March 2019

Deltaic Wetland Dynamics from Seasonal to Centennial Scales

Giancarlo A. Restreppo
Louisiana State University and Agricultural and Mechanical College

DELTAIC WETLAND DYNAMICS FROM SEASONAL TO CENTENNIAL SCALES

A Dissertation

Submitted to the Graduate Faculty of the
Louisiana State University and
Agricultural and Mechanical College
in partial fulfillment of the
requirements for the degree of
Doctor of Philosophy

in

The Department of Geology and Geophysics

by
Giancarlo A. Restreppo
B.A., California State University, Los Angeles, 2010
M.S., California State University, Los Angeles, 2015
May 2019

For my grandparents, Mimi and Ata, who left Ecuador for Los Angeles seeking a better future;

For my mother, Delia, who battled to provide two boys with every opportunity she could;

For my wife, Nadia, who's chasing a dream with me.

…You needn't die happy when your day comes, but you must die satisfied, for you have lived your life from beginning to end and ka is always served.

--Stephen King
The Dark Tower

ACKNOWLEDGEMENTS

First, thank you to my advisor and mentor, Dr. Samuel Bentley. Sam brought me into the fold with open arms and gave me everything I needed to grow as a researcher and to get this work done. Secondly, I'd like to thank my committee members, Dr. Kehui Xu and Dr. Carol Wilson. Both have been invaluable resources when I've been stuck on a problem or unsure of what direction to go. I'd like to thank past and future manuscript coauthors Dr. Jiaze Wang and Dr. Qihui Wu for their assistance with important portions of my research. Also, a huge thanks to Bill Gibson and Chris Cleaver at the CSI boat shop, who got me where I needed to be, when I needed to be there.

This project was funded in part by the Billy and Anne Harrison Endowed Chair in Sedimentary Geology, held by Dr. Bentley. Additional funding was provided by National Science Foundation Coastal SEES Award #1427389. I would also like to extend my deepest thanks to the Southern Regional Education Board and the LSU Board of Regents for funding my salary these past four years.

I'd like to acknowledge my many Bentley lab colleagues and undergraduate assistants, as well as LSU cohorts and friends, in alphabetical order: Jackie Brewster, Ryan Clarke, Daniela Colmenares, Brianna Crenshaw, Andrew Curtois, Jeff Duxbury, Rory Escobedo, Cameron Gernant, Suyapa Gonzalez, Brittney Gregory, Samantha Hall, Ross Harrison, Ethan Hughes, Greg Keller, Evan LeBlanc, Ryder Myers, Meg O'Connor, Patrick Robichaux, Richard Robinet, Rod Steiffel, and last but definitely not least, the Shannon & Crawford White. Y'all helped me through this in different ways, and I would like to express my profound thanks for being there.

To my old CSULA Geodudes, especially David Urita and future Dr. Ngoc Luu, thanks for the outings, laughs, and for the visits on the rare occasion we could make them happen. Thanks

Dr. Kim Bishop for checking in on me and for the Mojave advice, and Dr. Pedro Ramirez, my MS advisor, for the guidance and kind words of support that continued even after I left CSULA.

To my eternal friends from kinder and high school: Alex Aleman, Cesar Colín, Matt Green, Nick Lopez, Damaris and future JD Doug Valladares, and Henry Vasquez, thanks for making me feel like I still belong on the west coast. You guys are the best friends one could ask for.

Thanks to my Leyva family: Raquel, Checo, Chava, Roma, Beto, Omar, all the Houston folk, and the Tauts too. Thank you to my Coronel family: my mother Delia, Seppi, Ata, Coco, Azu, Gina & David Krashna, and George. Mom, Ata, Coco, I'm here principally because of you and the examples you set forth. Thank you for giving me something to strive for. Mimi, te extraño mucho y te dedico este volumen.

Finally, to my immediate family and "ka-tet" here in Baton Rouge, my wife and future super nurse Nadia, and our dogs Siana and Louie, you're my world. Thanks for being there through blood, sweat, tears, insect bites, complaints, etc. More importantly, thanks for sharing the new sights, new foods, new culture, and joys of this strange place called Louisiana. I love you deeply, and I couldn't have done this without you.

TABLE OF CONTENTS

ABSTRACT

The lower plain of the Mississippi River Delta contains approximately five coastal sedimentary basins that are topographically defined, and one shelf-crossing depocenter (the Birds Foot Delta). These depositional systems receive varying quantities of sediment from fluvial and marine sources and have rates of coastal land loss that are roughly inversely proportional to fluvial sediment supply. To combat land loss along these regions, Louisiana has launched a historic campaign to sustain and regrow coastal lands using, in part, river sediment diversions. Fine sediments constitute the majority of sediment load in the Mississippi River, but are under-studied with respect to dispersal processes, particularly in terms of sediment supply to distal deltaic bays and wetlands. To expand the knowledge of fine sediment dynamics along distal coastal marshes, two distinct, contrasting field areas along southeastern Louisiana are studied. The first, Fourleague Bay, is actively nourished by fresh sediment from the Atchafalaya River. The second, Terrebonne Bay, has not had an active fluvial connection in over a century. Using push cores, vibracores, carbon dating, grain size analysis, loss-on-ignition testing, bulk density, seismic CHIRP data, and natural and anthropogenic radioisotopes 7-beryllium, 210-lead, and 137-cesium, rates and patterns of sediment accumulation on both the shallow bay bottom and marsh platforms are calculated from seasonal to centennial timescales. Results indicate 1) riverine sphere of influence for nourishing mineral sediments is at least 25 km from the river mouth; 2) rhere exists a synergistic relationship between mineral sediment input and organic sediment production; 3) paleochannels may provide resiliency for marsh platforms established above them; 4) environmental processes control the physical properties of sediment.

CHAPTER 1. INTRODUCTION

1.1. Why?

As will be repeated multiple times throughout this volume, Louisiana is deep in the midst of a coastal crisis driven primarily from anthropogenic causes. The causes are well established, stemming from upriver damming of the Mississippi over the past centuries, which has substantially reduced sediment load to the coast, to climate driven responses in eustatic sea level, which is increasing annually. When the reduction in sediment is paired with a rise in sea level along a muddy coast already prone to compaction, consolidation, and subsidence, drastic changes in subaerial land area occurs. Louisiana's coast is disappearing (Fig. 1.1).

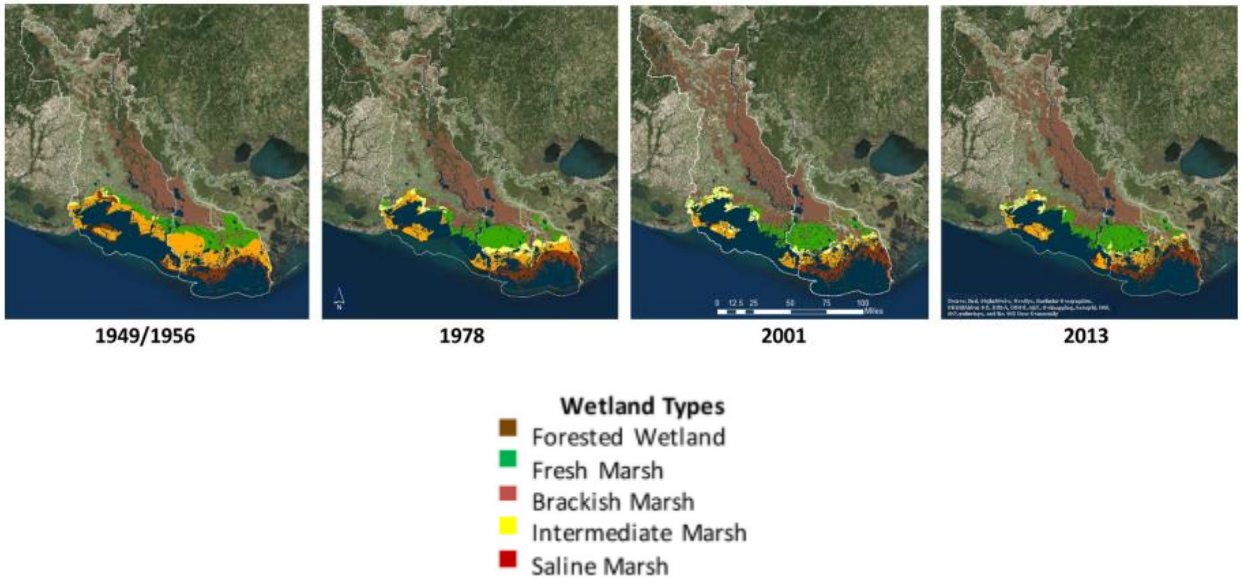

Figure 1.1. Wetland and marshes distribution in Terrebonne and Atchafalaya Basins, 1949/1956 - 2013 (modified from Twilley et al., 2016)

In response to our changing coastline, the state of the Louisiana has begun implementation of a Coastal Master Plan (CPRA, 2017). The Master Plan seeks to combat land loss using various methods, e.g. dredging and marsh creation, marsh restoration, and, most pertinent to this volume, river sediment diversions. In order for these diversions to work properly, and not just as small scale Band-Aids over a hemorrhaging coast line, it becomes necessary to understand how marsh

creation and sustainment occurs naturally over different time scales. Thus, analogues must be studied and sediment dynamics and delivery to the marsh platform must be thoroughly investigated.

1.2. Chapter Descriptions

Beginning with Chapter 2 and ending with Chapter 4, the work in this volume is presented in manuscript format, with each chapter published in or intended for publication in academic journals. Thus, while Chapter 5 briefly synthesizes all three chapters, each is intended to stand on its own.

Chapter 2, "Riverine Sediment Contribution to Distal Deltaic Wetlands: Fourleague Bay, Louisiana," uses the Atchafalaya River as an analogue for a sediment diversions. While proximal (river mouth) sandy sediment interaction with the marsh platform is relatively well studied, these interactions in distal wetlands are much less understood. In this chapter, push cores taken every two months of the marsh surface and bay bottom of Fourleague Bay, a semi enclosed, shallow, micro tidal bay southeast of the Atchafalaya mouth, were analyzed and used to deduce how much riverine fine sediment is delivered to the coastal fringes. The primary tool used to calculate our values is a short lived ($t_{1/2}$ = ~53 days) isotope, 7-beryllium. Since Fourleague has remained stable compared to the rest of the coast (Day et al., 2000; Barras et al., 2004; Twilley et al., 2016), this chapter provides some assumptions for how much sediment is necessary to sustain these coastal marshes.

To expand on the work done in Chapter 2, it became necessary to gather data from coastal marshes that have not been fed fresh sediment in some time. Thus, we moved into Terrebonne Bay, east of our Fourleague Bay field area and home of the fastest disappearing coastline in Louisiana (Penland and Ramsey, 1990; Jankowski et al., 2017). In Chapter 3, "Contrasting Recent Sedimentation Rates and Sediment Characteristics Between Fluvially Nourished and Self-

sustaining Distal Coastal Marshes in Southeastern Louisiana, USA," we compare push cores from Fourleague Bay with those from Terrebonne, in a direct "apples to apples" type contrast. Because Terrebonne is not fed directly by any major river, it became necessary to use longer lived isotopes for this study. The primary tools used in this study were the much longer lived isotopes 210-lead and 137-cesium ($t_{1/2}$ = ~22 and 30 years, respectively). Additionally, cores were fully analyzed for grain size, organic content (via loss-on-ignition), and density. A simple model for predicting how much longer certain coring sites will remain above sea level is also provided. The results are somewhat surprising, and a possible new diagnostic measurement for the health of a marsh platform is discussed.

Finally, Chapter 4 examines at the longer term (centennial) sedimentation rates and patterns of Terrebonne Bay. The full suite of analysis done in Chapter 3 is done once again to vibracores taken from ~4 to 6.5 m below the surface of both the marsh platform and bay bottom. However, instead of radioisotopes, carbon dating is used to calculate vertical accretion rates. Furthermore, seismic data of the subsurface just offshore of the marsh platform were gathered and interpreted. The major hypothesis of this chapter was geomorphological, in that perhaps the remaining fringes of coastline in Terrebonne Bay are built upon paleochannels, based on their appearance when seen in satellite view. While the hypothesis was not entirely proven, the seismic data were intriguing when aligned with the subaerial land mass.

In summary, this work seeks to establish 1) The amount of fine sediment making its way onto distal marsh platforms, and the mechanism by which this occurs; 2) The key differences in sediment characteristics between a marsh platform nourished by fresh sediment versus a platform sustained only by recycled sediment; 3) geotechnical reasons for marsh platform resilience, i.e. why do eroding coastal marshes in greatly at risk areas take the shape they do? Structurally, this

dissertation moves from seasonal to decadal to centennial time scales. These studies were done in the hopes of aiding ongoing and future coastal restoration efforts.

1.3. References

Barras, J. et al (2004) Historical and projected coastal Louisiana land changes: 1978-2050. USGS open file report 2003-334. https://doi.org/10.3133/ofr03334

Coastal Protection and Restoration Authority of Louisiana (CPRA) (2017) *Louisiana's Comprehensive Master Plan for a Sustainable Coast*. Web page at http://coastal.la.gov/our-plan/2017-coastal-master-plan/. Accessed January 17, 2019.

Day, J. W. et al. (2000) Pattern and process of land loss in the Mississippi Delta: A Spatial and temporal analysis of wetland habitat change. *Estuaries,* 23: 425-438.

Jankowski, K.L. et al. (2017) Vulnerability of Louisiana's coastal wetlands to present-day rates of relative sea-level rise. *Nature Communications* 8: 14792

Penland, S. and Ramsey, K.E. (1990) Relative sea-level rise in Louisiana and the Gulf of Mexico: 1908-1988. *Journal of Coastal Research*, 6(2): 323-342.

Twilley, R.R. et al. (2016) Co-evolution of wetland landscapes, flooding, and human settlement in the Mississippi River Delta Plain. *Sustain Sci.,* 11: 711-731.

CHAPTER 2. RIVERINE SEDIMENT CONTRIBUTION TO DISTAL DELTAIC WETLANDS: FOURLEAGUE BAY, LA

2.1. Introduction

The world's inhabited deltaic regions are at risk of drowning, due in large part to the interruption of natural sediment transport processes by humans. With the expected increase in eustatic sea level rise over the next century, the losses to these coastal regions will be catastrophic (Syvitski et al., 2009; Giosan et al., 2014). While research into sustainment and restoration of these coastal regions is already underway, the majority of this research focuses on coarse sediment that is deposited proximal to the river mouth (e.g., Kim et al., 2009; Nittrouer et al., 2012). However, the majority of sediment transported by these rivers is silt size or finer (Milliman and Mead, 1983; Milliman and Syvitski, 1992; Milliman and Farnsworth, 2011). Distal dispersal processes of these fine sediments, as well as their impact on the growth and sustainment of marshes distant from the sediment source, remain understudied. In the shallow, distal regions of the delta that are influenced by meteorological and astronomical tides, this fine sediment is susceptible to complex cycles of deposition and resuspension, forming intricate networks of exchange among initial sources and short-term and long-term sinks, such as river mouths, bay floors, and wetlands, respectively (Roberts et al., 2015; Ogston et al., 2017). These distal wetlands rely almost exclusively on cycles of fine sediment resuspension and exchange for sustainment. Maintenance of the deltaic landscape depends on the understanding of these fine sediment dispersal processes. This case study demonstrates the regional impact of muddy sediment dispersal and its ability to sustain and nourish

This chapter was previously published as Restreppo, G.A., Bentley, S.J., Wang, J., and Xu, K. (2019) Riverine sediment contribution to distal deltaic wetlands: Fourleague Bay, LA. *Estuaries and Coasts* 42(1): 55-67. The final publication is available at Springer via https://doi.org/10.1007/s12237-018-0453-0.

wetlands. This knowledge can be used with planned sediment diversions to better capture sediment to sustain and restore wetlands along the coast.

Between 1932 and 2010, Louisiana lost approximately 4877 km^2 of coastal land area. Calculated rate of land loss from 1985 through 2010 equates to 43 km^2 yr^{-1}, or the often quoted "one football field per hour" (Couvillion et al., 2011). Multiple factors drive the continued degradation of Louisiana's coast. One primary control is the upstream damming of the Mississippi River, which has drastically reduced the suspended sediment load carried by the river to Louisiana's muddy coast. This lack of new sediment, along with mud's natural tendency to compact over time, as well as rise in eustatic sea level, has led to an increasingly rapid decline in coastal land area in the Mississippi River Delta (Blum & Roberts, 2009). In order to combat land loss along the Mississippi River Delta, the State of Louisiana has launched a multi-decadal coastal engineering program to sustain and regrow coastal lands using, in part, river-sediment diversions (Peyronnin et al., 2012). The proposed diversions will capture both mud and sand-sized sediment that will be dispersed via natural coastal currents upon leaving conveyance channels (Allison and Meselhe, 2010). Modeling studies addressing fine-sediment dispersal for diversions often rely on highly simplified parameterizations for complex mud-dispersal processes (e.g., Brown et al., 2017). Some recent observational and modeling studies for diversions have examined controls on fine-sediment dispersal from river to bays to wetlands (Roberts et al., 2015; Allison et al., 2017). Nevertheless, because the properties of fine sediments that control erosion, transport, and deposition can evolve relatively rapidly due to consolidation and resuspension (Lo et al., 2014; Xu et al., 2016), confidently predicting coastal patterns of fine-sediment dispersal and deposition remains a challenge (Roberts et al., 2015), however critical these processes may be for maintaining deltaic wetlands.

2.2. Background

The fine-sediment dispersal system of the Atchafalaya River and associated bays and wetlands provide an excellent analog for future diversions as a means to study the radius of influence that a diversion provides, in terms of fine-sediment supply. The Atchafalaya Delta and a large swath of Louisiana's western coastline stand in sharp contrast to the Mississippi River and its delta. The marshes around the Atchafalaya have remained stable throughout the 20th and into the 21st centuries (Twilley et al., 2016). As a Mississippi River distributary, the Atchafalaya River is subject to the same limits on suspended sediment load as the parent river but is nevertheless building new deltaic wetlands at a substantial rate (Allen et al., 2012).

Several studies have concluded that major fluvial connections to Louisiana's coastal marshes are absolutely vital to their sustainment and growth (Day et al., 2007, 2016; Smith et al., 2015; Ko et al., 2017). Rates of accretion, both on and offshore, have been quantified using geochronology based on the relatively long-lived radioisotopes ^{137}Cs ($t_{1/2}$ = 30.17 y) and ^{210}Pb ($t_{1/2}$ = 22.3 y) (Smith et al., 2015; Keller et al., 2016). Studies of higher temporal resolution using ^{7}Be, which can be used to quantify the apparent mass deposition rate (AMDR), are less common along the same geographic region.

Fourleague Bay is a semi-enclosed bay with an active connection to the Atchafalaya River, which carries fine sediment into its nearby wetlands (Fig. 2.1). Most sand carried by the Atchafalaya River is trapped within the Atchafalaya and Wax Lake Deltas (Roberts et al., 2003). As such, Fourleague Bay serves as a choice field area for the study of fine-sediment dynamics and the role these sediments play in wetland growth and sustainability along the distal edge of a large deltaic depositional system.

Fourleague Bay spans approximately 17.5 km from its connection to Atchafalaya Bay in the north to Oyster Bayou, a tidal channel at its southern limits. The narrow (~0.3 km) Oyster Bayou tidal channel provides a path for water and sediment to exchange with the Gulf of Mexico. During the passage of southerly winds and large river pulses, Oyster Bayou limits flow into the Gulf, causing a backup of water and sediment in the bay that inundates the marshes (Perez et al., 1999). The maximum width of Fourleague Bay is approximately 7 km. Average bay depth, based upon bathymetric data gathered during this study, is $\leq$ 1 m, deepening to >3 m in the northern opening and >5 m in Oyster Bayou to the south. The marshes surrounding the bay are vegetated year-round.

According to Lane et al. (2010), less than 5% of the Atchafalaya's total discharge moves through Fourleague Bay. Even so, wetlands around the bay remain relatively stable against the deteriorative forces of subsidence, sea level rise, and wave erosion (Day et al., 2000; Twilley et al., 2016; Jankowski et al., 2017). This paper attempts to answer the following related questions: 1) At what rates do fine riverine sediments contribute to coastal marsh sustainment? 2) What processes transport these sediments to the marsh surface? As sea level rises, answers to these questions become more significant to degrading deltaic systems worldwide.

2.3. Radiochemistry

An extensive amount of research has been published on the utility of ^{7}Be as a proxy for the short-term erosion and deposition of fine sediment within aqueous environments under the influence of fluvial systems (Olsen et al., 1985; Casey, 1986; Hawley et al., 1986; Fitzgerald et al., 2001; Blake et al., 2002; Neubauer et al., 2002; Rotondo and Bentley, 2003; Walling, 2012; Guzmán et al., 2013; Keller et al., 2016). This study applies the same research techniques to the

distal, coastal-deltaic marshes of Fourleague Bay, Louisiana, in order to determine trends and rates of mass deposition.

Cosmogenic ^{7}Be is a naturally occurring radioisotope generated in the atmosphere by the bombardment of nitrogen and oxygen atoms with cosmic rays. The isotope precipitates back down to Earth, where it adsorbs onto fine sediment in both wet and dry settings, but is most concentrated in fluvial environments (Blake et al., 2002). With a half-life of approximately 54 days, ^{7}Be is an ideal tracer for relatively short-term sediment transfer within and from a fluvial environment. Since sediment from a surrounding watershed tends to collect in fluvial environments, rivers serve to funnel this sediment from a drainage basin to the coast. Thus, ^{7}Be active sediment is especially concentrated within rivers and the area influenced by a river's outlet. With inventory calculation during consecutive sampling periods, AMDR of recently deposited fluvial sediments can be determined (Fitzgerald et al., 2001; Blake et al., 2002; Walling, 2012; Keller et al., 2016).

2.4. Methodology

Between May 2015 and May 2016, push cores were taken once every two months at five sites along an aquatic transect down the center of Fourleague Bay, as well as in five adjacent sites along seasonally inundated marsh located within the eastern edge of the bay (Fig 2.1). All marsh sites are located approximately 50 m from the marsh edge and are 0.5-2 m in elevation, based on a 2011 USGS National Elevation Dataset LIDAR survey of Louisiana, referenced to NAD83 (U.S. Geological Survey, 2017). This data does not account for vegetation, however, and so is likely an overestimation of bare-earth elevation. A total of seven sampling events were undertaken and a total of 68 cores were analyzed. During April 2018, amid a significant flood event similar to that

seen in early 2016, an additional trip was undertaken to gather suspended sediment at four sites: a new northern site, FLB W1; and at three of the five bay sites, FLB 1, 3, and 5 (Fig. 2.1).

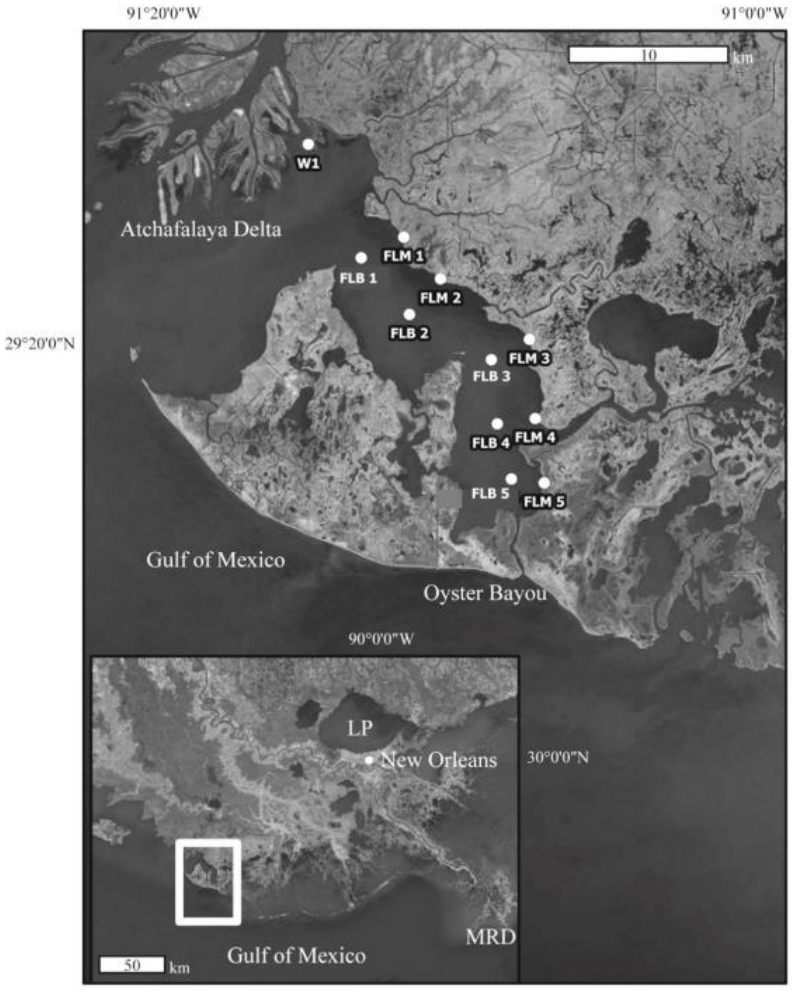

Figure 2.1. Location of Fourleague Bay and field sites in relation to the Mississippi River Delta (MRD) and Lake Pontchartrain (LP) Source: Esri, DigitalGlobe, GeoEye, i-cubed, USDA FSA, USGS, AEX, Getmapping, Aerogrid, IGN, IGP, swisstopo, and the GIS User Community.

After collection, the cores and water samples were taken to a cold room at Louisiana State University, Baton Rouge. Cores were then extruded in 2 cm intervals up to 20 cm in depth, weighed, dried for 48 hours at 60 ^{o}C, weighed again to determine gravimetric water content, then ground using a mortar and pestle. Water samples were allowed to settle for at least 48 hours, at which point the supernatant was removed and suspended sediment was concentrated and dried.

Suspended sediment was also ground once dry. Homogenized powder for both cores and suspended sediment were then weighed and sealed into tight-lid petri dishes. The sealed samples were placed within Canberra germanium gamma detectors for 20-24 hours to analyze for ^{7}Be activity. All samples from individual cores were counted for ^{7}Be in single detectors to reduce uncertainties in inter-detector calibration. The efficiency of the detectors for the 477 keV peak, which is associated with ^{7}Be activity, was determined via interpolation from adjacent peaks in National Institute of Standards and Technology and International Atomic Energy Agency standard reference materials (Keller et al., 2016).

In order to calculate ^{7}Be inventories, grain density measurements of the dry, powdered samples were made using a Quantachrome Ultrapyc 1200e gas pycnometer. With grain density known, the following suite of equations were used to calculate total inventory:

$$w_s = m_d/m_w \quad [2.1]$$

$$\rho_{db} = \rho_g w_s \quad [2.2]$$

$$A_2 = A_1 * \rho_{db} \quad [2.3]$$

$$I_t = z\Sigma A_2 \quad [2.4]$$

Where w_s is the solid mass fraction, m_d is the dry mass of the sample, m_w is the wet mass of the sample; ρ_{db} is the dry bulk density of the sample, ρ_g is the grain density of the sample; A_1 is measured massic activity (via gamma detection) of the sample, in Bq kg^{-1}; A_2 is volumetric activity at a specific depth in core in Bq m^{-3}; and finally, I_t is the total ^{7}Be inventory through the core at the date of sampling, in Bq m^{-2}, while z is the maximum depth of ^{7}Be penetration in cm. Expected soil inventory, or equilibrium inventory (I_{eq}), from both wet and dry precipitation (516.6 Bq m^{-2}; Baskaran et al. 1993 & 1997) is subtracted from the total inventory of marsh cores only, resulting

in surplus inventory (I_s). This was not done for bay cores as the bay floor is subaqueous year round, minimizing the effects of atmospheric fallout.

Once total or surplus inventory is calculated, fluvially sourced AMDR can be determined using the first sampling date, May 2015, as a zero point and following the method in Fitzgerald et al., (2001). To elaborate, inventory of the first sampling date is calculated and decay corrected to a second sampling date. This residual inventory (I_r) is then subtracted from the surplus or total inventory of the second sampling date, giving a "new" inventory (I_n) that can then be used to calculate time-dependent ^{7}Be flux for that given period of time (t_d):

$$\text{For marsh cores: } I_n = (I_t - I_{eq}) - I_r = I_s - I_r \quad [2.5]$$

$$\text{For bay cores: } I_n = I_t - I_r \quad [2.6]$$

$$\text{Time-dependent } ^7\text{Be flux for all cores} = I_n / t_d \quad [2.7]$$

This calculation can be carried through the entire year of sampling along consecutive sampling periods. If the calculated ^{7}Be flux value is positive, mass deposition occurred; if the value is negative, erosion or deposition of resuspended, ^{7}Be-free material occurred. If neither mass deposition nor removal occurred, flux would remain close to zero. To convert time-dependent ^{7}Be flux to apparent mass deposition rate, AMDR (Ψ), flux must be divided by the weighted average particle activity:

$$\Psi = {}^7\text{Be flux / weighted average particle activity} \quad [2.8]$$

This yields a mass accretionary rate in kg m^{-2} d^{-1}. Like ^{7}Be flux, a positive AMDR indicates mass deposition of relatively recent riverine sediment, and a negative AMDR can indicate either erosion, or deposition of resuspended older or coarser sediments that lack the ^{7}Be signature. If ^{7}Be activity was absent from a sample collected on a specific date, inventory from the previous sampling date

is decay corrected and used in its place. These values are considered a minimum erosion rate and may be an underestimation of the actual rate of erosion.

We refer to this rate estimate as an "apparent" mass deposition rate because it is not a direct measurement, but a proxy estimate (DeMaster et al., 1985; Lewis et al., 2002). This proxy estimate cannot differentiate between erosion versus deposition of unlabeled or organic sediment; this approach can only demonstrate the presence or lack of recently deposited fluvial sediment at the time of sampling. Because this approach is based on the inventory, not depth profile of ^{7}Be, the estimate of deposition rate is not sensitive to the effects of bioturbation (Muhammed et al., 2008).

Average AMDR estimates are compared to atmospheric data (wind speed, atmospheric pressure) from May 2015 to May 2016 gathered from NOAA's National Data Buoy Center website. The station used, "EINL1 – North of Eugene Island", is located ~15 km west of the northern entrance to Fourleague Bay. Atchafalaya discharge data was attained via the US Army Corp of Engineers website, from the discharge gauge at Simmesport, LA, ~185 km to the north.

2.5. Results

If present, ^{7}Be activity generally penetrated to a depth of 4 cm. There were three instances where activity penetrated to a depth of 6 cm. Overall ^{7}Be activities and inventories were lower in bay cores than in the marsh cores (Fig. 2.2). The highest individual surplus ^{7}Be inventory value within the marshes, (40.0 ± 12.7)E+2 Bq m^{-2}, was found in site FLM 3 during sampling on March 4, 2016, just after historic Atchafalaya discharge during January of that year. In the bay, the highest individual ^{7}Be inventory value, (27.6 ± 7.6)E+2 Bq m^{-2}, was found at site FLB 1 during sampling on May 15, 2015. See Tables 2.1 and 2.2 for all marsh and bay ^{7}Be inventory and flux data.

The largest individual AMDR in the marshes was 2.8 ± 1.0 kg m^{-2} d^{-1} at site FLM 3, once again during the March 4, 2016 sampling period. The most negative individual AMDR was at -2.1 ± 1.1 kg m^{-2} d^{-1} at site FLM 1 during the September 1, 2015 sampling period. It should be noted that this is a minimum erosion rate, as it was calculated using decayed activity from the May 15, 2015 sampling date. When AMDRs for all marsh sites are averaged, the largest rate calculated was 0.7 ± 0.2 kg m^{-2} d^{-1}, just after historic Atchafalaya discharge, on March 4, 2016. The lowest average marsh AMDR was -0.6 ± 0.2 kg m^{-2} d^{-1}, during the September 1, 2016 sampling period, which occurred at the start of annual low river discharge. Table 2.3 contains all marsh AMDR values through the year of sampling.

The largest individual bay AMDR, 2.9 ± 2.3 kg m^{-2} d^{-1}, was calculated at site FLB 2 during the July 7, 2015 sampling period. The most negative individual AMDR, -2.0 ± 3.6 kg m^{-2} d^{-1}, was calculated at site FLB 5 during the January 20, 2016 sampling period, coinciding with a historic river discharge event. When AMDR for all bay sites are averaged, the greatest rate of deposition was 1.2 ± 0.67 kg m^{-2} d^{-1}, during the sampling period of September 1, 2015, the period of annual low river discharge. The most negative average bay AMDR -0.9 ± 0.3 and -0.9 ± 1.2 kg m^{-2} d^{-1}, occurred twice; first during the July 7, 2015 sampling date which occurred close to peak seasonal river discharge; then again during the January 20, 2016 sampling period of historic high river discharge. Table 2.4 contains all bay AMDR values through the year of sampling. Table 2.5 contains all the averaged bay and marsh AMDR values for each period through the year of sampling.

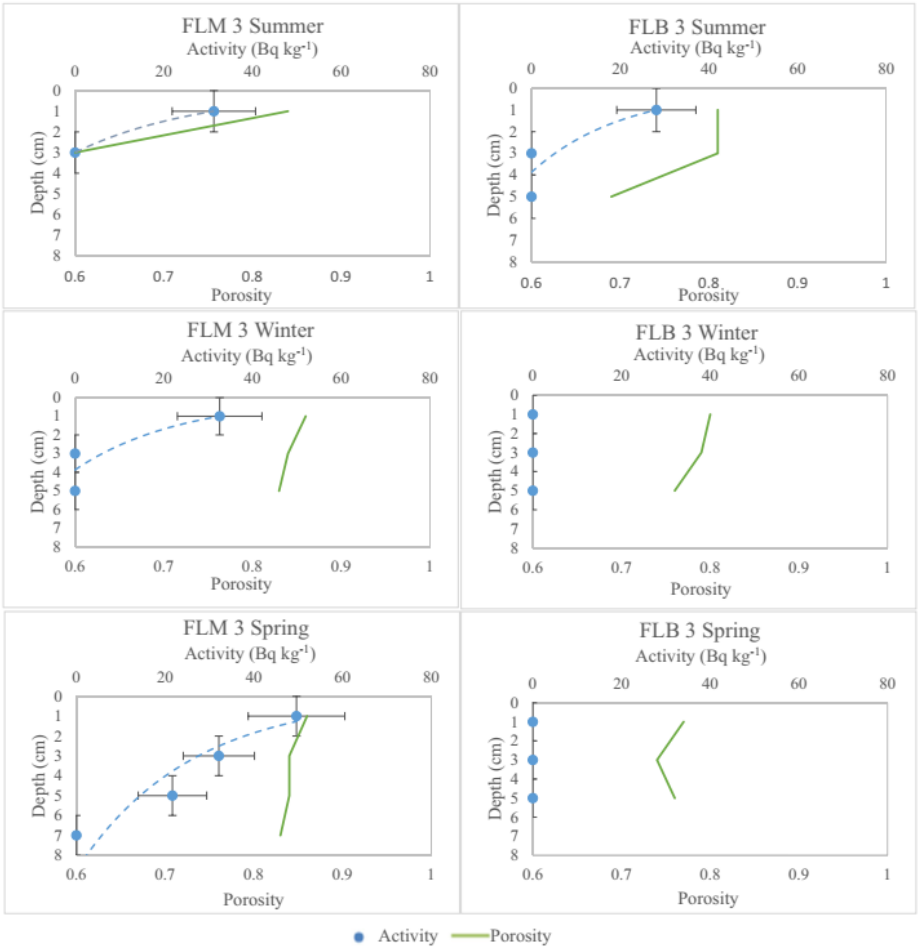

Figure 2.2. ^{7}Be activity and porosity with depth in marsh core FLM 3 and bay core FLB 3 through three seasons of sampling. Note depth of ^{7}Be penetration in the marsh core and relative inactivity in the bay core.

Activity of suspended sediments was substantially higher than any bay or marsh core in the first three, most northern sites, FLB W1, FLB 1, and FLB 3: 208.9 ± 36.0, 326.7 ± 90.9, and 207.8 ± 37.5 Bq kg^{-1}, respectively. Activity levels decreased drastically at the remaining, southern most site, FLB 5, with a value of 36.2 ± 11.3 Bq kg^{-1}. Overall, sediment from the bay opening southward, away from the river mouth, to Oyster Bayou (Sites FLB 1, FLB 3, and FLB 5) displays a gradient of decreasing ^{7}Be activity and increasing total suspended sediment concentration (TSSC). Table 2.6 contains activity, suspended sediment concentration, and salinity values for all four water sites.

Table 2.1. Marsh time-dependent ^{7}Be flux values.

Site	Date	Surplus inventory (eq. 5; Bq m^{-2}, E + 2)	Residual inventory (Bq m^{-2}, E + 2)	New inventory (Bq m^{-2}, E + 2)	Elapsed time (d)	Time-dependent ^{7}Be flux (Bq m^{-2} d^{-1})
FLM 1	5/15/2015	3.5 ± 3.8	–	–	–	–
	7/7/2015	19.6 ± 8.0	1.8 ± 1.9	17.8 ± 8.2	53	33.7 ± 15.5
	9/1/2015	− 5.2 ± 1.7	9.4 ± 3.8	− 14.6 ± 4.2	56	− 26.1 ± 7.5
	11/19/2015	17.3 ± 4.8	0	17.3 ± 4.2	79	21.9 ± 5.3
	1/20/2016	− 5.8 ± 1.7	7.7 ± 1.9	− 12.9 ± 2.5	62	− 20.8 ± 4.0
	3/4/2016	− 5.2 ± 1.7	0	− 5.2 ± 1.7	44	− 11.7 ± 3.8
	5/12/2016	− 2.6 ± 1.8	0	− 2.6 ± 1.8	69	− 3.8 ± 2.6
FLM 2	5/15/2015	14.9 ± 5.9	–	–	–	–
	7/7/2015	− 5.2 ± 1.7	7.5 ± 2.9	− 12.6 ± 3.4	53	− 23.8 ± 6.4
	9/1/2015	NS	–	–	56	–
	11/19/2015	− 5.2 ± 1.7	–	–	79	–
	1/20/2016	8.0 ± 2.7	0	8.0 ± 2.7	62	12.9 ± 4.4
	3/4/2016	− 5.2 ± 1.7	4.5 ± 1.5	− 9.7 ± 2.3	44	− 22.0 ± 5.1
	5/12/2016	− 5.2 ± 1.7	0	− 5.2 ± 1.7	69	− 7.5 ± 2.4
FLM 3	5/15/2015	− 5.2 ± 1.7	–	–	–	–
	7/7/2015	1.9 ± 2.4	0	1.9 ± 2.4	53	3.6 ± 4.5
	9/1/2015	2.3 ± 2.8	90.6 ± 1.2	1.4 ± 3.0	56	2.5 ± 5.4
	11/19/2015	− 5.2 ± 1.7	0.8 ± 1.0	− 6.0 ± 1.9	79	− 7.6 ± 1.2
	1/20/2016	− 0.7 ± 2.1	0	− 0.7 ± 2.1	62	− 1.2 ± 3.4
	3/4/2016	40.0 ± 7.0	0	40.0 ± 7.0	44	90.8 ± 16.0
	5/12/2016	13.8 ± 3.3	16.2 ± 2.9	− 2.5 ± 4.4	69	− 3.6 ± 6.4
FLM 4	5/15/2015	NS	NS	–	–	–
	7/7/2015	− 5.2 ± 1.7	–	–	53	–
	9/1/2015	− 2.3 ± 2.1	0	− 2.3 ± 2.1	56	− 5.2 ± 3.7
	11/19/2015	− 0.4 ± 2.2	0	− 0.4 ± 2.2	79	− 0.5 ± 2.8
	1/20/2016	− 1.0 ± 1.9	0	− 1.0 ± 1.9	62	− 1.6 ± 3.1
	3/4/2016	12.8 ± 3.8	0	12.8 ± 3.8	44	29.1 ± 8.7
	5/12/2016	3.9 ± 3.0	5.2 ± 1.6	− 1.4 ± 3.3	69	− 2.0 ± 4.8
FLM 5	5/15/2015	NS	NS	–	–	–
	7/7/2015	− 2.0 ± 2.5	–	–	53	–
	9/1/2015	− 1.3 ± 2.0	0	− 1.3 ± 2.0	56	− 2.3 ± 3.6
	11/19/2015	− 0.3 ± 2.1	0	− 0.3 ± 2.1	79	− 0.3 ± 2.7
	1/20/2016	7.1 ± 3.1	0	7.1 ± 3.1	62	11.5 ± 5.1
	3/4/2016	0.8 ± 2.1	4.0 ± 1.8	− 3.3 ± 2.8	44	− 7.4 ± 6.3
	5/12/2016	9.0 ± 3.8	0.3 ± 0.9	8.7 ± 3.9	69	12.6 ± 5.6

NS not sampled

Table 2.2. Bay time-dependent ^{7}Be flux values.

Site	Date	Total inventory (Eq. 6; Bq m^{-2}, E + 2)	Residual inventory (Bq m^{-2}, E + 2)	New inventory (Bq m^{-2}, E + 2)	Elapsed time (d)	Time-dependent ^{7}Be flux (Bq m^{-2} d^{-1})
FLB 1	5/15/2015	27.6 ± 7.6	–	–	–	–
	7/7/2015	0	13.8 ± 3.8	− 13.8 ± 3.8	53	− 26.1 ± 7.2
	9/1/2015	0	0	0	56	0
	11/19/2015	0	0	0	79	0
	1/20/2016	0	0	0	62	0
	3/4/2016	0	0	0	44	0
	5/12/2016	14.2 ± 2.6	0	14.2 ± 2.6	69	20.6 ± 3.7
FLB 2	5/15/2015	6.6 ± 3.3	–	–	–	–
	7/7/2015	0	3.3 ± 1.7	− 3.3 ± 1.7	53	− 6.3 ± 3.1
	9/1/2015	20.4 ± 11.5	0	20.4 ± 11.5	56	36.5 ± 20.5
	11/19/2015	6.9 ± 3.4	7.3 ± 4.1	− 0.4 ± 5.4	79	− 0.5 ± 6.8
	1/20/2016	0	3.1 ± 1.5	− 3.1 ± 1.5	62	− 4.9 ± 2.5
	3/4/2016	0	0	0	44	0
	5/12/2016	4.1 ± 1.6	0	4.1 ± 1.6	69	5.9 ± 2.3
FLB 3	5/15/2015	9.0 ± 4.2	–	–	–	–
	7/7/2015	0	4.5 ± 2.1	− 4.5 ± 2.1	53	− 8.5 ± 3.9
	9/1/2015	5.5 ± 2.0	0	5.5 ± 2.0	56	9.8 ± 3.6
	11/19/2015	0	2.0 ± 0.7	− 2.0 ± 0.7	79	− 2.5 ± 0.9
	1/20/2016	0	0	0	62	0
	3/4/2016	0	0	0	44	0
	5/12/2016	7.1 ± 2.4	0	7.1 ± 2.4	69	10.3 ± 3.5
FLB 4	5/15/2015	0	–	–	–	–
	7/7/2015	0	0	0	53	0
	9/1/2015	0	0	0	56	0
	11/19/2015	4.4 ± 2.2	0	4.4 ± 2.2	79	5.5 ± 2.8
	1/20/2016	0	1.9 ± 1.0	− 1.9 ± 1.0	62	− 3.1 ± 1.6
	3/4/2016	0	0	0	44	0
	5/12/2016	0	0	0	69	0
FLB 5	5/15/2015	0	–	–	–	–
	7/7/2015	0	0	0	53	0
	9/1/2015	4.5 ± 1.6	0	4.5 ± 1.6	56	8.1 ± 2.9
	11/19/2015	17.6 ± 6.9	1.6 ± 0.6	16.0 ± 6.9	79	20.2 ± 8.8
	1/20/2016	1.1 ± 1.9	7.8 ± 3.1	− 6.8 ± 3.6	62	− 10.9 ± 5.9
	3/4/2016	0	0.6 ± 1.1	− 0.6 ± 1.1	44	− 1.4 ± 2.5
	5/12/2016	1.9 ± 1.3	0	1.9 ± 1.3	69	2.7 ± 1.9

Table 2.3. Daily AMDR in marsh sites, per sampling period.

Site	Date	Time-dependent ^{7}Be flux (Bq m^{-2} d^{-1})	Average ^{7}Be particle activity (Bq kg^{-1})	Marsh AMDR (Ψ; kg m^{-2} d^{-1})
FLM 1	5/15/2015	–	–	–
	7/7/2015	33.7 ± 15.5	26.2 ± 8.1	1.3 ± 0.7
	9/1/2015	− 26.1 ± 7.5	12.6 ± 3.9[a]	− 2.1 ± 0.9[b]
	11/19/2015	21.9 ± 5.3	55.8 ± 9.7	0.4 ± 0.1
	1/20/2016	− 20.8 ± 4.0	24.9 ± 4.3[a]	− 0.8 ± 0.2[b]
	3/4/2016	− 11.7 ± 3.8	0	–
	5/12/2016	− 3.8 ± 2.6	32.6 ± 9.0	− 0.1 ± 0.1
FLM 2	5/15/2015	–	–	–
	7/7/2015	− 23.8 ± 6.4	12.1 ± 3.3[a]	− 2.0 ± 0.8[b]
	9/1/2015	–	NS	–
	11/19/2015	–	–	–
	1/20/2016	12.9 ± 4.4	37.6 ± 6.2	0.3 ± 0.1
	3/4/2016	− 22.0 ± 5.1	21.2 ± 3.5[a]	− 1.0 ± 0.3[b]
	5/12/2016	− 7.5 ± 2.4	0	–
FLM 3	5/15/2015	–	–	–
	7/7/2015	3.6 ± 4.5	40.7 ± 10.0	0.1 ± 0.1
	9/1/2015	2.5 ± 5.4	31.3 ± 9.4	0.1 ± 0.2
	11/19/2015	− 7.6 ± 1.2	11.2 ± 3.4[a]	− 0.7 ± 0.3[b]
	1/20/2016	− 1.2 ± 3.4	32.6 ± 9.5	− 0.04 ± 0.1
	3/4/2016	90.8 ± 16.0	32.3 ± 5.0	2.8 ± 0.7
	5/12/2016	− 3.6 ± 6.4	42.8 ± 6.6	− 0.1 ± 0.2
FLM 4	5/15/2015	–	NS	–
	7/7/2015	–	–	–
	9/1/2015	− 5.2 ± 3.7	12.2 ± 6.6	− 0.4 ± 0.4
	11/19/2015	− 0.5 ± 2.8	34.4 ± 10.3	− 0.01 ± 0.1
	1/20/2016	− 1.6 ± 3.1	29.7 ± 7.2	− 0.05 ± 0.1
	3/4/2016	29.1 ± 8.7	25.8 ± 5.0	1.1 ± 0.4
	5/12/2016	− 2.0 ± 4.8	21.4 ± 5.8	− 0.1 ± 0.2
S	5/15/2015	–	NS	–
	7/7/2015	–	–	–
	9/1/2015	− 2.3 ± 3.6	25.2 ± 7.3	− 0.1 ± 0.1
	11/19/2015	− 0.3 ± 2.7	33.8 ± 8.8	− 0.01 ± 0.1
	1/20/2016	11.5 ± 5.1	24.7 ± 5.0	0.5 ± 0.2
	3/4/2016	− 7.4 ± 6.3	34.2 ± 7.6	− 0.2 ± 0.2
	5/12/2016	12.6 ± 5.6	28.9 ± 6.4	0.4 ± 0.2

[a] Decay corrected from previous sampling interval

[b] Minimum erosion rate

NS not sampled

Table 2.4. Daily AMDR in bay sites, per sampling period.

Site	Date	Time-dependent ^{7}Be flux (Bq m^{-2} d^{-1})	Average ^{7}Be particle activity (Bq kg^{-1})	Bay AMDR (Ψ; kg m^{-2} d^{-1})
FLB 1	5/15/2015	–	–	–
	7/7/2015	−26.1 ± 7.2	24.9 ± 4.8[a]	−1.1 ± 0.4[b]
	9/1/2015	0	0	–
	11/19/2015	0	0	–
	1/20/2016	0	0	–
	3/4/2016	0	0	–
	5/12/2016	20.6 ± 3.7	67.7 ± 8.7	0.3 ± 0.1
FLB 2	5/15/2015	–	–	–
	7/7/2015	−6.3 ± 3.1	21.1 ± 9.4[a]	−1.2 ± 0.8[b]
	9/1/2015	36.5 ± 20.5	12.4 ± 7.0	2.9 ± 2.3
	11/19/2015	−0.5 ± 6.8	29.1 ± 13.1	−0.02 ± 0.2
	1/20/2016	−4.9 ± 2.5	13.0 ± 5.8[a]	−0.4 ± 0.3[b]
	3/4/2016	0	0	–
	5/12/2016	5.9 ± 2.3	15.8 ± 5.4	0.4 ± 0.2
FLB 3	5/15/2015	–	–	–
	7/7/2015	−8.5 ± 3.9	35.5 ± 14.6[a]	−0.2 ± 0.2[b]
	9/1/2015	9.8 ± 3.6	28.2 ± 8.9	0.4 ± 0.2
	11/19/2015	−2.5 ± 0.9	10.1 ± 3.2[a]	−0.3 ± 0.1[b]
	1/20/2016	0	0	–
	3/4/2016	0	0	–
	5/12/2016	10.3 ± 3.5	33.9 ± 9.7	0.3 ± 0.1
FLB 4	5/15/2015	–	–	–
	7/7/2015	0	0	–
	9/1/2015	0	0	–
	11/19/2015	5.5 ± 2.8	18.7 ± 8.5	0.3 ± 0.2
	1/20/2016	−3.1 ± 1.6	8.3 ± 3.8[a]	−0.4 ± 0.3[b]
	3/4/2016	0	0	–
	5/12/2016	0	0	–
FLB 5	5/15/2015	–	–	–
	7/7/2015	0	0	–
	9/1/2015	8.1 ± 2.9	22.0 ± 6.8	0.4 ± 0.2
	11/19/2015	20.2 ± 8.8	25.1 ± 6.5	0.8 ± 0.4
	1/20/2016	−10.9 ± 5.9	5.4 ± 9.3	−2.0 ± 3.6
	3/4/2016	−1.4 ± 2.5	3.1 ± 5.3[a]	−0.5 ± 1.1[b]
	5/12/2016	2.7 ± 1.9	8.0 ± 5.3	0.3 ± 0.3

[a] Decay corrected from previous sampling interval

[b] Minimum erosion rate

Table 2.5. Averaged AMDR for marshes and bays for each sampling period.

Sampling date	Avg. marsh AMDR ($kg\ m^{-2}\ d^{-1}$)	Avg. bay AMDR ($kg\ m^{-2}\ d^{-1}$)
5/15/2015	–	–
7/7/2015	-0.2 ± 0.3	-0.9 ± 0.3
9/1/2015	-0.6 ± 0.2	1.2 ± 0.7
11/19/2015	-0.1 ± 0.1	0.2 ± 0.1
1/20/2016	-0.02 ± 0.07	-0.9 ± 1.2
3/4/2016	0.7 ± 0.2	-0.5 ± 1.1
5/12/2016	0.04 ± 0.09	0.3 ± 0.1

Table 2.6. Salinity, TSSC, and ^{7}Be activity values for water samples

Sample	Salinity (ppt)	TSSC ($mg\ L^{-1}$)	Activity ($Bq\ kg^{-1}$)
W1	0.1	67.0	209 ± 36.0
FLB1	0.1	26.5	327 ± 90.9
FLB3	0.8	47.7	208 ± 37.5
FLB5	21.0	88.6	36 ± 11.3

2.6. Discussion and Implications

Within the limitations of our methodology, results show reciprocal patterns of ^{7}Be inventories in marsh and bay sediments that are indicative of sediment exchange between bay floor and wetland surface over seasonal timescales. Marsh and bay AMDR rates display a moderate, negative correlation (r = -0.51; Fig. 2.3). Results also show net positive AMDR in the three southernmost marsh sites, FLM 3, 4, and 5 over the course of the year (Fig. 2.4).

The trend of decreasing ^{7}Be activity in suspended sediments through the bay indicate that the fluvial environment concentrates and funnels these sediments to the coast. In Fourleague Bay, during periods of high river discharge, it appears that as these sediments move through the bay and towards the Gulf of Mexico, they are distributed into the marshes during periods of high water. Simultaneously, bay floor sediments are resuspended, most obvious in the suspended sediment of

site FLB 5 in the lower portion of the bay. The large reduction in ^{7}Be activity and increase in TSSC as one moves south through the bay may indicate: 1) Active sediment is indeed making its way into the marshes, thus reducing the active sediment concentration; 2) The increased discharge from the river during this period is agitating the bay bottom enough to resuspend inactive and organic sediments from the bay floor, also reducing active sediment concentration; or 3) Both are occurring simultaneously. In the marshes, this net sediment accumulation occurs over length scales of at least 25 km from the Atchafalaya River mouth.

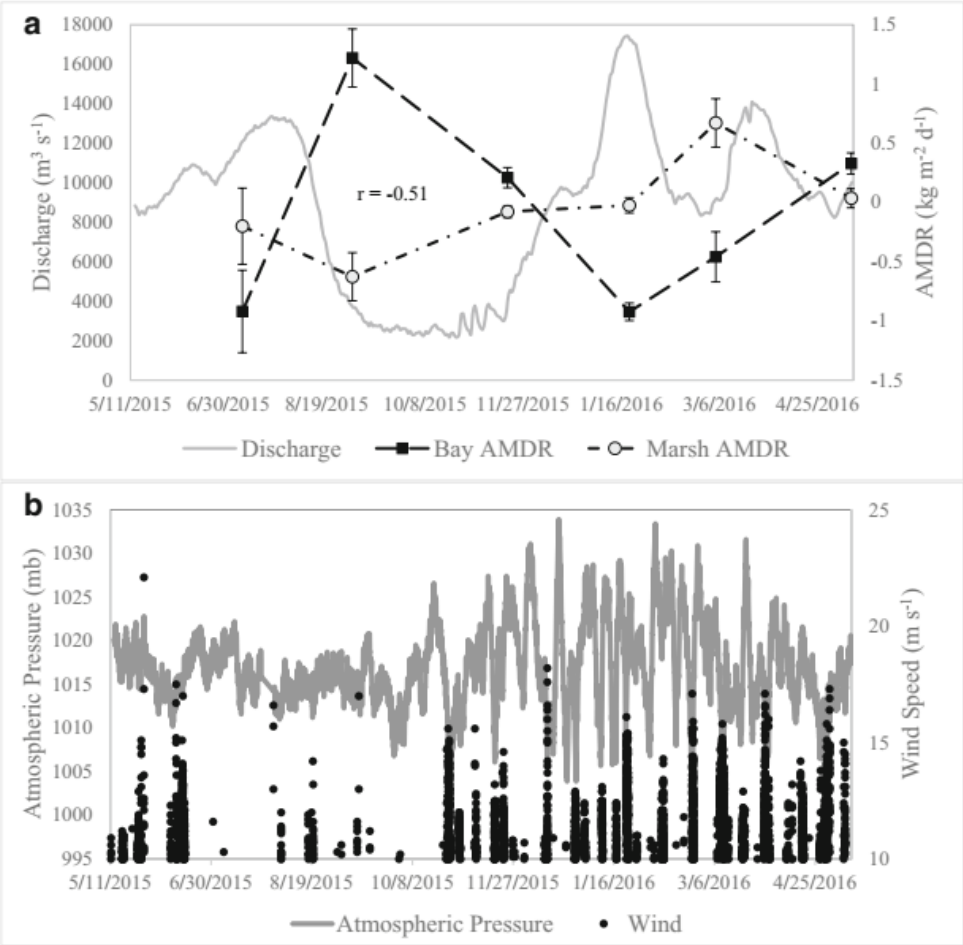

Figure 2.3. a: Average bay and marsh AMDR throughout the year of sampling with Atchafalaya discharge. b: Atmospheric pressure with wind speed; "columns" of wind represent the passage of a strong front, especially when lined up with a drop in atmospheric pressure.

Collectively, these findings are in agreement with the hydrodynamic time-series study of Wang et al., (2018), from which we and Wang et al. identify three sediment transport regimes in Fourleague Bay: 1) Fine sediment bypasses the bay floor and is delivered directly to the wetlands during periods of high river discharge, which occurred the first quarter of 2016 (Fig. 2.3); 2) Sediment is delivered from the river to the bay floor during minimal river discharge and calm atmospheric conditions, which occurred from approximately late July to October 2015. The surrounding marsh receives little to no riverine sediment input (Fig. 2.3); and 3) Sediment is delivered to the bay floor and then deposited onto the wetland surface via resuspension by local waves and currents during periods of minimal river discharge and energetic atmospheric conditions, which occurred from November until December 2015. It is believed that the marshes receive both fresh, recently deposited riverine sediment and resuspended older bay floor sediment during this time (Fig. 2.3). Limits to this approach include that these results only pertain to the contribution of ^{7}Be-labeled sediment, mostly of recent fluvial provenance. These AMDR values do not include in situ organic sediment production, inactive fluvial sediment, or wind-driven, resuspended older or coarser sediments coming from the bay floor that lack detectable ^{7}Be. While undetectable by the research methods of this paper, bay floor sediment that has been resuspended by moderate to strong atmospheric forcing is likely a substantial seasonal contributor to total sediment accretion in the marshes of Fourleague Bay. Perez et al., (1999), Roberts et al., (2015) and Wang et al., (2018) found that passage of a cold front through the region can raise water levels by up to 1 m, which then floods the marshes with sediment-laden water. The results presented above are in agreement with these findings, as AMDR values in the marshes generally increase during periods of frequent, strong winds. AMDR values in the bays only increase during periods

of both calm atmospheric conditions and low river discharge. An increase in winds during annual low river discharge leads to an increase in marsh AMDR and a decrease in the bay.

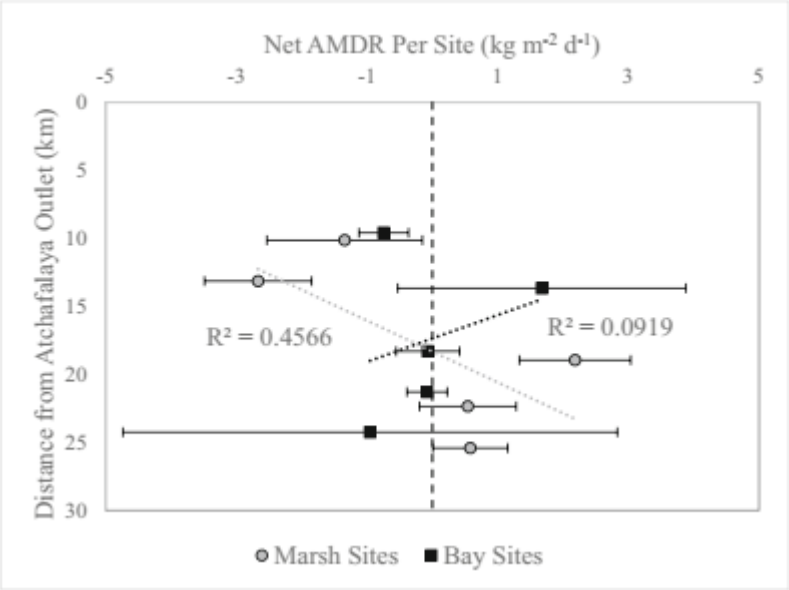

Figure. 2.4. Net AMDR per site vs. distance from Atchafalaya River mouth, with trend lines. Marsh sites trend positive, while bay sites trend negative.

While studies calculating ^{7}Be based AMDR in identical environmental settings could not be found, there have been studies that have calculated ^{7}Be inventories in analogous areas, such as diversion projects along the Louisiana coast or other coastal areas under direct river influence (Casey, 1986; Neubauer et al., 2002; Rotondo and Bentley, 2003; Andrus and Bentley, 2007; Kolker et al., 2012; Keller et al., 2016). When compared, the ^{7}Be inventory values calculated in this study are generally in agreement with those in the aforementioned studies. For example, Rotondo and Bentley (2003) found maximum ^{7}Be inventory of subaqueous sites along Louisiana's chenier plain coast, 100 km to the west of our field area, between 200 and 900 Bq m^{-2}, depending on the time of year. When ^{7}Be activity was present, inventory of subaqueous bay sites in our study area typically fall within this range, with the exception of northernmost site FLB 1 and two substantially higher values that occur during fall 2015 at sites FLB 2 and FLB 5. Kolker et al.

(2012) measured ^{7}Be inventory of cores in and around the West Bay Mississippi River Diversion and calculated maximum inventory at ~3700 Bq m^{-2}. All of our marsh inventory values fall well below this number, with the exception of core FLM 3 during spring 2016.

Average riverine AMDR within marshes and bays is, of course, primarily a factor of the amount of river discharge, but atmospheric forcing appears to enhance the effect. Average AMDR in the marshes rises during periods of increasing discharge, and peaks after the historically high Atchafalaya discharge event of early 2016 (sample date March 4, 2016). The most negative rate of mass deposition in the marshes, occurs during a drop in river discharge to an annual low, on September 1, 2015 (Fig 2.3; Table 2.5). AMDR begins to rebound when atmospheric forcing increases during the period before the November 19, 2015 sampling date and continues to rise through the period of historically high discharge.

Bay values indicate constant sediment bypass and erosion year-round, until annual low discharge from the Atchafalaya during the September 1, 2015. Wind also becomes more quiescent at this time. During this period, average AMDR within the bay peaks (Fig. 2.3; Table 2.5). Once river discharge and atmospheric forcing begin to increase, bay AMDR decreases substantially. When net AMDR per site for the year is plotted against distance (Fig. 2.4), maximum AMDR occurs at site FLM 3, the central marsh site. The two northern most marsh sites, FLM 1 and FLM 2 are at a net loss for the year. These lateral gradients in ^{7}Be active sediment deposition may be comparable to lateral gradients in sediment accumulation observed on many subaqueous deltaic clinoforms, for which low proximal deposition rates are limited by hydrodynamic energy, low distal rates are limited by lower sediment supply, and high medial rates are produced by high sediment supply and reduced bed shear stresses (e.g., Walsh et al., 2004; Denommee et al., 2017) The only bay site to achieve a net positive AMDR is site FLB 2, with all other bay sites trending

either near zero or negative. These observations suggest that, on average, most of the bay floor experiences bed shear stresses high enough to prevent long-term accumulation and shoaling of the bay floor during the length of this study.

2.7. Conclusion

To summarize, our results indicate that when river discharge is high, sediment bypasses the bay and directly feeds the marshes. Only when discharge is at an annual low, and with minimal atmospheric forcing, does sediment accrete onto the bay floor. Subsequent resuspension during periods of elevated water levels provide muddy sediments to distal marshlands, helping to offset the effects of relative sea level rise and other deteriorative forces that are erasing Louisiana's coast. In addition to a strong fluvial connection, the key factors in the sustainment of Fourleague Bay appear to be resuspension of bay floor sediments via wind, and possibly the bay's morphology. When paired with high discharge from the Atchafalaya River, marsh inundation is more likely and in fact a regular occurrence. Atmospheric forcing in this shallow environment serves to amplify the range and effects of inundation, even during annual low river discharge.

While Fourleague Bay receives only ~5% of the Atchafalaya's discharge, which translates to a primarily fine sediment load of 3.1 – 4 MT $year^{-1}$ based on 62 – 80 MT $year^{-1}$ sediment discharge from the river during flood years (Allison et al., 2012), the marshland surrounding Fourleague Bay has sustained itself for the better part of a century while the majority of Louisiana's coast continues to disappear. The use of river-sediment diversions for restoration and conservation of deltaic wetlands (in the Mississippi or other deltaic systems worldwide) should incorporate understanding of sediment-dispersal processes such as those that help sustain Fourleague Bay wetlands. If pulses of river water out of the diversion are timed correctly with seasonal

intensification of atmospheric forcing, surrounding marshland could feasibly be sustained, and perhaps even grow.

2.8. References

Allen, Y.C. et al. (2012) Using multitemporal remote sensing imagery and inundation measures to improve land change estimates in coastal wetlands. *Estuaries and Coasts,* 35(1): 190-200.

Allison, M.A. and Meselhe, E.A. (2010) The use of large water and sediment diversions in the lower Mississippi River (Louisiana) for coastal restoration. *Journal of Hydrology,* 387(3): 346-360.

Allison, M.A. et al. (2012) A water and sediment budget for the lower Mississippi-Atchafalaya River in flood years 2008-2010: Implications for sediment discharge to the oceans and coastal restoration in Louisiana. *Journal of Hydrology*, 432-433: 84-97.

Allison, M.A. et al. (2017) Observational and numerical particle tracking to examine sediment dynamics in a Mississippi River delta diversion. *Estuarine, Coastal and Shelf Science*, 194: 97-108.

Andrus, M.T. and Bentley, S.J. (2007) Sediment flux and fate in the Mississippi River Diversion at West Bay: observation study. In *Coastal Sediment '07: Proceedings of the Sixth International Symposium on Coastal Engineering and Science of Coastal Sediment Processes, May 13-17, New Orleans, Lousiana,* pp. 722-735. Kraus, N.C, and Rosati, J.D. eds. American Society of Civil Engineers.

Baskaran, M. et al. (1993) Atmospheric depositional fluxes of ^{7}Be and ^{210}Pb at Galveston and College Station, Texas. *Journal of Geophysical Research,* 98(D11): 20,555-20,571.

Baskaran, M. et al. (1997) Cycling of ^{7}Be and ^{210}Pb in a high DOC, shallow, turbid estuary of south-east Texas. *Estuarine, Coastal and Shelf Science,* 45: 165-176.

Blake, W. H. et al. (2002) Using cosmogenic beryllium-7 as a tracer in sediment budget investigations. *Geografiska Annaler, Series A: Physical Geography,* 84(2): 89-102.

Blum, M.D. and Roberts, H.H. (2009) Drowning of the Mississippi Delta due to insufficient sediment supply and global sea-level rise. *Nature Geoscience,* 2: 488-491

Brown, S. et al. (2017) *2017 Coastal Master Plan: Appendix C: Modeling Chapter 3 – Modeling Components and Overview*. Version Final. (p. 72). Baton Rouge, Lousiana: Coastal Protection and Restoration Authority.

Casey, W.H. (1986) The distribution of cosmogenic ^{7}Be in salt marsh sediments. *Geophysical Research Letters,* 13(4): 322-325.

Couvillion, B.R. et al. (2011) Land area change in coastal Louisiana from 1932 to 2010: U.S. Geological Surevey Investigations Map 3164, 12 p. pamphlet.

Davenport, C. and Robertson, C. (2016) Resettling the First American 'Climate Refugees'. *The New York Times,* 3 May 2016, pp. A1.

Day, J. W. et al. (2000) Pattern and process of land loss in the Mississippi Delta: A Spatial and temporal analysis of wetland habitat change. *Estuaries,* 23: 425-438.

Day, J.W. et al. (2007) Restoration of the Mississippi Delta: Lessons from Hurricanes Katrina and Rita. *Science,* 315: 1679-1684.

Day, J.W. et al. (2016) Large infrequently operated river diversions for Mississippi delta restoration. *Estuarine, Coastal, & Shelf Science,* 183(Part B):292-303.

DeMaster, D.J. et al. (1985) Rates of sediment accumulation and particle reworking based on radiochemical measurements from continental shelf deposits in the East China Sea. *Continental Shelf Research*, 4(1-2): 143-158.

Denommee, K.C. et al. (2017) Mechanisms of muddy clinothem progradation on the Southwest Louisiana Chenier Plain inner shelf. *Geo-Marine Letters,* doi.org/10.1007/s00367-017-0525-3

Fitzgerald, S. A. et al. (2001) Beryllium-7 as a tracer of short-term sediment deposition and resuspension in the Fox River, Wisconsin. *Environmental Science & Technology*, 35(2): 300-305.

Giosan, L. et al. (2014) Protect the world's deltas. *Nature*, 516: 31-33.

Guzmán, G. et al. (2013) Sediment tracers in water erosion studies: current approaches and challenges. *J Soils Sediments,* 13(4): 816-833.

Hawley, N. et al. (1986) The partitioning of 7beryllium in fresh water. *Geochimica et Cosmochimica Acta*, 50(6): 1127-1131.

Jankowski, K. L. et al. (2017) Vulnerability of Louisiana's coastal wetlands to present-day rates of relative sea-level rise. *Nat Commun,* 8: 14792, doi:10.1038/ncomms14792.

Keller, G. et al. (2016) River-plume sedimentation and $^{210}Pb/^{7}Be$ seabed delivery on the Mississippi River Delta Front. *Geo-Marine Letters,* 1-14.

Kim, W. et al. (2009) Is it feasible to build new land in the Mississippi River Delta? *EOS, Transactions American Geophysical Union,* 90(42): 373-374.

Kolker, A.S. et al. (2012) Depositional dynamics in a river diversion receiving basin: the case of the West Bay Mississippi River Diversion. *Estuarine, Coastal, and Shelf Science,* 106: 1-12.

Ko, J.Y. et al. (2017) Challenges in collaborative governance for coastal restoration: lessons from the Caernarvon river diversion in Louisiana. *Coastal Management*, 45(2):1-18.

Lane, R. R.. et al. (2010) Hydrologic and nutrient dynamics of a coastal bay and wetland receiving discharge from the Atchafalaya River. *Hydrobiologia*, 658(1): 55-66, doi:10.1007/s10750-010-0468-4.

Lewis, R.C. et al. (2002) Accumulation rate and mixing of shelf sediments in the Monterey Bay National Marine Sanctuary. *Marine Geology*, 181(1-3): 157-169.

Lo, E.L. et al. (2014) Experimental study of cohesive sediment consolidation and resuspension identifies approaches for coastal restoration: Lake Lery, Louisiana. *Geo-Marine Letters*, 34(6): 499-509.

Milliman, J.D. and Mead, R.H. (1983) World-wide delivery of river sediment to the oceans. *The Journal of Geology*, 91(1): 1-21.

Milliman, J.D. and Syvitski J.P.M. (1992) Geomorphic/tectonic control of sediment discharge to the ocean: the importance of small mountainous rivers. *The Journal of Geology*, 100: 525-544.

Milliman, J.D. and Farnsworth, K.L. (2011) Runoff, erosion, and delivery to the coastal ocean. *River discharge to the coastal ocean: a global synthesis.* Cambridge University Press, Cambridge, UK, pp 13-69.

Muhammed, Z. et al. (2008) Excess ^{210}Pb inventories and fluxes along the continental slop and basins of the Gulf of Papua. *Journal of Geophysical Research: Earth Surface*, 113(F1), doi: 10.1029/2006JF000676.

Neubauer, S.C. et al. (2002) Sediment deposition and accretion in a Mid-Atlantic (U.S.A.) tidal freshwater marsh. *Estuarine, Coastal, and Shelf Science,* 54: 713 -727.

Nittrouer, J.A. et al. (2012) Mitigating land loss in coastal Louisiana by controlled diversion of Mississippi River sand. *Nature Geoscience*, 5: 534-537.

Ogston, A.S. et al. (2017) Hydrodynamics and sediment dynamics in Mekong Delta distributary channels: how tidal rivers impact transfer of sediment from source to sink. *Oceanography*, 30(3): 22-33.

Olsen, C.R. et al. (1985) Atmospheric fluxes and marsh-soil inventories of ^{7}Be and ^{210}Pb. *Journal of Geophysical Research*, 90(D6): 10487-10495.

Perez, B.C. et al. (2000) Influence of Atchafalaya River discharge and winter frontal passage on suspended sediment concentration and flux in Fourleague Bay, Louisiana. *Estuarine, Coastal and Shelf Science,* 50: 271-290.

Peyronnin, N.S. et al. (2012) Louisiana's 2012 Coastal Master Plan: Overview of a science-based and publicly informed decision-making process. *Journal of Coastal Research,* 67(sp1): 1-15.

Roberts H.H., et al. (2003) An embryonic major delta lobe: a new generation of delta studies in the Atchafalaya-Wax Lake delta system. *Trans Gulf Coast Assoc Geol Soc*, 53: 690–703.

Roberts, H.H. et al. (2015) Floods and cold front passages: Impacts on coastal marshes in a river diversion setting (Wax Lake delta area, Louisiana). *Journal of Coastal Research,* 37(5): 1057-1068.

Rotondo, K.A., and Bentley, S.J. (2003) Deposition and resuspension of fluid muds on the western Louisiana inner continental shelf. *Gulf Coast Association of Geological Societies Transactions,* 53: 722-731.

Smith, J.E. et al. (2015) What role do hurricanes play in sediment delivery to subsiding river deltas? *Scientific Reports,* 5: 17582.

Syvitski, J.P.M. et al. (2009) Sinking deltas due to human activities. *Nature Geoscience,* 2: 681-686.

Twilley, R.R. et al. (2016) Co-evolution of wetland landscapes, flooding, and human settlement in the Mississippi River Delta Plain. *Sustain Sci.,* 11: 711-731.

U.S. Geological Survey (2017) The National Map, 2017, 3DEP products and services: The National Map, 3D Elevation Program Web page, at http://ned.usgs.gov. Accessed 19 Feb 2018.

Walling, D. E. (2012) Beryllium-7: The Cinderella of fallout radionuclide sediment tracers?, *Hydrol. Process.*, 27(6), 830-844.

Walsh, J.P. et al. (2004) Clinoform mechanics in the Gulf of Papua, New Guinea. *Continental Shelf Research,* 24(19): 2487-2510.

Wang, J. et al. (2018) The coupling of bay hydrodynamics to sediment transport and micro-tidal wetland stability under high rates of relative sea level rise. *Marine Geology,* 405: 68-76.

Xu, K. et al. (2016) Implications of texture and erodibility for sediment retention in receiving basins of coastal Louisiana diversions. *Water*, 8(1): 26.

CHAPTER 3. CONTRASTING RECENT SEDIMENTATION RATES AND CHARACTERISTICS BETWEEN FLUVIALLY NOURISHED VERSUS SELF-SUSTAINING DISTAL COASTAL MARSHES IN SOUTHEASTERN LOUISIANA, USA.

3.1. Introduction

Land loss trends along southeastern coastal Louisiana, USA, merit investigation into processes and rates of sedimentation in distal wetlands, which are the areas most susceptible to destruction. Recent studies on sea level rise and vertical accretion in the region rely on Coastwide Reference Monitoring System (CRMS) data, which are valid but chronologically constrained to the past ~10 - 20 years. This study uses ^{137}Cs and ^{210}Pb radioisotopes to contrast rates of sediment accumulation over the past century in Fourleague Bay, an area receiving fresh sediment from the Atchafalaya River, and Terrebonne Bay, an area with limited, regionally recycled sediment supply. Accumulation rates are then compared with local rates of relative sea level rise (RSLR). Both areas are susceptible to the same storm and cold front passages, as well as flooding; the key difference is amount and type of sediment supplied. With this study, we hope to illustrate long term (up to 100 years) response in these two distinct regions with starkly differing patterns of sediment delivery.

The opening to Fourleague Bay is located ~12.5 km southeast of the Atchafalaya River mouth (Fig. 3.1). Here, the rate of land loss is minimal compared to the rest of Louisiana's southeastern coast (Day et al., 2000; Twilley et al., 2016), thus standing out in its relative stability. The stability is due in large part to the sediment load carried by the Atchafalaya River, which has not been as substantially engineered as the Mississippi River. The almost "natural" flow of the Atchafalaya from the Old River Control Structure onward allows for a substantial amount of sediment to reach the coast. As a result, a new subaerial delta has emerged at the river mouth. Unlike the Mississippi Delta, which has suffered a precipitous decline over the past century, the area around the Atchafalaya outlet is thriving (Twilley et al., 2016). Thus, the Atchafalaya River

can be used as a natural analog for large scale river and sediment diversion projects being designed to sustain or grow the Louisiana coast.

There exists a large disparity in the rate and extent of coastal marsh retreat between Fourleague Bay and Terrebonne Bay, which is located approximately 50 km to the east (Twilley et al., 2016; Fig. 3.1). The topic of land loss within Terrebonne Bay is discussed in depth through various studies (Reed, 1995; Day et al., 2000; Barras et al., 2004), and is recognized as a catastrophic decline over the past century. Bayou Lafourche, the last major Mississippi River distributary to the area, and therefore last major source of fresh fluvial sediment, was cut off in 1905 (Reuss, 2004). Without and input of fresh mineral sediment to nourish the marshes, the subaerial portions of Terrebonne cannot withstand the deteriorative effects of subsidence, wave action, and sea level rise.

These two almost antipodal bays serve as field areas for this study contrasting recent sedimentation patterns. This study will compare and contrast isotopic, grain size, density, and loss-on-ignition profiles of shallow push cores from both Fourleague Bay and Terrebonne Bay to answer three questions: 1) How does sediment accretion on the marsh platform differ between an area with an active fluvial connection versus an area with only recycled bay floor and cannibalized marsh platform sediment? 2) At what rates are these distal marshes accreting? 3) How long can they outpace the effects of relative sea level rise?

3.2. Field Areas: History and Description

The Atchafalaya/Wax Lake Delta first emerged during the 1970s. A high flood event during 1973 maximized discharge from the Atchafalaya outlet, reaching levels that were double the average flow during standard flood events. The magnitude of discharge scoured sand stored within the river's channel and moved it down the Atchafalaya's natural outlet and man-made Wax

Lake Outlet to the west. The result is two growing subaerial deltas (Roberts, 1997; Roberts et al., 2003).

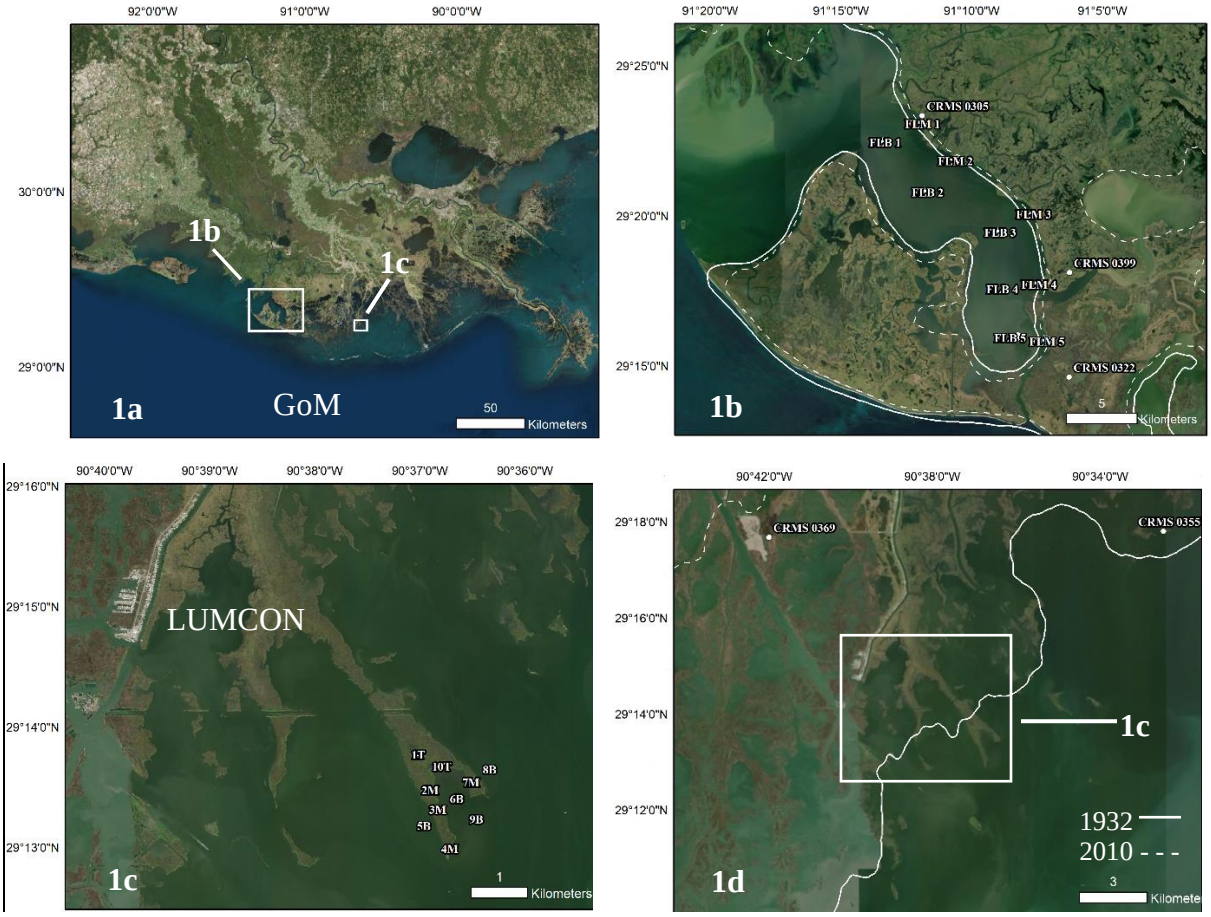

Figure 3.1. (a): Field areas in relation to the Louisiana coast and the Gulf of Mexico (GoM). (b): Fourleague Bay with the 10 coring sites, nearby Coastwide Reference Monitoring System (CRMS) sites, and 1932 and 2010 50% land to water ratio isopleths (Twilley et al., 2016). (c): The Terrebonne Crab Claw with coring sites and the Louisiana University Marine Consortium (LUMCON). (d): The Terrebonne Crab Claw with nearby CRMS and the 50% land to water isopleths from (b).

With the flood event pulsing approximately 20,000 $m^3 s^{-1}$ of water through the Atchafalaya River, an equally exceptional amount of sediment came with it (Roberts et al., 2003). Simultaneously, the force of the flow scoured the channel of the lower Atchafalaya River to 4 - 5 m below average depth. Roberts et al. (1980) indicate that the growth of the lobes within Atchafalaya Bay, and likely Wax Lake Outlet, is correlated to this scouring, which transferred

stored channel sediment (fine sand and coarse silt) downriver to the bays. This hypothesis is supported through sediment size comparisons, as the grains building the deltas are composed primarily of fine sand and silt (Keown et al., 1986).

Neighboring the Atchafalaya Delta ~8 km to the southeast is Fourleague Bay. Fourleague Bay spans approximately 23 km from its opening in the north to its outlet into the Gulf of Mexico, Oyster Bayou, a narrow tidal channel in the south. The shallow, semi-enclosed bay averages ~1 m in depth, deepening up to 5 m at its northern opening and Oyster Bayou (Restreppo et al., 2019). The bay is surrounded by seasonally inundated, perennially vegetated marshes. Flooding of the marsh platform tends to occur during maximum, seasonal river discharge, river flood events, and/or the passage of strong atmospheric fronts through the area (Wang et al., 2018; Restreppo et al., 2019). Less than 5% of the Atchafalaya's total discharge moves through Fourleague Bay (Lane et al., 2010). Even so, the area has maintained a stable marsh platform for the past century (Day et al., 2000; Twilley et al., 2016; Jankowski et al., 2017).

If the Atchafalaya Delta and Fourleague Bay represent the stable end of Roberts' (1997) deltaic spectrum, i.e. a growing and/or sustained subaerial land mass, Terrebonne Bay falls well into the declining phase. Terrebonne's foundation is composed of the Teche Delta Complex, formed between 5.5 – 3.5 kya and then reoccupied by the Lafourche Delta Complex, between 2.5 - 0.5 kya (Morgan, 1979; Wang et al., 1993; Blum and Roberts, 2012). When the Mississippi's distributary and Terrebonne Bay's last active channel, Bayou Lafourche, was dammed and sediment supply was cut off at Donaldsonville, approximately 105 km northwest of our field area (Morgan, 1979; Reuss, 2004). As commonly seen along Louisiana's coast, damming of the bayou led to a massive reduction in sediment delivery to the wetlands, in effect allowing the rate of erosion and subsidence to greatly outpace any land growth or sustainment.

The Terrebonne field area is located 55 km east of Fourleague Bay, and 5 km southeast of the Louisiana Universities Marine Consortium (LUMCON), in Cocodrie, Louisiana. The study area is smaller than that of Fourleague Bay, spanning a micro-bay feature dubbed the "Crab Claw" based on its shape. The Crab Claw encompasses a ~4 km^2 area with two "legs," one in the east and one in the west, as well as a tidal flat located at its apex. Immediately to the east is Lake La Graisse, to the west is Bay Chaland, and to the south is Bay Lost Reef. The marsh platform is perennially vegetated salt marsh, excluding the tidal flat which was never observed to be vegetated. The depth of the bay within the two legs is $\leq$ 1 m, with depths just outside the legs around 2 m, based on a survey done during this study. It is unknown when the marsh platform is inundated.

3.3. Radioisotopes

An extensive amount of research has been published on the utility of ^{210}Pb and ^{137}Cs radioisotopes as proxies for the deposition and reworking of fine organic and inorganic sediment within aqueous environments, including depositional environments within the Mississippi River Delta (Wilson and Allison, 2008; Guzmán et al., 2013; Corbett and Walsh, 2015; Smith and Bentley, 2015; Smith et al., 2015; Keller et al., 2016). ^{210}Pb ($t_{1/2}$ = 22.3 yr), part of the decay series of ^{238}U, is found naturally within the matrix of rock and sediment grains. ^{210}Pb's parent isotope, ^{222}Rn, is created by the decay of ^{226}Ra. ^{210}Pb within sediment can be divided into two categories, supported and excess: $^{210}Pb_{Supported}$ is generated within rock and sediment from its parent isotope, and so is continuously replaced; however, because ^{210}Pb's parent isotope is ^{222}Rn, an inert gas, some ^{222}Rn escapes into the atmosphere and continues to decay, generating $^{210}Pb_{Excess}$ which precipitates and then adsorbed onto the surface of sediment grains. Due to its relative immobility once adsorbed, $^{210}Pb_{Excess}$ can be a useful indicator of sedimentary processes over the past century

(Appleby and Oldfield, 1993; Corbett and Walsh, 2015). A simple equation for the calculation of total ^{210}Pb is provided by Corbett and Walsh (2015):

$$^{210}Pb_{Total} = {}^{210}Pb_{Excess} + {}^{210}Pb_{Supported} \quad (3.1)$$

^{210}Pb dating methods require certain assumptions during their calculation, and thus ^{210}Pb calculations benefit from validation by an independent approach whenever possible (Baskaran et al., 2014). Commonly, this approach is ^{137}Cs geochronology. ^{137}Cs ($t_{1/2}$ = 30.2 yr) is generated through nuclear fission of ^{235}U, and thus is directly linked to nuclear and hydrogen bomb testing. Depending on geographic location, two peaks can be seen through gamma spectrometry: 1963, the year when hydrogen bomb testing reached maximum levels in the northern hemisphere; and 1986, the year Chernobyl had a meltdown. The onset of activity is dated at 1954, when testing began (UNSCEAR, 2000; Corbett and Walsh, 2015). The location of field area used for this study limits activity to the 1954 onset and 1963 peak. If a peak in ^{137}Cs activity can be identified within a core, that specific depth interval can be assigned a date of 1963, giving the researcher an average amount of accretion since 1963. If no clear peak is visible, but isotope activity drops to zero, that interval can be assigned the year 1954. While not the highest resolution, ^{137}Cs dating certainly provides insight into total deposition over the last 50+ years. Additionally, the lack of any ^{137}Cs activity within a core may signify a very active environment.

3.4. Methodology

Push cores up to 0.5 m in depth were collected from ten sites in Fourleague Bay during April 2015. Of these ten cores, five were pulled from a transect along the middle bay bottom, labeled FLB, and five were taken from the vegetated marsh platform along the eastern edge of the bay, labeled FLM, located about 50 m inland (Fig. 3.1). During April 2017, ten push cores were also taken from Terrebonne Bay; these cores include four from the vegetated marsh platform

(designated TER #M), four from the bay bottom (designated TER #B), and two from the unvegetated tidal flat and intertidal zone (designated TER #T) (Fig. 3.1). Regardless of where they were sourced, all cores were sealed and taken back to Louisiana State University, Baton Rouge, and placed into cold storage until they were extruded at 2 cm intervals. The extruded slices were then weighed, dried in a 60° C oven for at least 24 hours, homogenized using a mortar and pestle, and placed into sealed petri dishes.

The sealed samples were allowed to equilibrate for at least 15 days, and then placed into Canberra germanium gamma detectors for 24 hours to analyze for the presence ^{137}Cs and ^{210}Pb. In the case of ^{210}Pb, 100 second transmissions were also run using a radioactive source in order to correct $^{210}Pb_{supported}$ values (Cutshall et al., 1983; Cable et al., 2001).

Calculation of vertical accretion rate (VAR) using ^{137}Cs data is straightforward. A large ^{137}Cs activity peak is seen at depth z (cm) with decreasing activity both above and below marks the 1963 horizon, during which global hydrogen bomb testing was at its maximum (Eq. 3.2). If no such peak is seen downcore, then the depth at which ^{137}Cs activity is first detected can be used instead, substituting 1953, the year testing began, for 1963 (Eq. 3.3). Vertical accretion rate (VAR; cm yr^{-1}) is calculated by:

$$z/(t_{current} - 1963) \quad (3.2)$$

$$z/(t_{current} - 1953) \quad (3.3)$$

Similar to ^{137}Cs, which provides a bulk estimate for accretion since 1953 or 1963, ^{210}Pb analysis can provide the researcher with a constant rate of sedimentation. Three models for this calculation are provided in Corbett and Walsh (2015); the constant flux-sedimentation (CFCS), or "simple" model; the constant rate of supply (CRS) model; and the constant initial concentration (CIC) model. Only one model, CFCS, was found to be appropriate for this study.

The CFCS model assumes a constant accumulation rate, constant flux of $^{210}Pb_{Excess}$, and a resulting constant initial activity upon deposition using the equation (Corbett and Walsh, 2015):

$$A_z = A_0\, e^{-\lambda(z/S)} \quad (3.4)$$

Where:

A_z = $^{210}Pb_{Excess}$ activity at depth z (dpm g^{-1})

A_0 = initial $^{210}Pb_{Excess}$ activity at deposition

λ = decay constant for Pb^{210}, 0.031 (yr^{-1})

S = VAR (cm yr^{-1})

Two variations of this model were used to calculate VAR. The first is a Sigmaplot© least-squares regression for Eq. 3.4 (Smith and Bentley, 2015; Keller et al., 2016). This method worked best in cores with a more unsteady ^{210}Pb profile. The second method involves dividing λ by the regression of the natural log of activity vs. depth (Nittrouer and Sternberg, 1981; Wilson and Allison, 2008). This method worked best with more steady state ^{210}Pb profiles, but also generated a larger error value. The value closest to the rate of sedimentation calculated from ^{137}Cs was selected for each site. For sites in which no ^{137}Cs VAR could be obtained, the smallest value was selected to err on the side of caution.

Regardless of which variation of the CFCS model was used, if dry bulk density is known, one can then calculate the mass accumulation rate (MAR; g cm^{-2} y^{-1}), which will vary through time:

$$MAR = \rho_{db} * S \quad (3.5)$$

Where*:*

ρ_{db} = dry bulk density (g cm^{-3})

One benefit to using the CFCS method is that it does not need inventory calculations and works with simple activity measured at dpm g^{-1}. While the CFCS model does make several assumptions about initial conditions and constant rates of accumulation and activity, it proves to be dependable when paired with ^{137}Cs data for comparison and validation.

All isotopic profiles are evaluated for grain size effects, i.e. any extreme deviation in the profile of ^{210}Pb, if paired with an abrupt change in grain size, was not used in the overall calculation of VAR or MAR. Both radioisotopes, ^{210}Pb and ^{137}Cs, do not readily sorb onto coarse grains. These pockets of coarser material within the core may be the results of storms, which may winnow finer particles away while depositing coarser material, and so do not represent normal background sedimentation (He and Walling, 1996). Additionally, some rates were calculated based on weighted averages from separate intervals within the core. This was done specifically when the ^{210}Pb activity profile did not appear steady state, i.e. these profiles displayed "stair stepping" downcore (Bentley et al., 2002). Such deviations could be the product of bioturbation and/or changes in sedimentation and are addressed later.

Grain size analysis was done using a Beckman Coulter LS 13 320 Laser Diffraction Particle Size Analyzer. Samples were taken from the same 2 cm intervals that were analyzed for isotope activity, processed with hydrogen peroxide to oxidize organics, and then run through the analyzer in a 0.05% sodium phosphate solution to prevent flocculation of fine particles. Grain density measurements were done using a Quantachrome helium pycnometer, again using the same 2 cm intervals.

Finally, loss-on-ignition (LOI) testing was done on these intervals to determine organic and mineral-mass percentages. For LOI, a small sample is weighed, dried in an oven at 105^{o} C to remove water content, weighed again, and is then heated to 550^{o} C in a muffle furnace to incinerate

all organic matter (Heiri et al., 2001). The remaining material is also weighed. The differences in weight at all three stages produce a percentage of water content, organic sediment, and mineral sediment, respectively. With organic and mineral percentage known, sediment-type-specific MAR can be calculated by multiplying MAR by percent organic sediment and percent mineral sediment. The ratio of organic mass accumulation rate (OMAR) to mineral mass accumulation rate (MMAR) provides a dimensionless ratio with which to compare and contrast different sites and field areas.

3.5. Results: Fourleague Bay

3.5.1. Grain Size and LOI

Mean grain sizes for all cores generally fall into the clay and silt categories, with occasional packets of coarse silt to fine sand. Overall, marsh cores tend to trend finer as one moves farther south, while bay cores trend flat throughout the bay (Fig. 3.2). Two of the five marsh cores, FLM 1 and FLM 2, contained coarse silt to fine sand intervals in which the ^{210}Pb profile deviated in a negative fashion before rebounding to their original pattern. In FLM 1, this occurs from approximately 28 - 34 cm in depth, while in FLM 2, it occurs from approximately 18 - 28 cm. LOI data from these same intervals contain a decrease in organic content as well (Fig. 3.3). Both FLM 3 and FLM 5 also contain a coarse silt to fine sand packet, with the interval in FLM 3 also containing a drop in organic percentage. However, these cores do not display the ^{210}Pb profile deviation. All core data can be found in Appendix A.

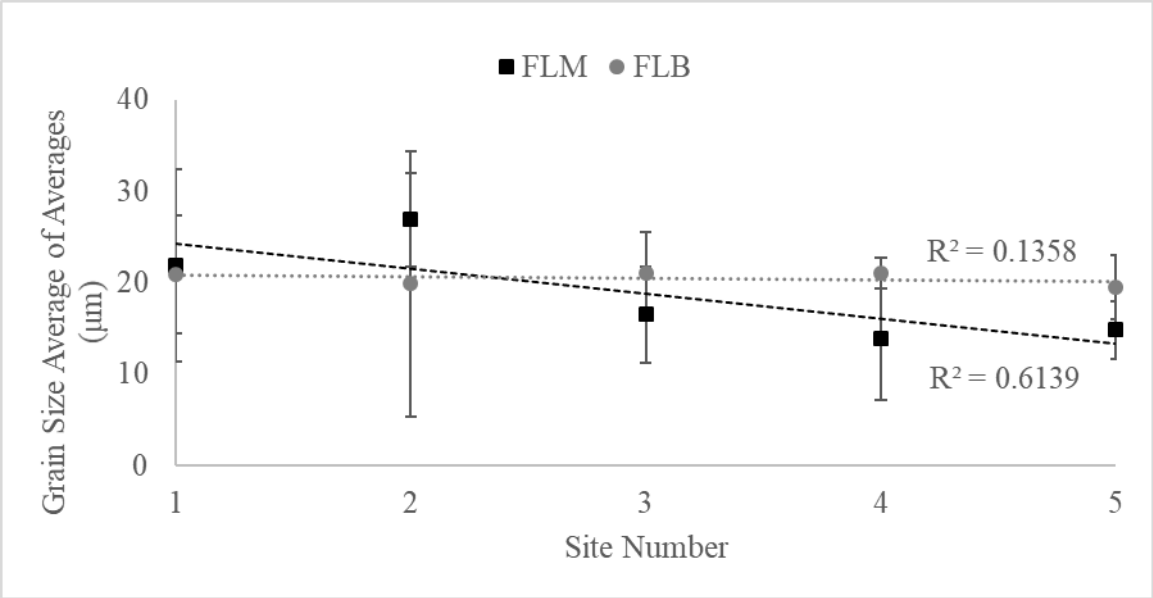

Figure 3.2. Grain size trends in marsh (FLM) and bay (FLB) cores through Fourleague Bay, as one moves from the northern opening to the south.

Mean grain size in bay cores is slightly coarser, with a higher amount of coarse silt and fine sand throughout. The grain size paired ^{210}Pb profile deviations are not readily obvious in these cores, aside from perhaps the bottom 12 cm of core FLB 3 and the top 8 cm of FLB 4. The authors are reluctant to assign these packets to storms, however, as grain size values do not differ significantly from the rest of the core.

Average dry mass organic content in marsh cores varied downcore, with organic content higher at the top and decreasing downcore or within storm intervals. Average dry mass organic content across all marsh cores is 16%, with individual organic content per 2 cm interval ranging from 2 – 35%. Not surprisingly, dry mass organic content in bay cores is significantly lower than that of the vegetated marsh cores, at an average value of 4.4%. Unlike marsh cores, organic content in bay cores tends to remain stable downcore.

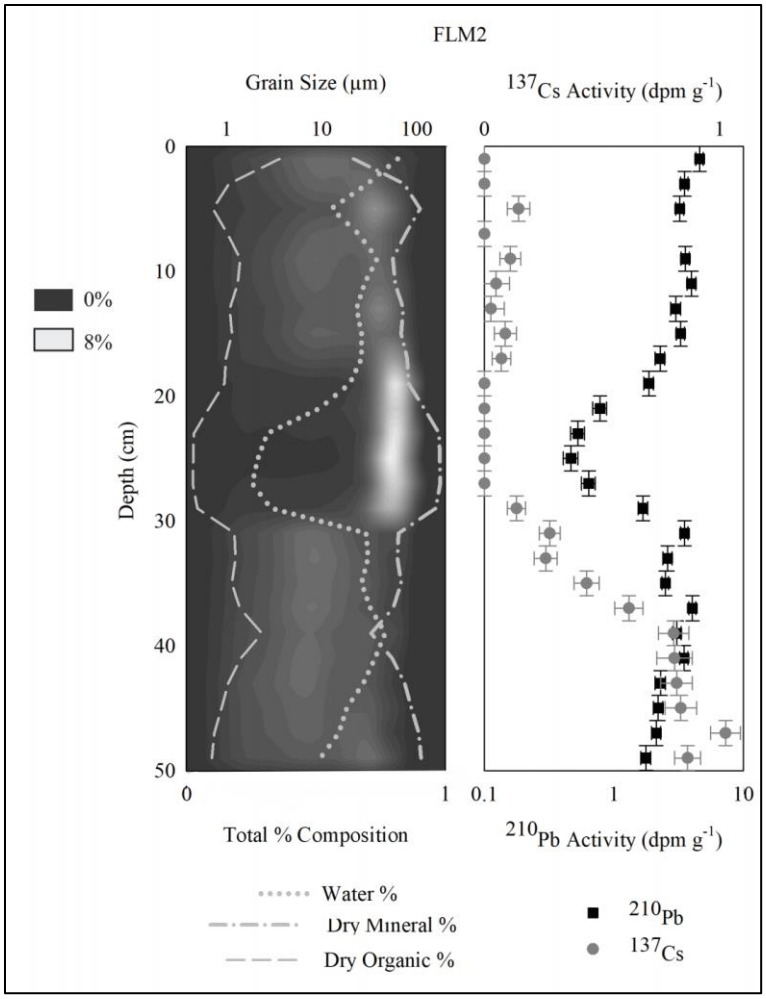

Figure 3.3. Grain size frequency & LOI data (left), ^{137}Cs & ^{210}Pb profiles (right) for core FLM 2. Note the deviation in both isotopes at approximately 20-30 cm, with an increase in grain size frequency and mineral percentage.

3.5.2. Marsh Rates

All stated ranges are the minimum and maximum across all cores for VAR, and per interval across all cores for MAR. Errors are calculated via root sum of squares method and propagated when necessary. Table 3.1 contains all rate data for Fourleague Bay. The five marsh sites yield ^{210}Pb VARs between 0.67 ± 0.40 cm yr^{-1} at FLM 5 in the far south to 1.45 ± 0.33 cm yr^{-1} at FLM 1 near the bay opening, with an average vertical accretion rate of 1.11 ± 0.79 cm yr^{-1}. Site FLM 1 contains no clear ^{137}Cs peak nor did activity fall to zero, and so only a minimum ^{137}Cs based VAR could be calculated, at 0.61 cm yr^{-1}. When checked against ^{137}Cs calculated rates, the ^{137}Cs/^{210}Pb

ratio for four of the five marsh sites falls between 0.64 to 1.02, where 1 is equality. Site FLM 4 contains the largest discrepancy between the two radioisotopes, and site FLM 3 contained the smallest. It should be noted that the methods used to calculate average VAR from ^{210}Pb data incorporate different time scales depending on the core; for example, deeper cores are expected to extend further back in time. As such, rates could differ over particular time scales and sections of a core. Average ^{137}Cs derived sedimentation rate across all four viable marsh cores is 0.81 cm yr^{-1}. With storm deposits removed, MARs also vary in all five cores, spanning 0.31 to 2.30 g cm^{-2} yr^{-1}. Average MAR across all four marsh cores is 0.79 ± 1.00 g cm^{-2} yr^{-1}.

3.5.3. Bay Rates

Two of the five bay cores, FLB 1 and 2, contained no detectable ^{137}Cs activity and so ^{210}Pb derived rates stand alone. ^{210}Pb calculated vertical accretion rates in all bay cores range from 0.46 ± 0.19 to 1.20 ± 1.09 cm yr^{-1}, with an average of 0.83 ± 1.06 cm yr^{-1}. ^{137}Cs VARs in viable cores range from 0.48 – 0.64 cm yr^{-1}, with an average of 0.58 cm yr^{-1}. MAR in all bay cores range from 0.46 to 1.83 g cm^{-2} yr^{-1}. Average MAR across all bay cores is 1.06 ± 0.66 g cm^{-2} yr^{-1}.

3.6. Results: Terrebonne Bay

3.6.1. Grain Size and LOI

Five of the ten cores (TER 1T, TER 2M, TER 3M, TER 7M, and TER 9B) were analyzed for grain size. LOI testing was done for all ten sites. All core data can be found in Appendix A. Grain size varies from clay to fine sand but are generally more evenly distributed through the core than their Fourleague Bay counterparts, i.e. not containing any major pockets of coarser material deviating from the rest of the core (Fig. 3.4). Marsh cores from the western leg, 2M and 3M, contain majority silt to fine sand, evenly distributed. Core 7M from the eastern leg displays two regimes, with clay and silt dominating the top 13 cm and then switching to silt and very fine sand

for the bottom half. The tidal flat core, 1M, displays an evenly distributed concentration of sediment from clay to very fine sand. Finally, the bay core, 9B, contains very fine sand almost exclusively.

Dry mass organic content in bay cores ranges from 3 – 15%, increasing with depth in several cores. Core 5B, however, is an outlier as it increases to approximately 50% organic content in its bottom four centimeters. The sediment from the bottom of this core appeared charcoal-like when dried. Cores from the tidal flat and intertidal area, 1T and 10T, are composed of 10 – 25% organic matter. Organic content in these cores decreases with depth. Finally, organic content in marsh cores ranges from 7 – 20.5% and remains stable downcore in half the cores while decreasing in the other half.

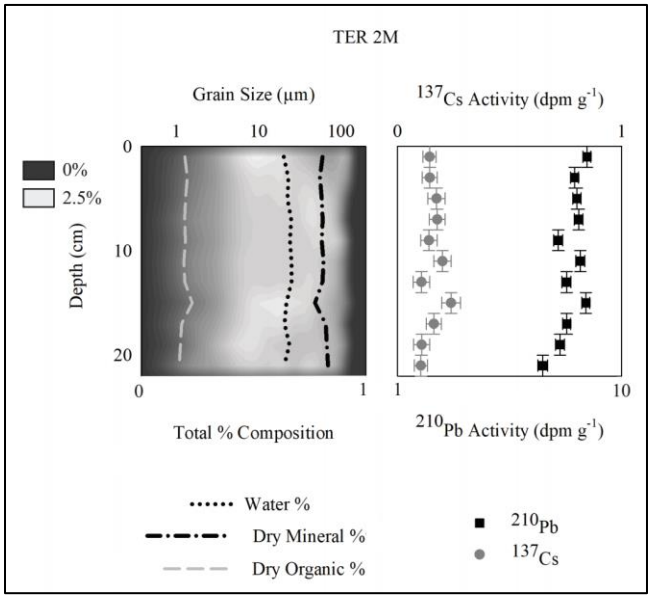

Figure 3.4. Grain size frequency & LOI data (left), ^{137}Cs & ^{210}Pb profiles (right) for core TER 2M. Note the much more even frequency distribution in grain size.

3.6.2. Marsh Rates

Table 3.2 provides all rate data for the Terrebonne Crab Claw. ^{210}Pb based VARs of the four marsh cores in Terrebonne Crab Claw are drastically smaller than those in Fourleague Bay, ranging from 0.23 ± 1.44 to 0.86 ± 0.38 cm yr^{-1}, a drop of approximately 40 – 66%. Average

^{210}Pb VAR for all marsh cores is 0.56 ± 0.88, or half of the average value in Fourleague Bay. None of the Crab Claw marsh cores contained an identifiable ^{137}Cs peak, nor did any drop to undetectable levels. As such, only minimum ^{137}Cs derived VAR values could be provided, and range from 0.33 – 0.45 cm yr^{-1}, with an average of 0.37 cm yr^{-1}. MARs vary from 0.17 to 1.01 g cm^{-2} yr^{-1}, also substantially lower than previous marsh cores. Average MAR across all four marsh cores is 0.48 ± 0.76 g cm^{-2} yr^{-1}, an almost 40% decrease.

3.6.3. Bay Rates

^{210}Pb based vertical accretion rates in all Crab Claw bay cores ranged from 0.37 ± 0.71 to 0.76 ± 0.62 cm yr^{-1}, with an average of 0.55 ± 1.06 cm yr^{-1}. These values represent a less significant drop than when comparing marsh cores, with the average bay VAR falling by 35% when compared to FLB cores. ^{137}Cs activity was present in all bay cores, with activity ceasing at a given depth in each core. ^{137}Cs based VARs were approximately one third lower than those calculated in Fourleague Bay cores, extending from 0.36 – 0.42 cm yr^{-1}, with an average value of 0.38 cm yr^{-1}. ^{137}Cs/^{210}Pb ratios (0.97 and 0.98, respectively) were substantially higher for bay bottom sites 6B and 9B, which came from between the two "legs" of the Crab Claw. Sites 5B and 8B, which came from the open, deeper waters outside each leg, contained ratios of 0.51 and 0.57, respectively. MAR in all bay bottom cores ranges from 0.19 to 1.47 g cm^{-2} yr^{-1}. Average MAR across all bay cores is 0.65 ± 1.11 g cm^{-2} yr^{-1}, which is again 40% less than the average value of bay bottom Fourleague Bay cores.

Table 3.1. Fourleague Bay VARs, MARs, and ratios.

Core	^{210}Pb*				^{137}Cs	
	VAR (cm yr^{-1})	Mineral MAR (g cm^{-2} yr^{-1})	Organic MAR (g cm^{-2} yr^{-1})	Average OMAR/MMAR	VAR (cm yr^{-1})	^{137}Cs/^{210}Pb VAR Ratio
FLB 1[1]	0.46 ± 0.19	0.43-0.84 ± 0.19	0.01-0.03 ± 0.01	0.04	-	-
FLB 2[2]	0.90 ± 0.96	0.95-1.38 ± 0.92	0.04-0.06 ± 0.05	0.04	-	-
FLB 3[1]	0.90 ± 0.20	0.72-1.71 ± 0.19	0.04-0.06 ± 0.01	0.05	0.63[a]	0.7
FLB 4[1]	0.69 ± 0.19	0.61-1.13 ± 0.18	0.03-0.05 ± 0.01	0.05	0.48[b]	0.7
FLB 5[2]	1.20 ± 1.09	1.32-2.45 ± 1.04	0.06-0.09 ± 0.05	0.06	0.64[a]	0.53
FLM 1[1]	1.45 ± 0.33	0.47-1.98 ± 0.26	0.11-0.26 ± 0.07	0.26	0.61[d]	0.42
FLM 2[2]	1.13 ± 2.90	0.26-1.20 ± 2.39	0.07-0.20 ± 0.52	0.24	0.90[c]	0.8
FLM 3[2]	0.96 ± 1.19	0.44-1.07 ± 1.04	0.07-0.14 ± 0.15	0.15	0.98[c]	1.02
FLM 4[2]	1.36 ± 2.07	0.40-1.31 ± 1.74	0.08-0.23 ± 0.33	0.19	0.87[b]	0.64
FLM 5[1]	0.67 ± 0.40	0.23-0.57 ± 0.47	0.03-0.10 ± 0.09	0.19	0.48[b]	0.72

Table 3.2. Terrebonne Crab Claw VARs, MARs, and ratios.

Core	^{210}Pb*				^{137}Cs	
	VAR (cm yr^{-1})	Mineral MAR (g cm^{-2} yr^{-1})	Organic MAR (g cm^{-2} yr^{-1})	Average OMAR/MMAR	VAR (cm yr^{-1})	^{137}Cs/^{210}Pb VAR Ratio
TER 1T[1]	2.46 ± 1.46	0.76-1.78 ± 0.30	0.20-0.33 ± 0.18	0.21	0.52[a]	0.21
TER 10T	1.75 ± 0.35	0.58-1.43 ± 0.30	0.15-0.20 ± 0.06	0.18	0.45[d]	0.26
TER 2M[2]	0.76 ± 1.53	0.41-0.49 ± 1.29	0.09-0.14 ± 0.29	0.24	0.33[d]	0.43
TER 3M[2]	0.23 ± 1.44	0.16-0.21 ± 1.30	0.02 ± 0.14	0.11	0.36[d]	1.57
TER 4M[1]	0.86 ± 0.38	0.58-0.90 ± 0.33	0.10-0.16 ± 0.06	0.16	0.45[d]	0.52
TER 7M[1]	0.40 ± 0.18	0.22-0.34 ± 0.16	0.03-0.04 ± 0.02	0.11	0.34[d]	0.85
TER 5B[2]	0.76 ± 0.62	0.08-1.43 ± 0.54	0.04-0.12 ± 0.08	0.09	0.39[a]	0.51
TER 6B[2]	0.37 ± 0.71	0.39-0.66 ± 0.67	0.02-0.03 ± 0.04	0.06	0.36[a]	0.97
TER 8B[2]	0.63 ± 1.97	0.49-0.75 ± 1.78	0.06-0.08 ± 0.19	0.1	0.36[a]	0.57
TER 9B[2]	0.43 ± 0.49	0.38-0.75 ± 0.47	0.01-0.03 ± 0.04	0.03	0.42[a]	0.98

*Normalized to grain size and with extreme outliers removed
[1]Least Squares Regression; [2]λ/regression.
^{137}Cs VAR: [a]1954, [b]1963, [c]Assumed 1963, [d]Minimum Rate (core bottom)
- No ^{137}Cs activity

3.6.4. Tidal and Intertidal Rates

Finally, VARs from the tidal flat and intertidal cores, 1T and 10T, contain the highest ^{210}Pb based VARs seen across both field sites, at 2.46 ± 1.46 and 1.75 ± 0.35 cm yr^{-1}, respectively. ^{137}Cs activity in core 1T fell to zero at the bottom interval, yielding a VAR of 0.52 cm yr^{-1}. Activity in core 10T did not fall to zero, and so only a minimum value of 0.45 cm yr^{-1} could be calculated. MARs at these two sites ranged from 0.77 to 2.00 g cm^{-2} yr^{-1}, with an average of 1.34 ± 0.47 g cm^{-2} yr^{-1}; once again, the highest rate seen across all sites.

3.7. Discussion

3.7.1. Contrasting Core Data: Riverine Influence

Fourleague Bay's size and proximity to a major river outlet allowed us to graph changes in VAR and MAR along a distance gradient from the northern opening to Oyster Bayou in the south. ^{210}Pb calculated VARs on the marsh platform decline from north to south, while the bay VARs rise (Fig. 3.5). Average MARs reflect the same pattern; marsh MARs decrease farther south, while bay MARs increase. Simultaneously, the ratio of OMAR to MMAR falls in the marshes as one moves farther south, indicating less organic accumulation. The bay ratio of OMAR to MMAR increases slightly. Hence, sites in Fourleague Bay with greater amounts of mineral sediment input appear to be associated with greater organic content, and greater overall vertical accumulation. The Terrebonne Crab Claw, which has no fresh mineral sediment input, shares similar rate and sediment characteristics with southernmost Fourleague Bay site FLM 5. Plotting OMAR/MMAR ratio vs. VAR of FLB marsh sites and Crab Claw marsh and tidal sites yields a linear trend (r^2 = 0.31) for the former and an asymptotic trend (r^2 = 0.5) for the latter (Fig. 3.6).

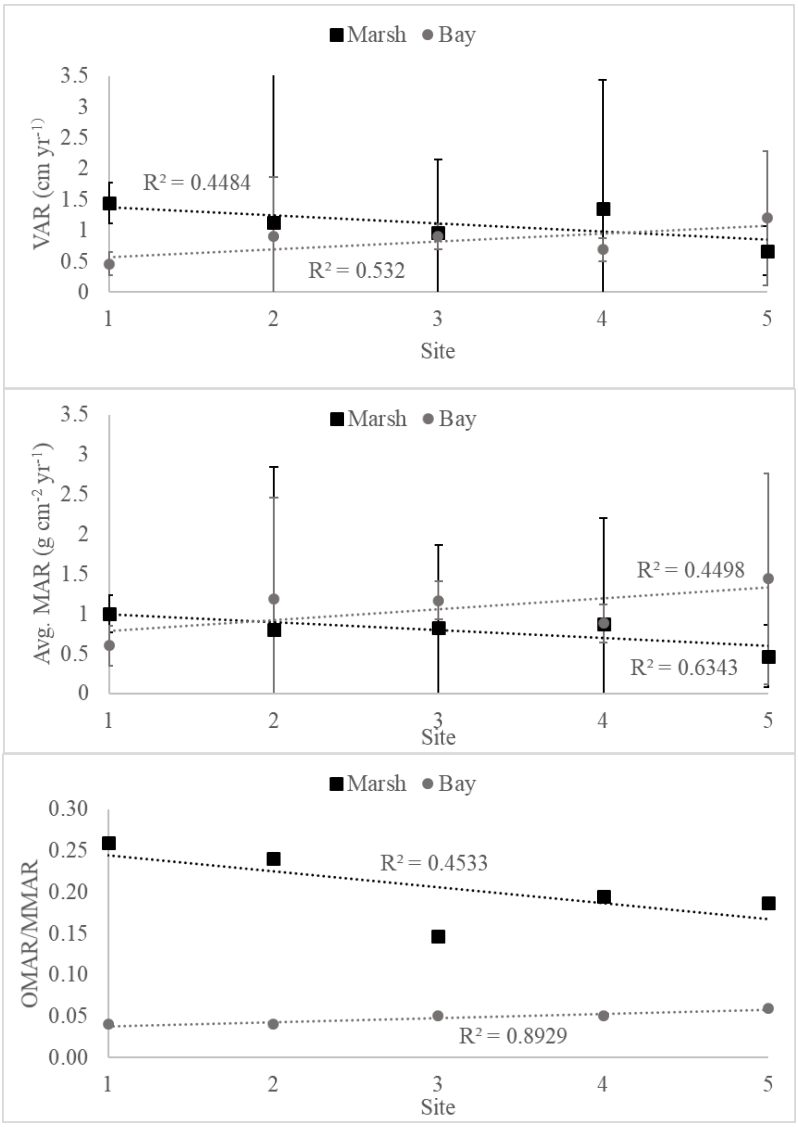

Figure 3.5. Down gradient vertical accretion (top), average mass accumulation rates (middle), and organic to mineral sediment accumulation ratios (bottom) in Fourleague Bay. Notice trends as one moves further south, from site 1 to site 5.

There exists a 40 – 66% disparity between VARs and MARs of the Fourleague Bay and the Terrebonne Crab Claw marsh platform (Fig. 3.7). If only ratios are compared, that is to say the ratio of average OMAR vs. MMAR (Fig. 3.7), a ~25% disparity exists between the two marsh platforms. However, bay bottom cores display an opposite pattern, where the Terrebonne Crab Claw bay bottom sediment contains a higher organic percentage than the FLB sediment by almost 30%. On the marsh platform, we theorize that this occurs because the heavier mineral sediment

works to anchor organic sediments in place. Without denser, fresh mineral sediment on which to adsorb, organics in the southern end of Fourleague Bay and in the Crab Claw are more likely to be eroded during tidal changes or when waves are high. While it is established that organic sediment produced from plants, etc., also works to stabilize mineral sediment in place (Whitehouse et al., 2000), this relationship may be more symbiotic than once thought.

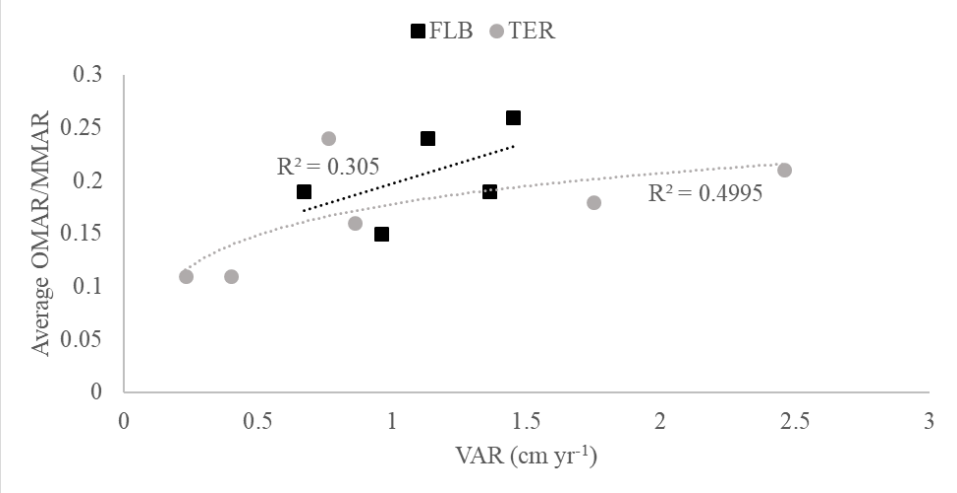

Figure 3.6. Average OMAR/MMAR ratio vs. VAR for subaerial sites. Note asymptotic trend in TER values, while trend in FLB values increases.

Keil and Mayer (2014) discuss the stabilization of organic matter by mineral sediment at the microscopic level. Organic sediment will sorb onto mineral particles, in this case clays, which then aggregate and shield the organics from oxidation and perhaps also from external forcing. For interactions between clay and organic particles, "…we can surmise that it was the aggregation effect itself that likely protected the organic matter".

Nyman et al. (1993) studied the relationship between vegetal growth, vertical accretion, and mineral sediment in Terrebonne Bay using bulk density calculations, LOI analysis at a lower temperature, and ^{137}Cs VAR calculations (notably, ^{210}Pb based calculations were not used). That study concluded that "inadequate vertical accretion resulted from inadequate organic matter accumulation." This lack of organic accumulation, Nyman et al. (1993) argue, is a product of

flooding stresses and a lack of mineral sediment accumulation. This appears to be exactly what our results display, especially when compared to the relatively stable sites in Fourleague Bay. A healthy marsh platform requires fresh mineral sediment, which provides nutrients for marsh growth and aids in the preservation of organic sediment (Keil and Mayer, 2014). When one type of sediment is deficient, it may be an indicator that the entire surface is at risk.

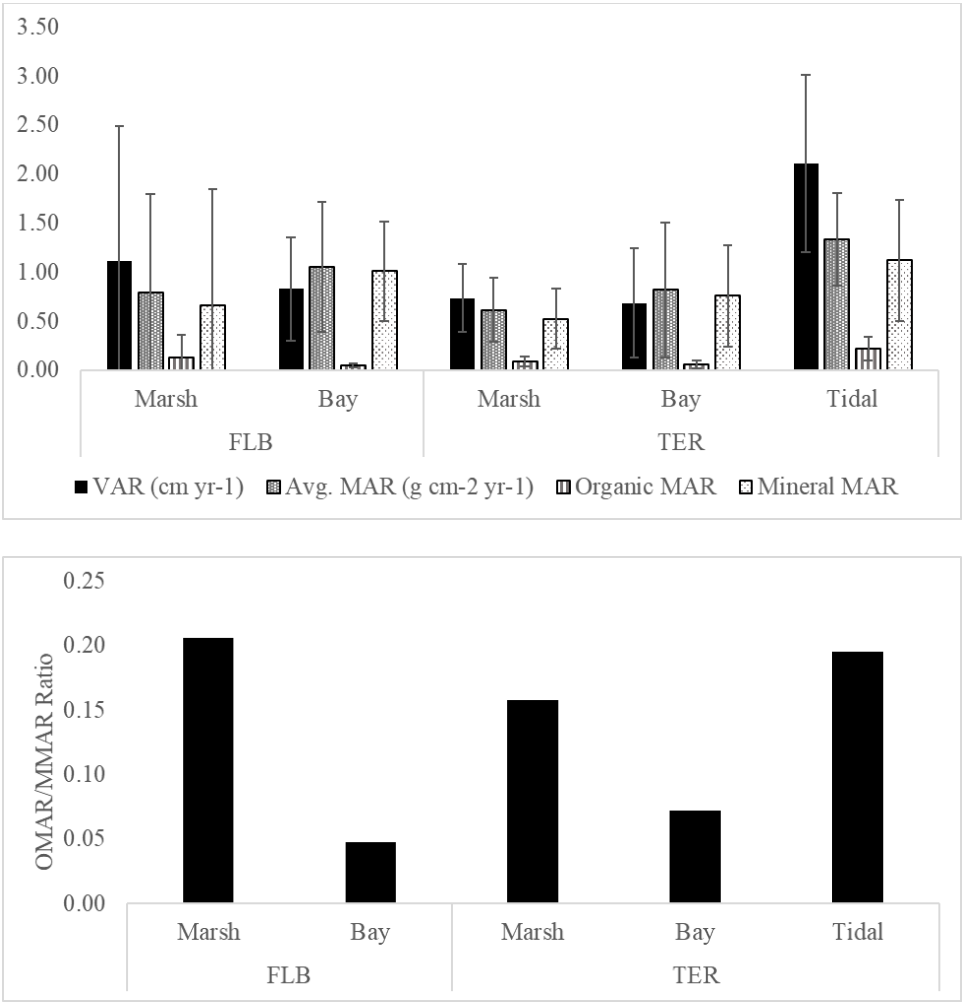

Figure 3.7. Top figure illustrates VAR, MAR, organic MAR, and mineral MAR of marsh and bay Fourleague Bay cores, and marsh, bay, and tidal flat Crab Claw Cores. Bottom figure displays organic MAR to mineral MAR ratios of each of the same areas.

The question then arises what critical amount of mineral sediment is necessary to keep the marsh platform stable. Looking once again at Tables 3.1 and 3.2, the significant difference in MMAR between both marsh platforms lies within maximum values. In Fourleague Bay, the

maximum MMAR averages 1.2 g cm^{-2} yr^{-1}. In the Crab Claw, the average is 0.49 g cm^{-2} yr^{-1}. Thus, average maximum mineral sediment input to the marsh platform in Fourleague Bay is more than double that of the Crab Claw. More data points are needed, but our study illuminates the crucial nature of regular riverine flood pulses for coastal marsh sustainment. It is established that the marshes of Fourleague Bay are regularly inundated during Atchafalaya flood events (Wang et al., 2018; Restreppo et al., 2019). Arguably, the high-end FLB values can only be achieved from input from an outside source. The Terrebonne Crab Claw is limited to the same recycled material already in place, essentially cannibalizing itself. Without a new source of mineral sediment, the Crab Claw cannot sustain itself.

3.7.2. Mass Balance: Effect of Relative Sea Level Rise in Fourleague Bay

To illustrate the actual effects of nourished versus abandoned distal coastal wetlands, it becomes necessary to incorporate relative sea level rise (RSLR) data into our VARs. The substantial difference in VAR and MAR in the two contrasting field areas becomes most evident when paired with this data. We have created a simple model to predict how long the marsh platform at a given coring site will remain above sea level. We use the current eustatic sea level rise (ESLR) rate, 2 mm yr^{-1}, which is then added to localized subsidence rates gathered from CRMS sites and calculated by Jankowski et al. (2017). VARs are also compared with average maximum value for RSLR, 13.2 mm yr^{-1} (Blum & Roberts, 2009, Jankowski et al., 2017). For elevation data, we use the USGS National Elevation Dataset (USGS NED, 2018). Each year the model is run increases ESLR by 2 mm, compounding over time. Thus, for the current year, ESLR generates 2 mm of space, which increases to 4 mm the following year, then 6 mm, and so on. This is a simple addition/subtraction model in which RSLR generates accommodation space (AS), increasing annually, while VAR for a given site fills that space, also at an annual rate:

$$Elevation_{resultant} = Elevation_{original} + Total\ Sediment\ Supply - Accommodation\ Space \quad (3.5)$$

Where, for current year 1:

$$Sediment\ Supply = VAR\ (cm\ yr^{-1}) \quad (3.6)$$

$$AS_{total} = RSLR = Subsidence\ (cm\ yr^{-1}) + ESLR\ (cm\ yr^{-1}) \quad (3.7)$$

For year n:

$$Total\ Sediment\ Supply = VAR*2 \quad (3.8)$$

$$AS_{total} = (Subsidence + (ESLR*n)) + AS_{Prior\ Year} \quad (3.9)$$

The model runs until elevation of a coring site falls below zero.

Three of our Fourleague Bay coring sites, FLM 1, 4, and 5, had neighboring CRMS sites: CRMS 0305, 0322, and 0399 (Fig. 3.1). These sites allowed our model to use rates of localized subsidence for a more accurate measure of RSLR. CRMS0305 is situated near site FLM 1 and so can also be used to check our VAR calculation for FLM 1 independently. Short-term accretion data at CRMS0305 is 1.36 cm yr^{-1}, with an RMS error of 3.34, and an RSLR rate of 1.19 cm yr^{-1} (Jankowski et al., 2017). Our long-term VAR for FLM 1 is 1.45 cm yr^{-1}, very close to Jankowski et al.'s (2017) value. Our model predicts relative stability of FLM 1 until about 2020, when the increase in eustatic sea level begins to take its toll. Using localized RSLR values, the model predicts this site to be at sea level in the year 2040 ± 2 years. If we use the RSLR average maximum, FLM 1 subsides by 2039 (Fig. 3.8).

Sites FLM 4 and 5 have their CRMS stations, 0355 and 0369, somewhat farther away and so we do not compare our VAR rate with theirs. However, the subsidence rates for these sites may still be valid. Using these localized subsidence rates, our model predicts FLM 4 to reach sea level by 2041, and FLM 5 by 2035. Using the average maximum RSLR value extends FLM 4's viability two years, to 2043, but FLM 5 deteriorates faster and is lost by 2035 (Fig. 3.8).

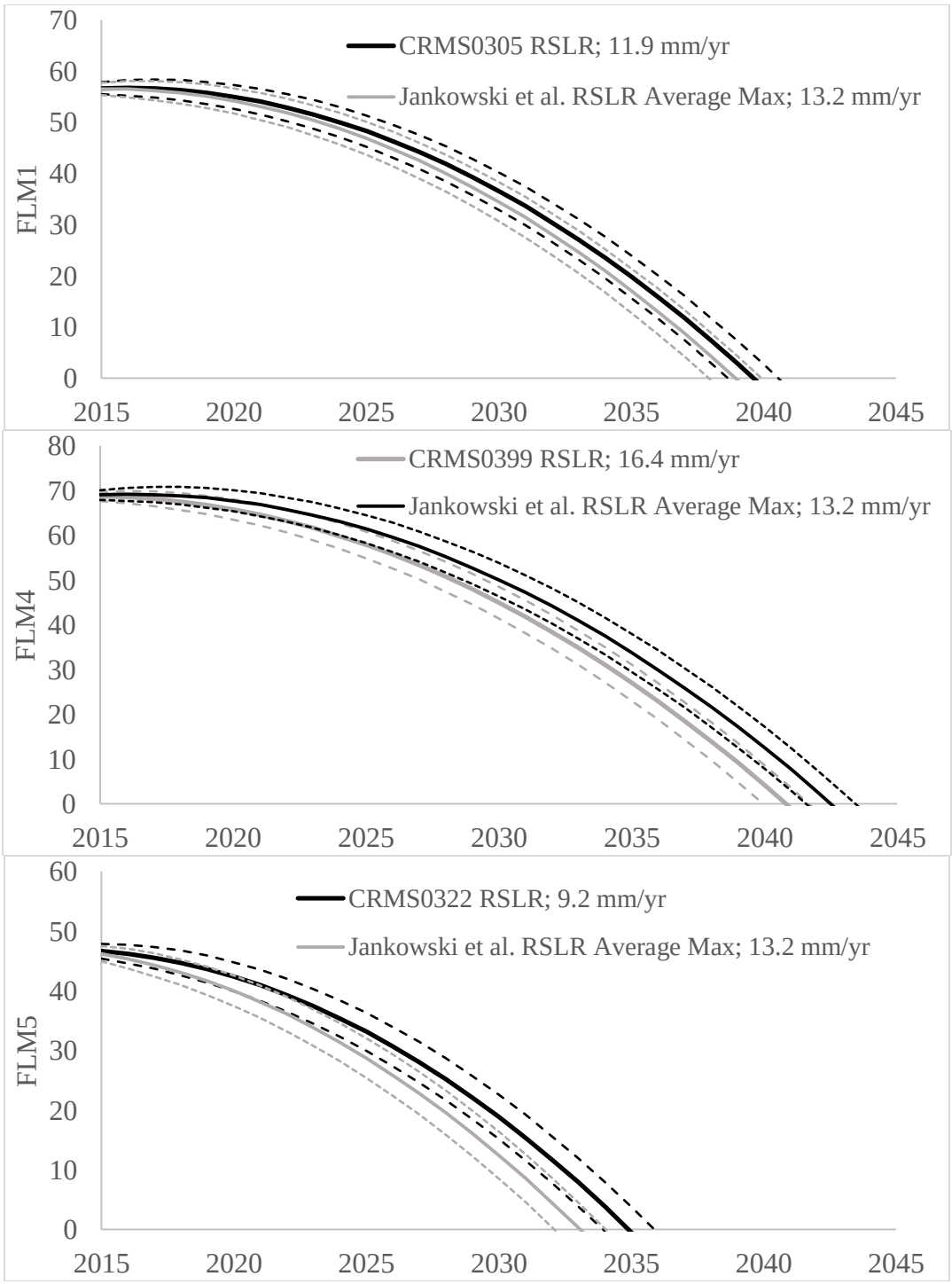

Figure 3.8. Projected elevation model (in cm) for three Fourleague Bay marsh platform coring locations, based on our calculated VAR and RSLR (calculated by Jankowski et al., 2017) of nearby CRMS stations. Top: FLM1; middle: FLM4; bottom: FLM5.

3.7.3. Mass Balance: Effect of Relative Sea Level Rise in the Terrebonne Crab Claw

The Terrebonne Crab Claw a smaller field area than Fourleague Bay and is not under the influence of any major river distributaries. Thus, there is no proper way to determine regional gradient trends as we did in FLB. Instead, we use Crab Claw marsh data and average it, producing an average VAR of 0.74 ± 0.62 cm yr^{-1}. We use two CRMS sites for the Crab Claw RSLR model, 0355 and 0369, located to the northeast and northwest, respectively (Fig. 3.1). These two CRMS sites have drastically different RSLR rates, at 2.02 and 1.11 cm yr^{-1}, respectively. When modelled along with average maximum RSLR, the Crab Claw reaches sea level between 2031 and 2034, ± 2 years (Fig. 3.9).

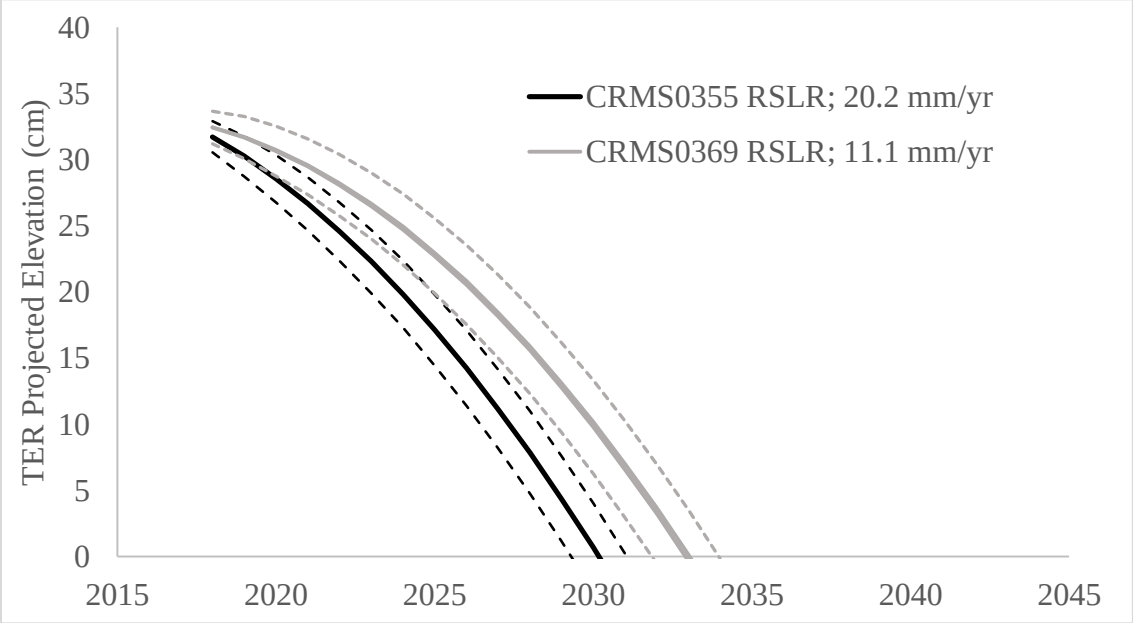

Figure 3.9. Projected elevation model for the Terrebonne Crab Claw as a whole. Average maximum RSLR was not included, as it mirrored the model for CRMS0369. Compare to Fig. 3.8.

These results are, of course, somewhat simplistic as they ignore any changes in RSLR, sediment supply, and the effects of marsh edge erosion, which are likely a nonlinear, accelerating function of wave power in a bay with ever increasing area. Recent estimates within Terrebonne Bay place the rate of landward migration at 218 m yr^{-1} (Twilley et al., 2016). However, they are

in line with prior studies, which indicate marsh edge loss in parts of our field areas by 2050 (Barras et al., 2004; Day et al., 2005), and should induce a sense of urgency. The best-case scenario, assuming no increase in eustatic sea level rise or subsidence rates, is areas of the marsh platform in Fourleague Bay not subsiding beneath sea level until ~2045. The Terrebonne Crab Claw's future is direr, with large portions of this feature sinking by ~2035. When compared to trends in 50% land to water isopleths from Twilley et al. (2016), the fragile nature of these landforms becomes especially evident (Fig. 3.1). While Fourleague Bay's marsh edge retreat is significantly less than that seen in Terrebonne Bay, both field areas have seen erosion since between 1932 and 2010. This trend will continue.

3.8. Conclusion

In summary and to answer the three questions posed in the Introduction, when the primary mechanism of marsh sustainment shifts from fresh mineral sediment input to the recycling of local sediment, fundamental changes occur in several measurable sediment characteristics. This is most clearly visible when comparing VAR and MAR through time, as well as the ratio of organic to mineral sediment MARs. In this study, rates between a fluvially connected distal marsh platform and a disconnected platform differed between 40 – 60%, with the disconnected marsh containing the lowest rates. Organic to mineral sediment ratios differed as much as 30%, with marshes in the Crab Claw containing a lower organic mass accumulation rate. The bay bottom cores displayed an opposite relationship; FLB cores contained a lower OMAR than those in the Crab Claw.

Our accommodation space model paints a grim picture of sustainability in both coastal areas. The equation is uncomplicated, and so only one factor need change to delay or reverse deterioration of the marsh platform: either eustatic sea level rise is slowed and reversed, which is

not likely, or sediment input in drastically increased, which is feasible. However, action must be taken promptly as time is indeed running out.

3.9. References

Appleby, P.G. and Oldfield, F. (1993) Application of lead-210 to sedimentation studies. In *Uranium-Series Disequilibrium: applications to Earth, Marine and Environmental Science 2nd Edition.* Ivanovich, M. and Harmon, R.S. Eds. pp. 731-783. United Kingdom: Clarendon Press.

Barras, J. et al. (2004) Historical and projected coastal Louisiana land changes: 1978-2050. USGS open file report 2003-334. https://doi.org/10.3133/ofr03334

Baskaran, M. et al. (2014) Problems with the dating of sediment core using excess ^{210}Pb in a freshwater system impacted by large scale watershed changes. *Journal of Environmental Radioactivity*, 138: 355-363.

Bentley, S.J. et al. (2002) The origin and preservation of a major hurricane event bed in the northern Gulf of Mexico: Hurricane Camille, 1969. *Marine Geology*, 186: 423-446.

Blum, M.D., and H.H. Roberts. (2009). Drowning of the Mississippi Delta due to insufficient sediment supply and global sea-level rise. *Nature Geoscience* 2(7): 488–491.

Blum, M.D. and Roberts, H.H. (2012) The Mississippi Delta region: past, present, and future. *Annu. Rev. Earth Planet. Sci.*, 40: 655-683.

Cable, J. et al. (2001) Empirical assessment of gamma ray self-absorption in environmental analyses. *Radioactivity and Radiochemistry,* 12: 30-39.

Corbett, D.R. and Walsh, J.P. (2015) ^{210}Lead and ^{137}Cesium: establishing a chronology for the last century. In *Handbook of Sea-Level Research, First Edition.* Shennan, I., Long, A.J., and Horton, B.P. Eds. Pp. 361-372. John Wiley & Sons, Ltd.

Cutshall, N.H. et al. (1983) Direct analysis of ^{210}Pb in sediment samples: self-adsorption corrections. *Nuclear Instruments and Methods,* 206: 309-312.

Day, J. W. et al. (2000) Pattern and process of land loss in the Mississippi Delta: A spatial and temporal analysis of wetland habitat change. *Estuaries,* 23: 425-438.

Day, J.W. et al. (2005) Implications of global climatic change and energy cost and availability for the restoration of the Mississippi Delta. *Ecological Engineering*, 24(4): 253-265.

Guzman, G. et al. (2013) Sediment tracers in water erosion studies: current approaches and challenges. *J. Soils Sediments*, 13: 816-833.

He, Q. and Walling, D.E. (1996) Interpreting particle size effects in the adsorption of ^{137}Cs and unsupported ^{210}Pb by mineral soils and sediments. *J. Environ. Radioactivity*, 30(2): 117-137.

Heiri, O. et al. (2001) Loss on ignition as a method for estimating organic and carbonate content in sediments: reproducibility and comparability of results. *Journal of Paleolimnology*, 25: 101-110.

Jankowski, K.L. et al. (2017) Vulnerability of Louisiana's coastal wetlands to present-day rates of relative sea-level rise. *Nature Communications* 8: 14792.

Keil, R.G. and Mayer, L.M. (2014) 12.12 - Mineral Matrices and Organic Matter. Eds. Holland, H.D. and Turekian, K.K. *Treatise on Geochemistry (Second Edition*): 337-359. Elsevier.

Keller, G., et al. (2016). River-plume sedimentation and $^{210}Pb/^{7}Be$ seabed delivery on the Mississippi River Delta front. *Geo-Marine Letters*: 1–14.

Keown, M.P. et al. (1986) Historical trends in the sediment flow regime of the Mississippi River. *Water Resources Research*, 22: 1555-1564.

Lane, R.R., et al. (2010) Hydrologic and nutrient dynamics of a coastal bay and wetland receiving discharge from the Atchafalaya River. *Hydrobiologia*, 658(1): 55–66.

Morgan, J.P. (1979) Recent geological history of the Timbalier Bay area and adjacent continental shelf. *Rice Institute Pamphlet – Rice University Studies*, 65(4): 575-589.

Nittrouer, C.A. and Sternberg, R.W. (1981) The Formation of sedimentary strata in an allochthonous shelf environment: The Washington continental shelf. *Marine Geology*, 42(1-4): 201-232.

Nyman, J.A. et al. (1993) Relationship between vegetation and soil formation in a rapidly submerging coastal marsh. *Marine Ecology Progress Series*, 96: 269-279.

Reed, D. J. Ed. (1995) *Status and Historical Trends of Hydrologic Modification, Reduction in Sediment Availability, and Habitat Loss/Modification in the Barataria and Terrebonne Estuarine System*. BTNEP Publ. No. 20, Barataria-Terrebonne National Estuary Program, Thibodaux, Louisiana, 338 pp. plus Appendices.

Restreppo, G.A. et al. (2019) Riverine sediment contribution to distal deltaic wetlands: Fourleague Bay, LA. *Estuaries and Coasts*, 42(1): 55-67.

Reuss, M. (2004) *Designing the Bayous: The Control of Water in the Atchafalaya Basin, 1800-1995*. Texas A&M University Press.

Roberts, H.H. (1997) Dynamic changes of the Holocene Mississippi River delta plain: The delta cycle. *Journal of Coastal Research*, 13(3): 605-627.

Roberts, H.H. et al. (1980) Evolution of a sand-dominant subaerial phase, Atchafalaya Delta, Louisiana. *American Association of Petroleum Geologists,* 64: 264-279.

Roberts H.H. et al. (2003) An embryonic major delta lobe: a new generation of delta studies in the Atchafalaya-Wax Lake delta system. *Trans Gulf Coast Assoc Geol Soc,* 53: 690–703.

Smith, J.E. et al. (2015) What role do hurricanes play in sediment delivery to subsiding river deltas? *Scientific Reports,* 5: 17582.

Smith, M. and Bentley, S.J. (2015) Sediment capture in flood plains of the Mississippi River: A case study in Cat Island National Wildlife Refuge, Louisiana. *Proc. IAHS*, 367: 442-446. doi:10.5194/piahs-367-442-2015

Twilley, R.R. et al. (2016) Co-evolution of wetland landscapes, flooding, and human settlement in the Mississippi River Delta Plain. *Sustain Sci.,* 11: 711-731.

United Nations Scientific Committee on the Effects of Atomic Radiation, UNSCEAR (2000) *Sources and Effects of Ionizing Radiation, Vol. 1: Sources*. United Nations, New York.

U.S. Geological Survey (2018) The National Map, 2018, 3DEP products and services: The National Map, 3D Elevation Program. Web page at https://www.usgs.gov/core-science-systems/ngp/tnm-delivery/. Accessed September 5, 2018.

Whitehouse, R. et al. (2000) *Dynamics of Estuarine Muds: A Manual for Practical Applications*. Thomas Telford Publishing, Thomas Telford Ltd, Heron Quay, London.

Wilson, C.A. and Allison, M.A. (2008) An equilibrium profile model for retreating marsh shorelines in southeast Louisiana. *Estaurine, Coastal, and Shelf Science*, 80(4): 483-494.

Wang, F.C. et al. (1993) Intertidal marsh suspended sediment transport processes, Terrebonne Bay, Louisiana. *Journal of Coastal Research,* 9(1): 209-220.

Wang, J. et al. (2018) The coupling of bay hydrodynamics to sediment transport and its implication in micro-tidal wetland sustainability. *Marine Geology,* 405: 68-76.

CHAPTER 4. THE EFFECTS OF INHERENT SEDIMENT CHARACTERISTICS AND BURIED PALOECHANNELS ON DELTAIC WETLAND RESILIENCE

4.1. Introduction

The muddy landscape along the Louisiana coast is disappearing, partially due to increasing sea level, but primarily due to subsidence of the underlying strata along with a substantial decrease in fresh, nourishing sediment previously deposited by the Mississippi River and its distributaries. Diversions and river engineering may alleviate the severe sediment reduction, but will newly established subaerial land be able to withstand oscillating wave energy from the passage of storms, or unidirectional current energy from new diversions? This study seeks to establish: 1) the maximum critical erosional shear stress of the transgressive Terrebonne marsh platform and bay bottom can withstand, and 2) why the bifurcating morphology of the marsh platform along the fringes of the Terrebonne coastline are prominent.

For question 1, we use the critical erosional shear stress calculated from density measurements and paired with grain size analysis and carbon dating of whole vibracores to reconcile age with consolidation characteristics of the cohesive sediment. For question 2, we posit that ancient rivers and distributaries, or simply channels, are among the most resilient features along the Louisiana coast. Marshes built upon paleochannel strata will remain viable after marshes built upon interdistributary and overbank deposits have subsided beneath the waves. Thus, the rheological properties of the sediment beneath the marsh platform, including currently submerged former platforms, will be interpreted from age, sediment type, and a seismic profile.

The logic behind the hypothesis in question 2 is simple. Channels are filled with the coarsest and densest sediment relative to the organic, fine, and muddy deposits found outside the channel. Because channel fill is coarser, 25 – 40% denser (Kuecher, 1994), and contains more mineral sediment, it is not prone to the level of compaction seen in the muds composing the rest

of the coast. When everything outside the channel has subsided, the innate resistance to compaction of channel fill keeps it from subsiding for a longer period of time. Therefore, any marshes that transgress previous channels subside slower (Bomer et al., in review). To provide an analogy, one can think of the resulting morphology as a film negative, where what was once above water has sunk below, and the channel is now the only subaerial feature remaining.

4.2. Background

4.2.1. Terrebonne Bay and Subsidence

Underneath modern Terrebonne Bay lies the Teche Complex, formed between 5.5 - 3.5 kya and then reoccupied by the Lafourche Complex between 2.5 - 0.5 kya (Morgan, 1979; Wang et al., 1993; Blum and Roberts, 2012). When Mississippi River distributary and Terrebonne's last active channel, Bayou Lafourche, was dammed in 1905, the supply of fresh sediment was cutoff at Donaldsonville, approximately 105 km northwest of our field area (Morgan, 1979; Reuss, 2004). Damming resulted in a substantial reduction of fresh sediment delivery to the wetlands, in effect allowing the rate of erosion and subsidence to greatly outpace any land growth or sustainment.

Our specific Terrebonne field area is located 5 km southeast of the Louisiana Universities Marine Consortium (LUMCON), in Cocodrie, Louisiana, encompassing a micro-bay feature dubbed the "Crab Claw" based on its shape. The Crab Claw spans a ~4 km^2 area with two "legs," one in the east and one in the west, as well as a tidal flat located at its apex (Fig. 4.1). Qualitatively, the eastern leg appears derelict when compared to the western leg; ponding is prominent and the marsh surface itself is softer, easily giving way when walking across. The western leg has a firmer surface, no obvious ponding, and is bisected by several ~1-2 m wide tidal channels. Immediately to the east of the Crab Claw is Lake La Graisse, to the west is Bay Chaland, and to the south is Bay Lost Reef. The marsh platform is perennially vegetated by *S. alterniflora* (spartina), excluding the tidal flat which was never observed to be vegetated. The depth of the bay within the two legs

is ≤ 1 m, with depths just outside the legs around 2 m, based on a survey done during this study. It is unknown when the marsh platform is inundated.

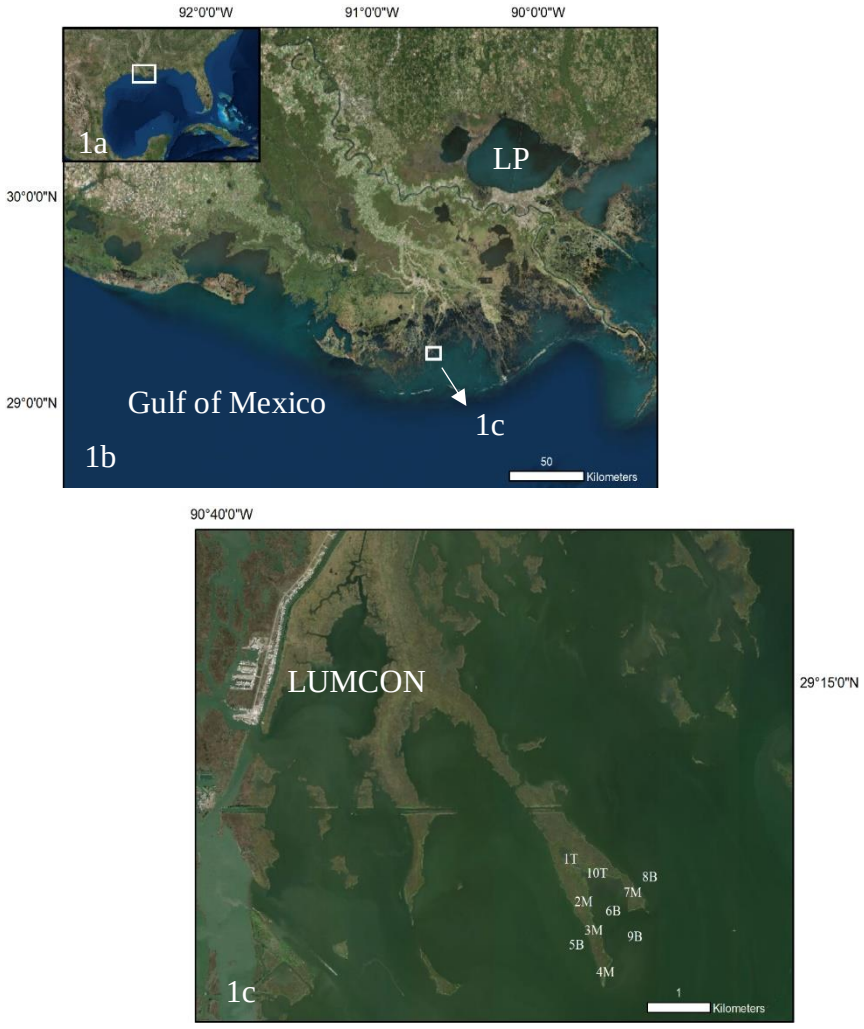

Figure 4.1. (a) Map of the Terrebonne Crab Claw field area in relation to the Gulf of Mexico; (b) to the Louisiana Coast and Lake Pontchartrain (LP); and (c) the Louisiana University Marine Consortium (LUMCON).

Based on Coastwide Reference Monitoring System (CRMS) data, relative sea level rise (RSLR) rates of western Terrebonne Bay range between 14.3 to 20.2 mm yr^{-1} (Jankowski et al., 2017). Overall, Terrebonne Parish experiences the highest RSLR rates in the state of Louisiana (Penland and Ramsey, 1990). Satellite photography of the area displays a curious bifurcating morphology in subaerial land at the fringes of the coast, including the Crab Claw itself. These

land masses, remnants of marsh platforms that have since subsided, are all that remain along the bay edge. This bifurcation appears visually similar to that seen when rivers split into distributaries proximal to their deltas, such as in the neighboring Atchafalaya Delta. The bifurcating morphology is of principal interest of this study.

The deterioration of Terrebonne Bay is rooted primarily in two causes: Lack of fresh sediment, discussed earlier, and the inherent tendency of mud composing the marshes to compact. This characteristic is especially problematic along the Louisiana coast, as the low elevation paired with ever increasing eustatic sea level makes the area critically susceptible to land loss. Without fresh riverine sediment to counteract the effects of RSLR, subsidence has overwhelmed much of Terrebonne Bay as predicted in models of delta evolution (Roberts, 1997). The existing subaerial land mass is only a fraction of what it was previously (Twilley et al., 2016). Satellite imagery of the field area clearly illustrates the amount of land loss experienced over the past 30 years (Fig. 4.2).

In southeastern coastal Louisiana, the top most sedimentary strata is separated into two distinct groups; a coarser, Pleistocene substratum, which is resistant to compaction, and a superseding Holocene layer of finer sediments which varies in thickness across the delta plain (Fisk et al., 1954; Kuecher et al., 1993; Meckel et al., 2006). Western Terrebonne Bay sits upon a relatively thick layer of the Holocene stratum, almost equal to that of the Mississippi River Valley itself (Meckel et al., 2006). It has been argued that compaction of this Holocene strata is a significant driver in coastal land loss and increases in RSLR (Tornqvist et al., 2008).

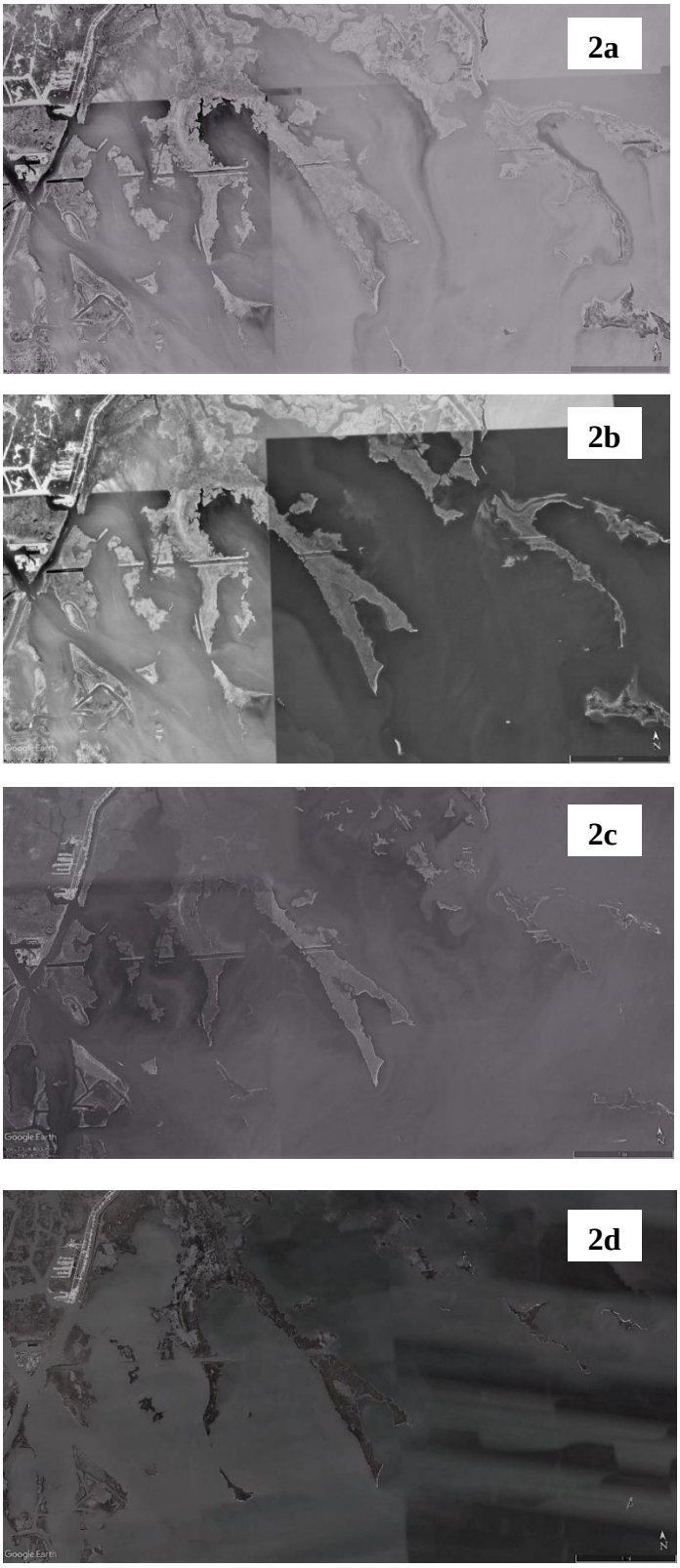

Figure 4.2. Satellite imagery of the Terrebonne Crab Claw over 25 years; (a) 1990, (b) 1998, (c) 2005, and (d) 2015 [Google Earth].

4.2.2. On Cohesive Sediment and Erodibility

Previous studies on consolidation of cohesive sediment with implications for coastal restoration have taken place in laboratory settings and have focused primarily on short term (days to months) consolidation of fluid muds within settling columns (Trimbak et al., 1985; Whitehouse et al., 2000; Lo et al., 2014; Sha et al., 2018). These tests reaffirmed the concept of increased shear stress resistance as the fluid mud settles and consolidates with depth and through time, with consolidation rates "inversely and exponentially related to initial sediment concentrations". However, Sha et al. (2018) note that organic material can substantially reduce the amount of erosional resistance expected with time. Nonetheless, the literature on the subject of long term, in situ cohesive sediment consolidation is significantly lacking. While the erodibility of non-cohesive sediment is well established, predicting the erodibility of cohesive sediment remains exceedingly difficult due to inherent physical properties within the mud (Grabowski et al., 2011).

Grabowski et al. (2011) thoroughly discuss the history of consolidation research to the near present. To paraphrase, the research of erodibility of cohesive sediment is primarily complicated by the attractive, interparticle forces and platy shape that cause the so called "stickiness" of fine sediment (Winterwerp and Van Kesteren, 2004; Grabowski et al., 2011). With coarser, more rounded, non-cohesive sediment, the charge that causes attraction is negligible and so each grain moves independently when acted upon by a force. This makes predictive modelling easier, as one particle behaves like all others of the same size and composition. It should be noted that the inclusion of clay and silt with coarse sand can increase resistance to erosion in sandy beds, as the pore space between the coarser material is filled in by the fine. At a sufficiently high clay concentration, non-cohesive sandy sediment may behave cohesively (Lick et al., 2004; Winterwerp and Van Kesteren, 2004; van Ledden et al., 2004; Grabowski et al., 2011). Second,

cohesive sediment is heterogenous, incorporating mineral and organic sediment of different sizes. While permeability is diminished, total porosity within uncompacted cohesive sediment is significantly greater than that of non-cohesive, coarse sediment (Fetter, 2000; Winterwerp and Van Kesteran, 2004). Thus, intergranular pore pressure and fluid movement becomes much more difficult to predict (Fetter, 2000). With additional fluid between interstitial pore space, cohesive sediments are more prone to consolidation from overburden as pressure forces the fluid to escape. More deeply buried cohesive sediment will become consolidated and therefore denser than relatively unconsolidated cohesive sediment near surface (Whitehouse et al., 2000; Bale et al., 2007).

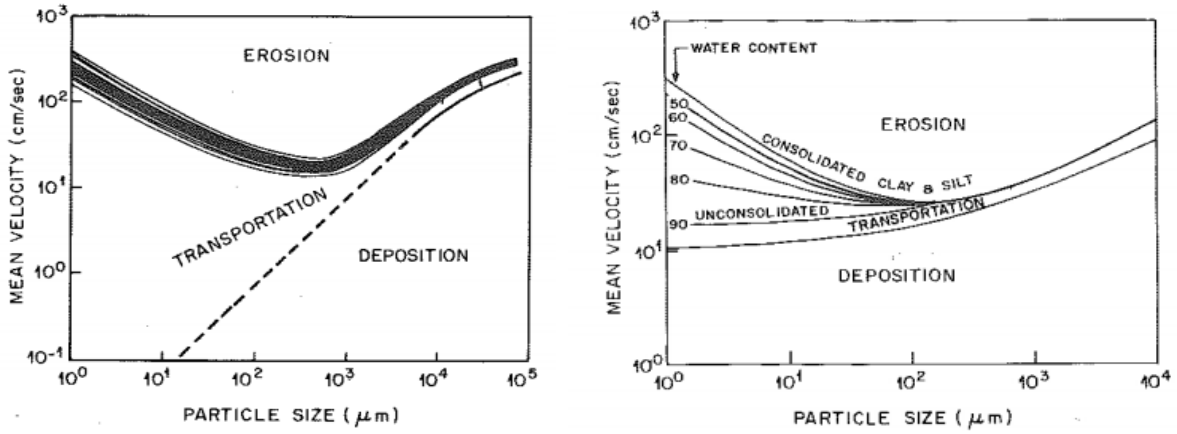

Figure 4.3. Hjustrom (left) and Postma (right) diagrams, modified from Dade et al., (1992). Both plots illustrate the mean velocity necessary to transport particles of a specific size. Note the increase in velocity needed to erode consolidated cohesive sediment.

Due to the post depositional behavior of cohesive sediment, erosional characteristics will vary as well. In essence, the critical erosional shear stress of a cohesive bed increases with time and depth. Thus, the more consolidated a unit is, the more erosional force is required to resuspend the bed. This is illustrated by the foundational work of Shields (1936) and Hjulstrom (1939) and expanded upon by Postma (1967) and Dade et al. (1992) (Fig. 4.3). Increase in erosional resistance of cohesive sediment with depth and consolidation is true no matter the type of forcing, e.g.

oscillating waves or unidirectional flow (Mehta et al., 1982; Parchure and Mehta, 1985; Maa and Mehta, 1987).

4.3. Methodology

CHIRP seismic data were gathered by Dr. Kehui Xu and Dr. Qihui Wu during May 2018 using an Edgetech 2000 DSS combined sidescan sonar & subbottom profiler system, with a frequency range of 2 – 12 kHz. Vertical resolution is between 6 – 10 cm, and penetration depth is up to 60 m. A special pontoon floating device was created to gather data in the shallow water within and around the Crab Claw study area. The transect used for this study, A – A', is illustrated in Fig. 4.4.

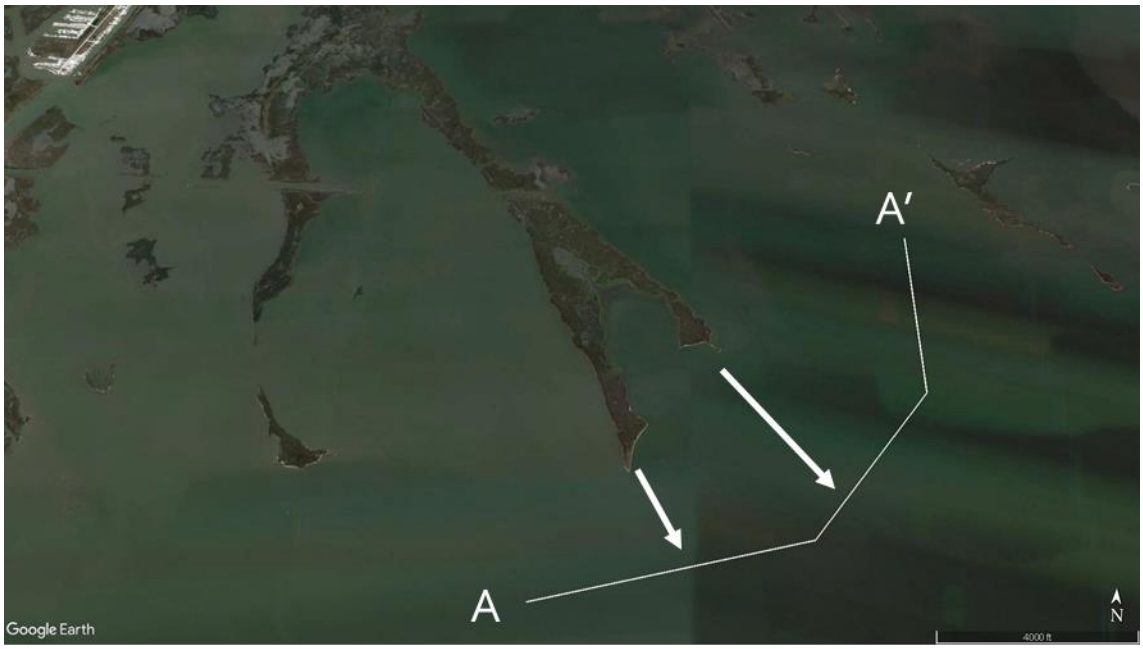

Figure 4.4. The transect used for CHIRP data collection. Arrows indicate paleochannel locations in Figure 4.5.

Ten vibracores, four on the marsh platform, four from the bay bottom, and two from the tidal flat and intertidal zone, were gathered during April 2017 (Fig. 4.1) with depth of acquisition ranging from 3.4 – 6.6 m. Vibracores were first run whole through a gamma density logger to collect bulk density data and then split and imaged using a Geotek core logger. Five vibracores

were subsampled at 2 cm intervals with the other five subsampled between 5 and 10 cm. Each interval was analyzed for grain size using a Beckman Coulter LS 13320 Laser Diffraction Particle Size Analyzer. Loss-on-ignition (LOI) testing was run on four of the ten cores to gather data on organic and mineral sediment percentage as well as water content, based on the method provided in Heiri et al. (2001).

Ten peat and plant samples from six cores core were sent to Beta Analytics for radiocarbon dating of what is presumed to be the previous marsh surface. Dating the most recent subaerial surface allows for the calculation of vertical accretion, as well as a general idea of when the area was previously above water. Dating of even older marsh surfaces allows the estimation of deltaic cycles and provides even more insight into the evolution of the landscape through time.

Critical erosional shear stress downcore was calculated using whole core density measurements with the equation below, given by Whitehouse et al. (2000):

$$\tau_e = E3(\rho_B - 1000)^{E4} \quad (4.1)$$

where:

τ_e is critical erosional shear stress (N m^{-2})

ρ_B is bulk density (kg m^{-3})

E3 and E4 are dimensionless, site-specific coefficients. In our case, to gain understanding of relative strength and because no local experimental results are available, default values of 0.015 & 0.73, respectively, were used (Whitehouse et al., 2000).

4.4. Results

4.4.1. CHIRP Data

Seismic data display two distinct channels of coarse material extending along the path of each Crab Claw leg (Fig. 4.4). The channels measure ~50 m in width, and are buried under

planar, continuous, acoustically opaque, organic-rich mud. The interdistributary mud between the channels is composed of disrupted, but continuous strata. Overall, paleochannel sediment is coarser and thicker, between 2 - 6 m, and pinches out laterally (Fig. 4.5). Four core images, those most proximal to the transect, have been emplaced upon the seismic profile to compare vibracores with the profile.

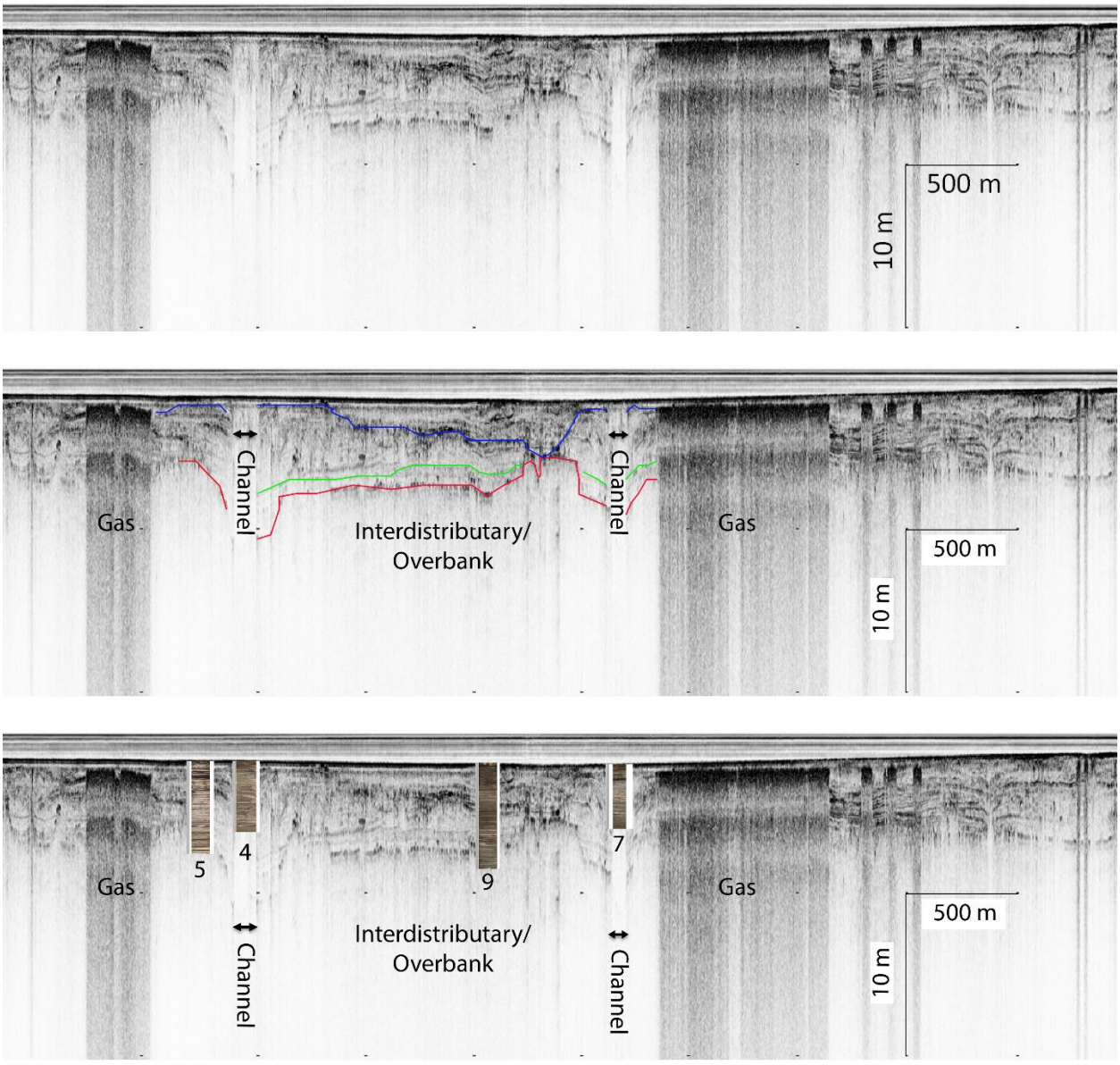

Figure 4.5. Top is an uninterpreted seismic profile of transect A – A'. Middle is the author's interpretation of the profile. Bottom contains the four most proximal vibracores (labeled 4, 5, 7,

9) hung across the profile; core depth is to scale, but core width is greatly exaggerated. Note the buried channels, which extend from the Crab Claw legs in Figure 4.4.

4.4.2. Critical Erosional Shear Stress

Three facies are visible downcore when pairing erosional shear stress with grain size (Fig. 4.6; Appendix B). The first facies reflects the low erosional resistance of loosely consolidated/fluid mud of the marsh platform near surface. τ_e values of Facies 1 are usually < 1 Pa, however coarser pockets of sand may increase erosional resistance beyond that value. Facies 2 is composed of consolidated older mud with τ_e values significantly higher than those in the first facies, generally ranging from ≥ 1 Pa to ≤ 2 Pa. Facies 3 is composed of much coarser and non-cohesive sandy sediment, which inherently has a higher erosional shear stress due to grain size and density. This facies displays the highest resistance to erosion, withstanding from ≥ 1 Pa to < 2.5 Pa.

4.4.3. Grain Size and LOI

Mean grain size across all vibracores fall into the clay to very fine silt range with occasional coarsening into medium silt (< 1 – 200 μm). This is not to say sand was not present, as several vibracores contained up to very coarse sand; these are simply average frequency values for each interval. The change into coarser grain size is usually rather abrupt and is present 200 to 400 cm below the surface, regardless of where the vibracore was taken.

Dry organic sediment percentage tends to be inversely proportional with coarsening sediment and increasing τ_e (Figs. 4.6 and 4.7; Appendix B). Facies 1 generally contains the highest amount of organic sediment, as do occasional pockets of low resistivity fine sediment downcore. The lowest organic values are linked with the coarse sediment of Facies 3. Of special note, core TER 1T contains a chaotic section with spiking organic percentage, grain size, and erosional

resistance grouped into Facies 1 (Fig. 4.6). This is the only core to display this pattern with this intensity, and it may be due to bioturbation at depth in the tidal flat.

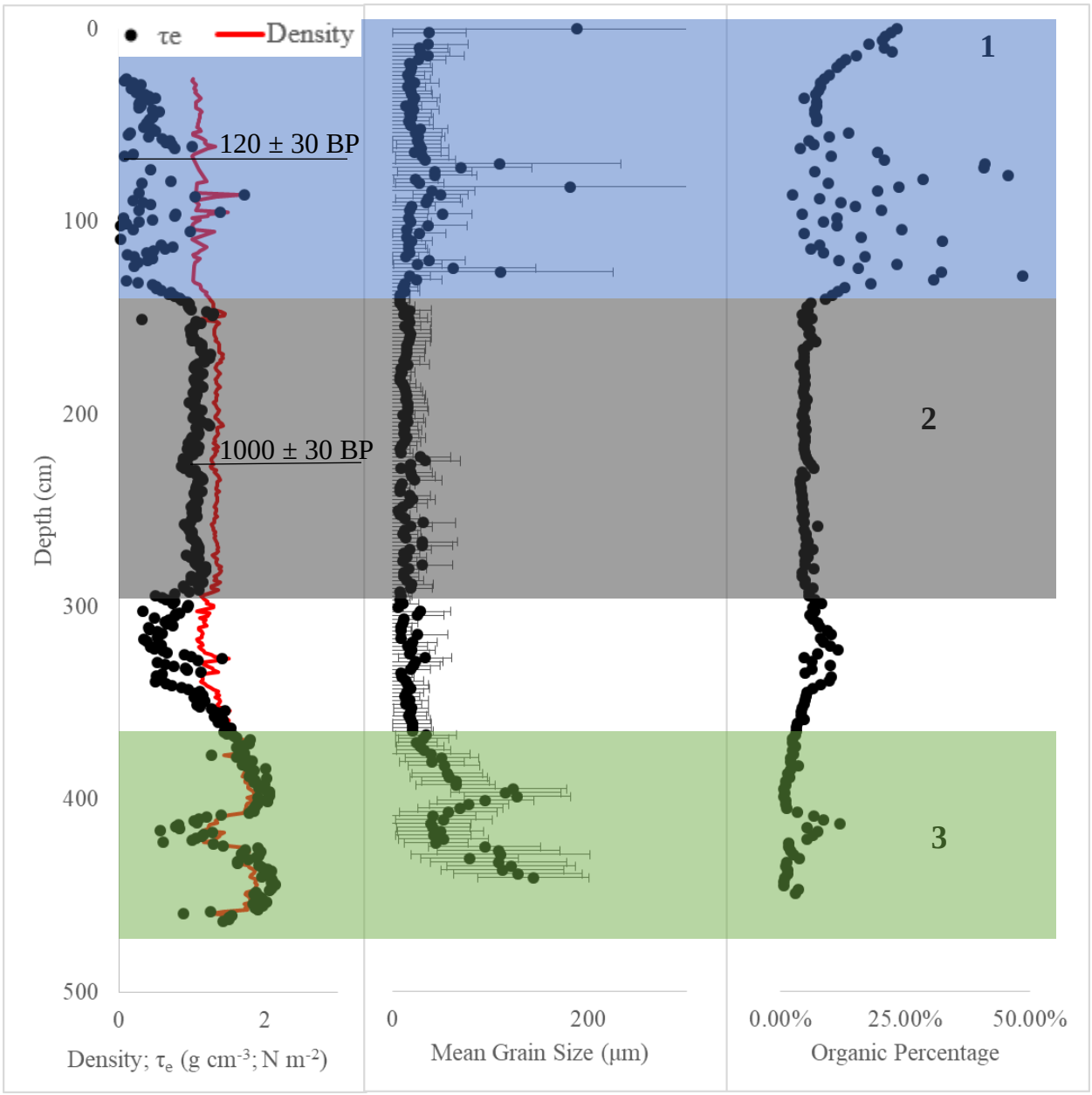

Figure 4.6. Bulk density from the gamma logger, critical erosional shear stress (τ_e), mean grain size, carbon dates, and dry mass organic in core TER 1T. Three prominent facies are visible in most vibracores. Facies 1 is unconsolidated/fluid sand and mud with low erosional resistance; 2 is consolidated mud with moderate to strong erosional resistance; 3 is sandy deposits with high erosional resistance. Note chaotic pattern midway through Facies 1.

4.4.4. Carbon Dates

Dating of previous marsh surfaces from several cores ranged from modern (~c. 1955, base of the current marsh surface) to 1000 ± 30 years BP (Table 4.1). Dates for the previous marsh surface in are in agreement in cores 2M and 3M, at approximately 880 ± 30 years BP. The marsh surface below that is also within the margin of error for each, between 950 and 940 ± 30 years before present. The ages of previous marsh surfaces in bay bottom cores are not in agreement, as those dates range from 380 to 680 ± 30 years before present. Dates from core TER 3M are especially of interest as the core display a classic consolidation profile throughout, consisting of loose mud at the surface and quickly strengthening downcore (Fig. 4.7).

Table 4.1. Carbon dates and vertical accretion rates (VAR) for previous marsh surfaces in six vibracores.

Core	Depth (cm)	^{14}C Age (yrs BP)	VAR (cm yr^{-1})
1T	67	120 ± 30	0.45 - 0.74
	221	1000 ± 30	0.21 - 0.23
2M	191	880 ± 30	0.21 - 0.22
	240	950 ± 30	0.24 - 0.26
3M	30.5	Modern (c. 1955)	0.49
	192	880 ± 30	0.21 - 0.23
	225	940 ± 30	0.23 - 0.25
5B	40	380 ± 30	0.10 - 0.11
8B	41	520 ± 30	0.07 - 0.08
9B	132	680 ± 30	0.19 - 0.20

4.5. Discussion and Conclusion

4.5.1. Vertical Accretion Rates

Vertical accretion rates (VARs) are calculated using carbon dates (Table 4.1). Samples from ~2 – 2.5 m below the marsh cores 2M and 3M are in close agreement, with a VAR of 0.21 – 0.26 cm yr^{-1}. The bottom of the vegetated marsh surface in core 3M dated to approximately 1955,

and so provides a much higher VAR of 0.47 cm yr^{-1}. This difference in rate is due to the compaction of older sediment from deeper within the vibracore.

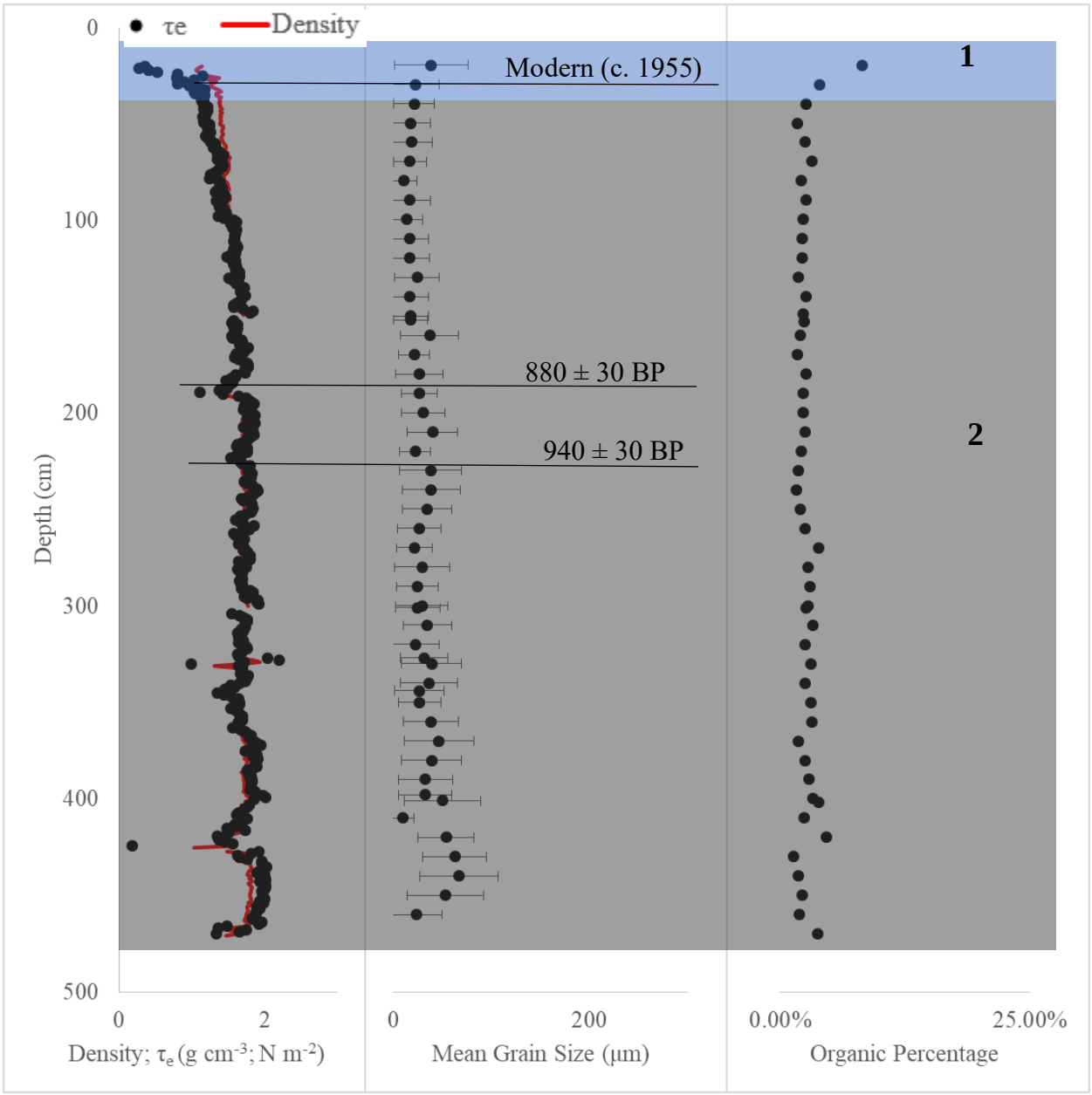

Figure 4.7. Downcore bulk density, critical erosional shear stress, mean grain size, and organic percentage of core TER 3M, with carbon dates assigned. Note the classic consolidation profile and lack of Facies 3.

VAR in the bay cores, 5B, 8B, and 9B was less than half of those calculated for the marshes and varied from 0.07 – 0.20 cm yr^{-1}. The differences between the marsh surface and bay bottom

rates is likely tied to the subaerial and subaqueous environments, respectively, as fine particles are less likely to settle in the more easily agitated shallow bay bottom surface.

Finally, the rates from the tidal flat core, 1T, ranged from 0.45 – 0.74 cm yr^{-1} at 67 cm below the surface (Facies 1) and falling to 0.21 – 0.23 cm yr^{-1} at 221 cm below the surface (Facies 2; Fig. 4.6). Notably, the shallow rate for this core is similar to that seen for the shallow portion of core 3M. It may be that VAR can be used as a proxy for consolidation in that an older, well consolidated mud will display a lower VAR, while recently deposited beds (~100 years BP to modern) will display VARs greater than double those of older beds.

Importantly, a VAR of ~0.20 cm yr^{-1} seems to be the hard limit for well consolidated beds in this area, as this number is seen in both marsh cores, 2M and 3M, and the tidal flat core 1T. In cores 2M and 1T, this value is valid until the mud contacts coarser sand. In core 3M, penetration of the vibracore was not deep enough to reach the sandy bed, but the VAR hovered around the 0.20 cm yr^{-1} amount for two older mud samples within the vibracore.

4.5.2. Consolidation and Erosional Shear Stress Resistance

Based on calculations in Whitehouse et al. (2001), the loosely consolidated zone, Facies 1, in both the marsh surface and bay bottom would be unable to withstand current flows with a bed shear stress approaching 1 Pa, or up to a depth averaged velocity of 1 m s^{-1} in saline water. On the marsh surface, including the tidal flat, this zone extends from ~30 to 130 cm below the surface; on the bay floor, this zone extends much deeper, from ~180 – 330 cm below the surface. However, once a zone of either consolidated mud or coarse sand is reached, erosion would not initiate until flows reach up to a depth averaged velocity of ~1.3 m s^{-1}. Importantly, critical erosional shear stress in Facies 2 and 3 appears to reach equilibrium with depth and therefore time. This is expected in coarser sediment packets, as τ_e is almost purely a function of individual grain size and

density in non-cohesive sediment. However, with cohesive sediments this may allude to a critical point where consolidation via overburden and dewatering is no longer a factor, at least at the near surface.

Relevant to this discussion is the expected shear stress generated by atmospheric forcing in the shallow bay environment. Xu et al. (2016) produced several plots illustrating shear stress as a function of wind speed, fetch, and depth. When our maximum critical erosional shear stress data for each facies is fitted to Xu et al.'s (2016) figures, it becomes clear that the marsh platform surface facies (F1) of loosely consolidated soil is at substantial risk to erosion in windy conditions.

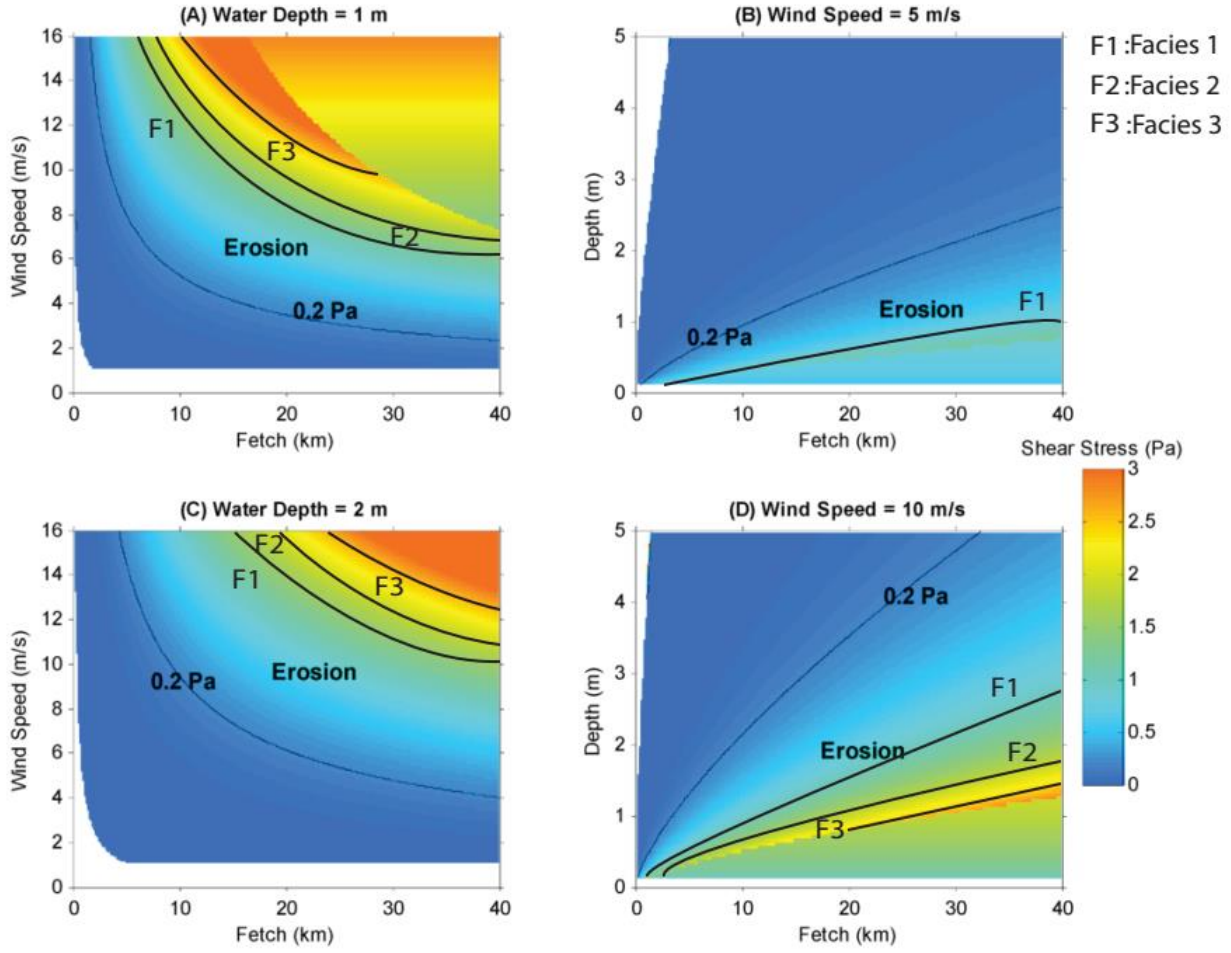

Figure 4.8. Modified from Xu et al. (2016), maximum critical erosional shear strength data for our three facies, F1-F3, is plotted against shear stress generated from specific wind speeds, fetch, and depth.

4.5.3. Channel Foundations and Marsh Platform Resilience

As stated earlier, the calculated erosional shear stress resistance values of sandy, coarse sediments are the most resistant to shear stresses. Therefore, any filled channels will likely withstand both current flows and wave action better than surrounding interdistributary or overbank deposits. This fact, paired with the inherent inability of coarse sediment to compact under non-metamorphic conditions, establishes paleochannels as resilient foundations for marsh platforms. The strongest evidence for this hypothesis emerges from the results of the seismic survey.

The seismic data gathered for this study indicate that the two legs of the Crab Claw were built upon ancient channels. When compared to satellite photography from the 1980s and 1990s, it becomes apparent that both legs once extended subaerially farther seaward toward the seismic channel track, A-A'. While the study area is only one example, these results are intriguing.

Returning to the original questions posed in the introduction, we can answer that: 1) Once consolidated to what appears to be a local maximum, older mud can withstand up to ~2 Pa of shear stress. Less consolidated or fluid mud near surface can only tolerate a maximum of <1 Pa. 2) The bifurcating morphology visible along the coastal fringe of Terrebonne Bay may be a byproduct of subsurface paleochannels, which are inherently less susceptible to compaction and consolidation and which may form a resilient foundation for the marsh platform. An expanded survey of remaining marsh platform is necessary to confirm these results, and the best tools to do so are seismic profiles.

4.6. References

Bale, A.J. et al. (2007) Critical erosion profiles in macro-tidal estuary sediments: implication for the stability of intertidal mud and the slope of mud banks. *Continental Shelf Research*, 27(18): 2303-2312.

Blum, M.D. and Roberts, H.H. (2012) The Mississippi Delta region: past, present, and future. *Annu. Rev. Earth Planet. Sci.*, 40: 655-83.

Bomer, E.J. et al. (in review) Deltaic morphodynamics and stratigraphic evolution of Middle Barataria Bay and Middle Breton Sound regions, Louisiana, USA: Implications for river-sediment diversions. *Estuarine, Coastal, and Shelf Science.*

Dade, W.B. et al. (1992) Predicting erosion resistance of muds. *Marine Geology*, 105: 285-297.

Fetter, C.W. (2000) *Applied Hydrogeology Fourth Edition*. Pearson Education Limited, England.

Fisk, H. N. (1954), Sedimentary framework of the modern Mississippi Delta, *J. Sediment. Petrol.*, 24(2), 76–99.

Grabowski, R.C. et al. (2011) Erodibility of cohesive sediment: The importance of sediment properties. *Earth-Science Reviews,* 105(3-4): 101-120

Heiri, O. et al. (2001) Loss on ignition as a method for estimating organic and carbonate content in sediments: reproducibility and comparability of results. *Journal of Paleolimnology*, 25: 101-110.

Hjulstrom, F. (1939) Transportation of detritus by moving water. In *Recent Marine Sediments*. P.D. Trask (Ed.). Am. Assoc. Pet. Geol., Tulsa. Pp. 5-31.

Jankowski, K.L. et al. (2017) Vulnerability of Louisiana's coastal wetlands to present-day rates of relative sea-level rise. *Nature Communications,* 8: 14792.

Kuecher, G. L., et al. (1993), Consolidation settlement potential in south Louisiana. In *Coastal Zone '93: Proceedings of the Eighth Symposium on Coastal and Ocean Management*, pp. 175–192, Am. Soc. of Civ. Eng., New York.

Kuecher, G. L. (1994), *Geologic Framework and Consolidation Settlement Potential of the Lafourche Delta, Topstratum Valley Fill; Implications for Wetland Loss in Terrebonne and Lafource Parishes, Louisiana*. Ph.D. thesis, 346 pp., La. State Univ., Baton Rouge.

Lick, W., et al. (2004) Initiation of movement of quartz particles. *Journal of Hydraulic Engineering-ASCE*, 130(8): 755-761.

Lo, E.L. et al. (2014) Experimental study of cohesive sediment consolidation and resuspension identifies approaches for coastal restoration: Lake Lery, Louisiana. *Geo-Marine Letters*, 34(6): 499-509.

Maa, P.-Y. and Mehta, A.J. (1987) Mud erosion by waves: a laboratory study. *Continental Shelf Research*, 7(11-12): 1269-184.

Meckel, T.A., Ten Brink, U.S., Williams, S.J. (2006) Current subsidence rates due to compaction of Holocene sediments in southern Louisiana. *Geophysical Research Letters*, 33, L11403, doi: 10.1029/2006GL026300.

Mehta, A.J. et al. (1982) Resuspension potential of deposited cohesive sediment beds. In *Estuarine Comparisons Proceedings of the Sixth Biennial International Estuarine Research Conference, Gleneden Beach, Oregon, November 1-6 1981*. Kennedy, V.S. ed. Academic Press, New York. Pp. 591-609.

Morgan, J.P. (1979) Recent geological history of the Timbalier Bay area and adjacent continental shelf. *Rice Institute Pamphlet – Rice University Studies*, 65(4): 575-589.

Parchure, T.M. and Mehta, A.J. (1985) Waves over mud: Modeling erosion. In *Proceedings of the 3rd International Symposium on River Sedimentation*. S.Y. Wang, H.W. Shen, and L.Z. Ding, eds. The University of Mississippi, Jackson, Mississippi. Pp. 588-601.

Penland, S. and Ramsey, K.E. (1990) Relative sea-level rise in Louisiana and the Gulf of Mexico: 1908-1988. *Journal of Coastal Research*, 6(2): 323-342.

Postma, H. (1967) Sediment transport and sedimentation in the estuarine environment. In *Estuaries*. G.H. Lauff (Ed.). AAAS, Washington, D.C. Publ. 83. Pp. 158-179.

Reuss, M. (2004) *Designing the Bayous: The Control of Water in the Atchafalaya Basin, 1800-1995*. Texas A&M University Press.

Roberts, H.H. (1997) Dynamic changes of the Holocene Mississippi River delta plain: The delta cycle. *Journal of Coastal Research*, 13(3): 605-627.

Sha, X. et al. (2018) Characterization and modeling of sediment settling, consolidation, and suspension to optimize coastal Louisiana restoration. *Estuarine, Coastal, and Shelf Science*, 203: 137-147.

Shields, I.A. (1936) Anwendung der Aehnlichkeitsmechanilr und der Turbulenzforschung ad die Geschiebe - bewegung , " Mitteilungen der Preussischen Versuchsanstalt fur Nassexbau nd Schiffbau. Translated by Ott, W.P. and Uchelen, J.C. Soil Conservation Service Cooperative Laboratory, CalTech, Pasadena, California.

Tornqvist, T.E. et al. (2008) Mississippi Delta subsidence primarily caused by compaction of Holocene strata. *Nature Geoscience*, 1: 173-176.

Trimbak, M.P. et al. (1985) Erosion of soft cohesive sediment deposits. *J. Hydraul. Eng.,* 111(10): 1308-1326.

Twilley, R.R. et al. (2016) Co-evolution of wetland landscapes, flooding, and human settlement in the Mississippi River Delta Plain. *Sustain Sci.,* 11: 711-731.

Van Ledden, M. et al. (2004) A conceptual framework for the erosion behaviour of sand-mud mixtures. *Contental Shelf Research,* 24(1): 1-11.

Wang, F.C. et al. (1993) Intertidal marsh suspended sediment transport processes, Terrebonne Bay, Louisiana. *Journal of Coastal Research,* 9(1): 209-220.

Whitehouse, R., et al. (2000) *Dynamics of Estuarine Muds: A Manual for Practical Applications.* Thomas Telford Publishing, Heron Quay, London.

Winterwerp, J.C. and van Kesteren, W.G.M. (2004). *Introduction to the Physics of Cohesive Sediment in the Marine Environment*. Elsevier, Amsterdam.

Xu, K. et al. (2016) Implication of texture and erodibility for sediment retention in receiving basins of coastal Louisiana diversions. *Water,* 8(1): 26.

CHAPTER 5. CONCLUSIONS

5.1. Significance of Research

Each chapter attempts to extend the depth and breadth of knowledge regarding fine sediment behavior in and around distal marsh platforms in Louisiana. Chapter 2 estimates how much riverine sediment would be expected to accumulate onto the marsh platform from a large source, e.g. the Atchafalaya River, as well as a sphere of influence for this riverine sediment over seasonal time scales. This data is useful for planning sediment diversions for restoration along the coast.

Chapter 3 provides a characteristic by which it may be possible to diagnose the health of an existing platform. The ratio of organic sediment to mineral sediment appears to be an important factor in stable platforms, with the platform in Fourleague Bay containing more organic matter even with fresh outside mineral sediment making its way onto the marsh surface. Terrebonne, on the other hand, contained less organic sediment and more mineral sediment. It appears as though the input of fresh mineral sediment enhances the retention and growth of organic material.

Finally, Chapter 4 provides a possible geotechnical mechanism for coastal resilience, with buried paleochannels providing natural resistance to compaction of overlying marsh. Additionally, a range of erosional resistance values are provided for three facies found near surface in Terrebonne Bay.

5.2. Future Research

Various avenues exist to expand upon the research provided in the volume. As for Chapter 2, a steady state fallout inventory of atmospherically derived ^{7}Be needs to be established for coastal Louisiana. The inventory used in Chapter 2 is specific to Galveston, TX, and is the nearest one available. Variations between Galveston and coastal Louisiana may be significant enough to

warrant such a venture. This would be difficult on the marsh surface, as gathering this data requires regular sampling, analysis, and a controlled environment, but it would be valuable one could be calculated.

The results from Chapter 3 are intriguing and could benefit greatly from further testing from other marsh platforms along the coast to establish a sort of baseline ratio for the region. Our results, at least for the Terrebonne Crab Claw, are somewhat limited in scale. Data from eastern Terrebonne Bay, Barataria Bay, Vermilion Bay, and the Chenier Plain of western Louisiana would substantially expand the impact of these findings.

Finally, Chapter 4 would also be improved by a more data, in this case CHIRP data around fringe coastal marsh platforms in Terrebonne and perhaps Barataria Bays. Additional vibracores could aid in testing the hypothesis of that chapter, but they would need to come from deeper below the surface and ideally from the CHIRP transect. Regardless, much more real-world data is necessary.

APPENDIX A. GRAIN SIZE, LOI, AND RADIOISOTOPE DATA FOR CHAPTER 3

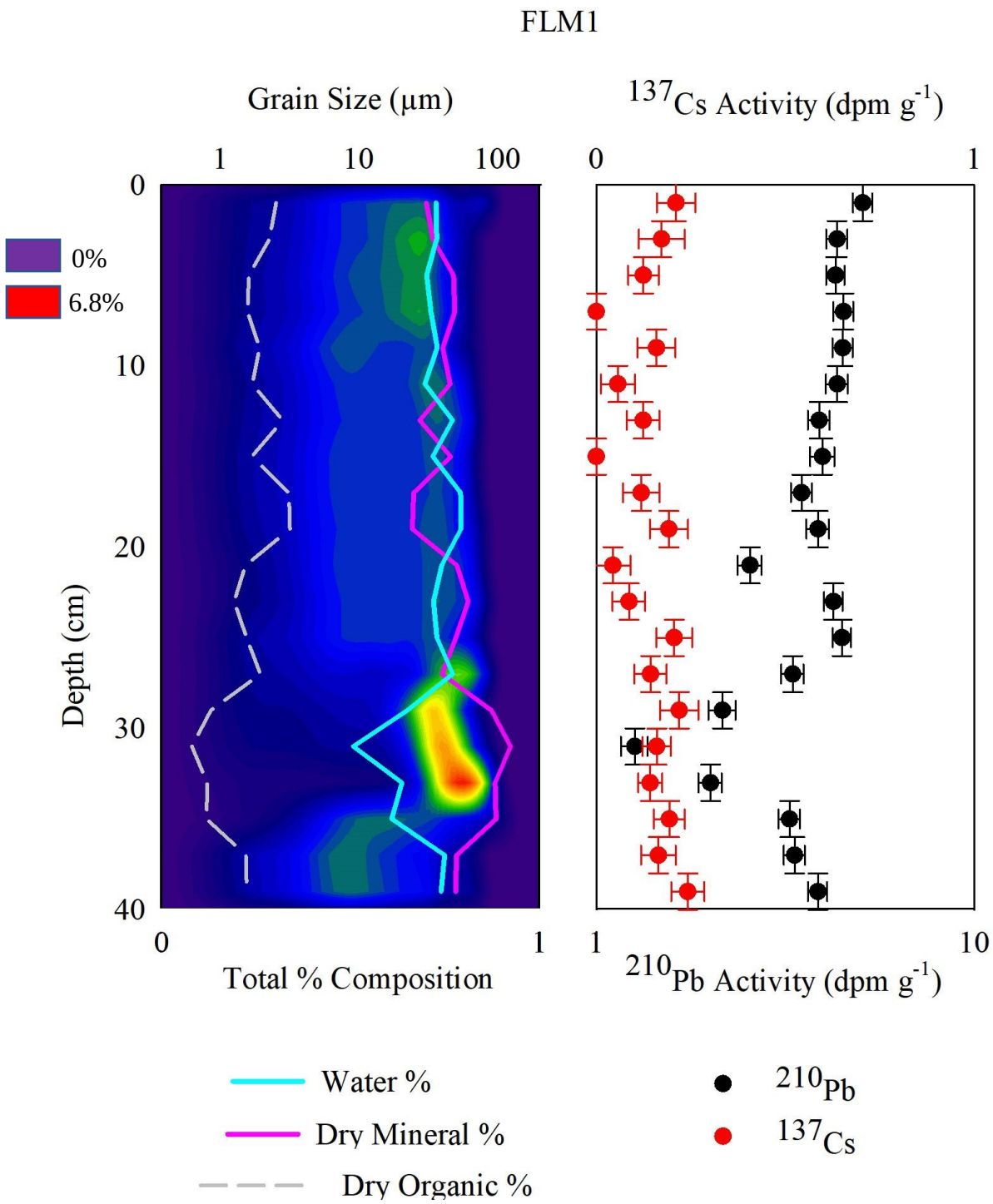

FLM2

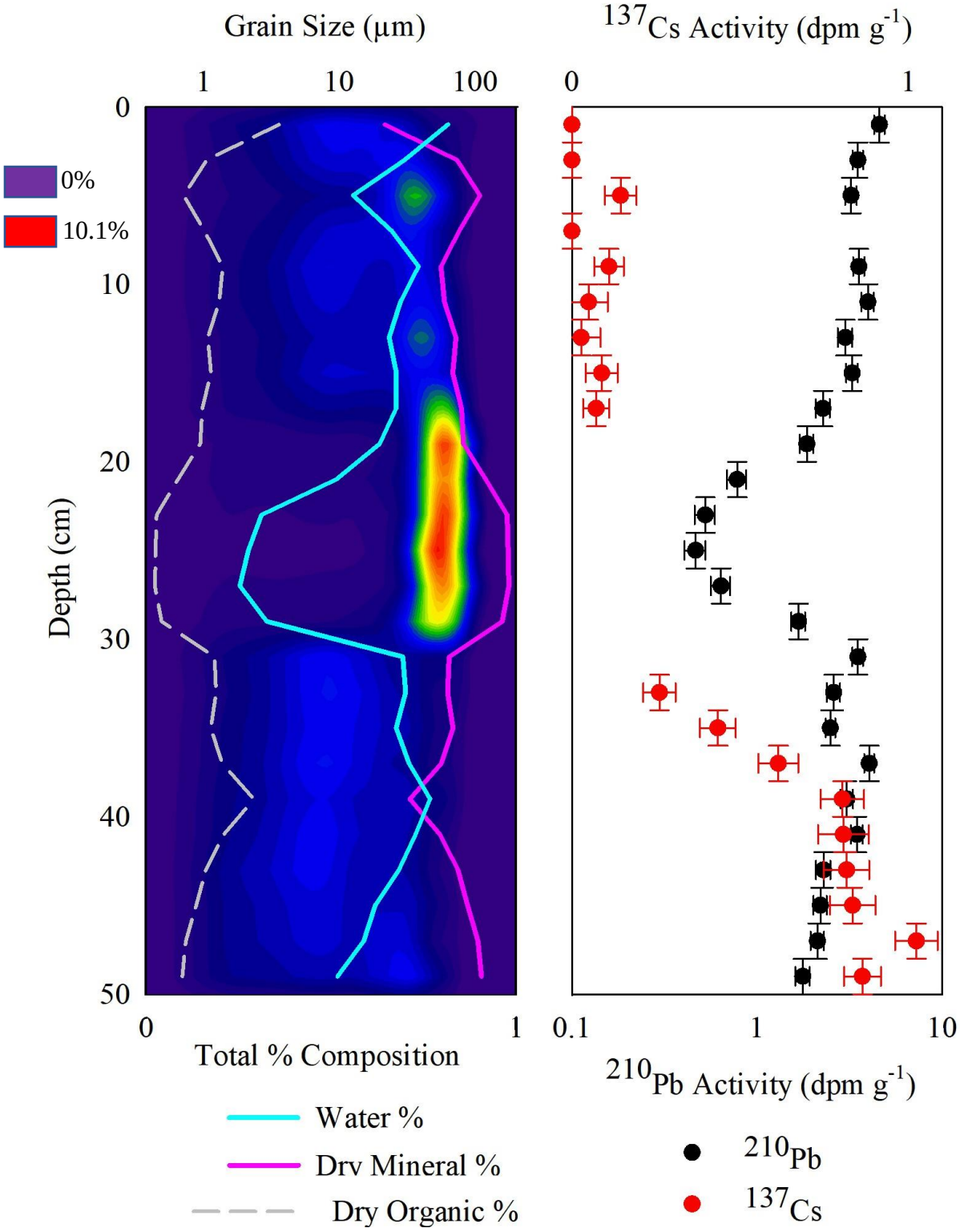
Grain Size (µm)
1
10
100
0
10
20
30
40
50
Depth (cm)
0%
10.1%
0
1
Total % Composition
Water %
Dry Mineral %
Dry Organic %
137Cs Activity (dpm g-1)
0
1
0.1
1
10
210Pb Activity (dpm g-1)
210Pb
137Cs

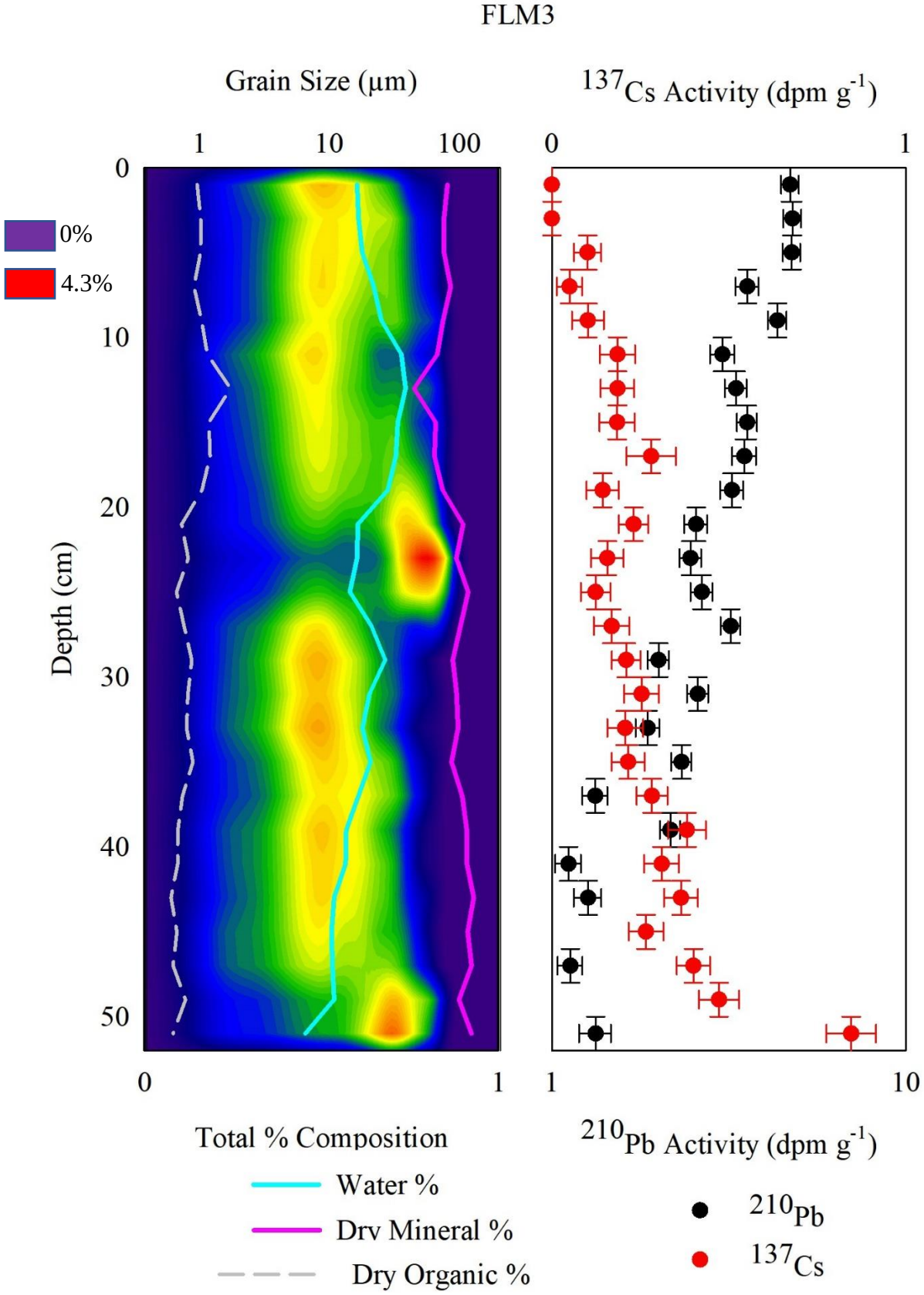
FLM3
Grain Size (µm)
1
10
100
0
10
20
30
40
50
Depth (cm)
0%
4.3%
0
1
Total % Composition
Water %
Drv Mineral %
Dry Organic %
137Cs Activity (dpm g-1)
0
1
1
10
210Pb Activity (dpm g-1)
210Pb
137Cs

FLM4

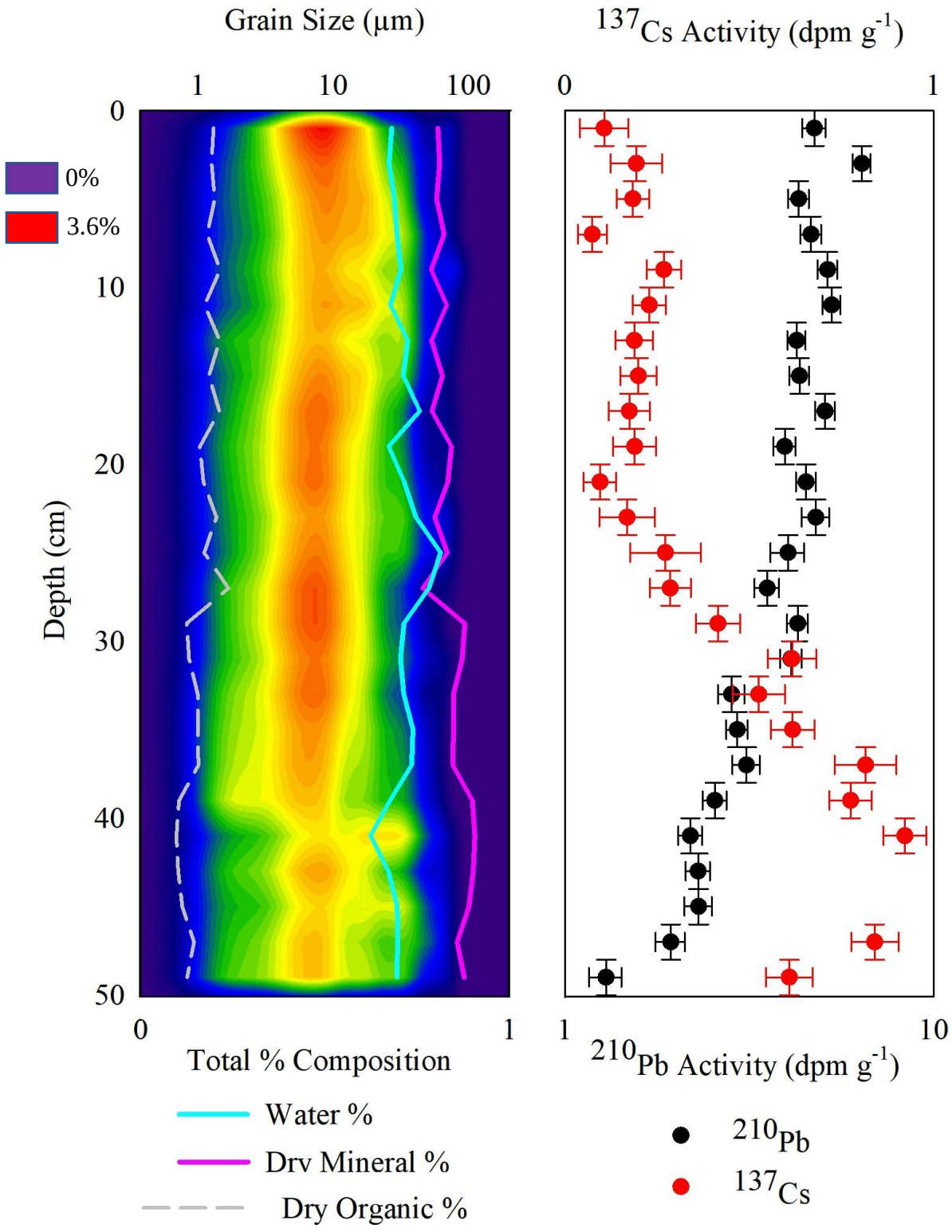
Grain Size (µm)
1
10
100
0%
3.6%
Depth (cm)
0
10
20
30
40
50
0
1
Total % Composition
Water %
Drv Mineral %
Dry Organic %
137Cs Activity (dpm g-1)
0
1
1
10
210Pb Activity (dpm g-1)
210Pb
137Cs

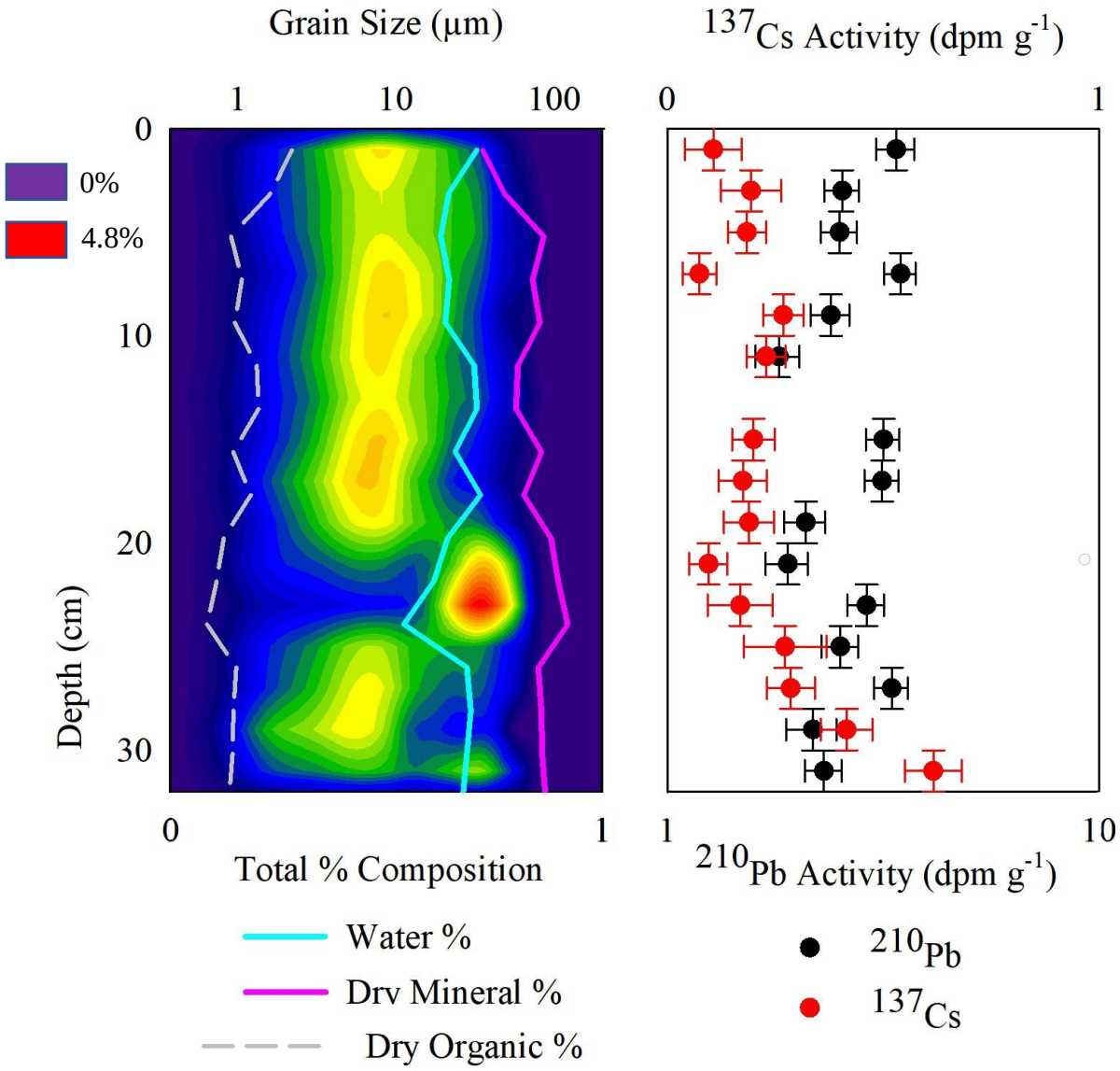
FLM5
Grain Size (µm)
1
10
100
0
10
20
30
Depth (cm)
0%
4.8%
0
1
Total % Composition
Water %
Drv Mineral %
Dry Organic %
137Cs Activity (dpm g-1)
0
1
1
10
210Pb Activity (dpm g-1)
210Pb
137Cs

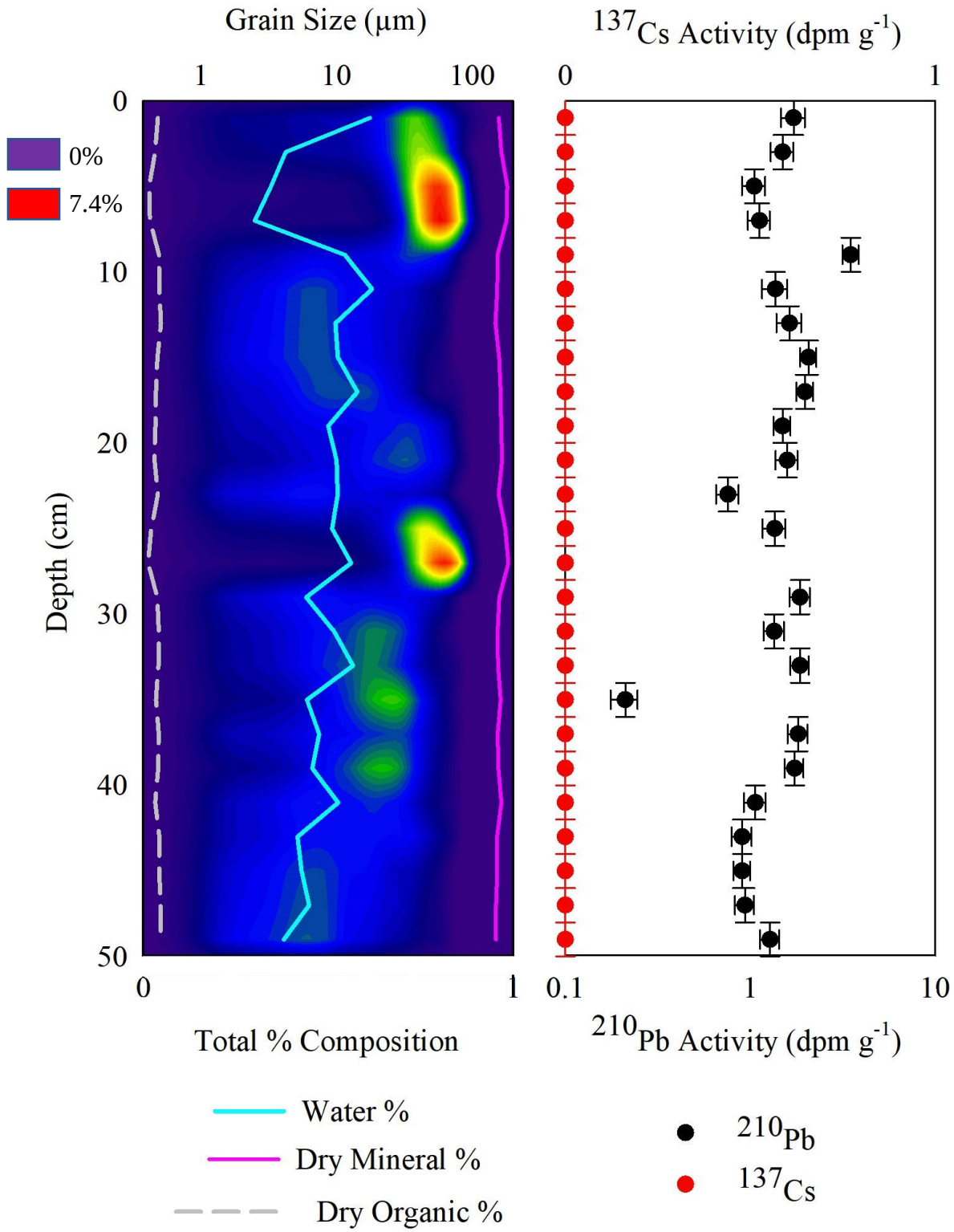
FLB1
Grain Size (µm)
1
10
100
0%
7.4%
Depth (cm)
0
10
20
30
40
50
0
1
Total % Composition
Water %
Dry Mineral %
Dry Organic %
137Cs Activity (dpm g-1)
0
1
0.1
1
10
210Pb Activity (dpm g-1)
210Pb
137Cs

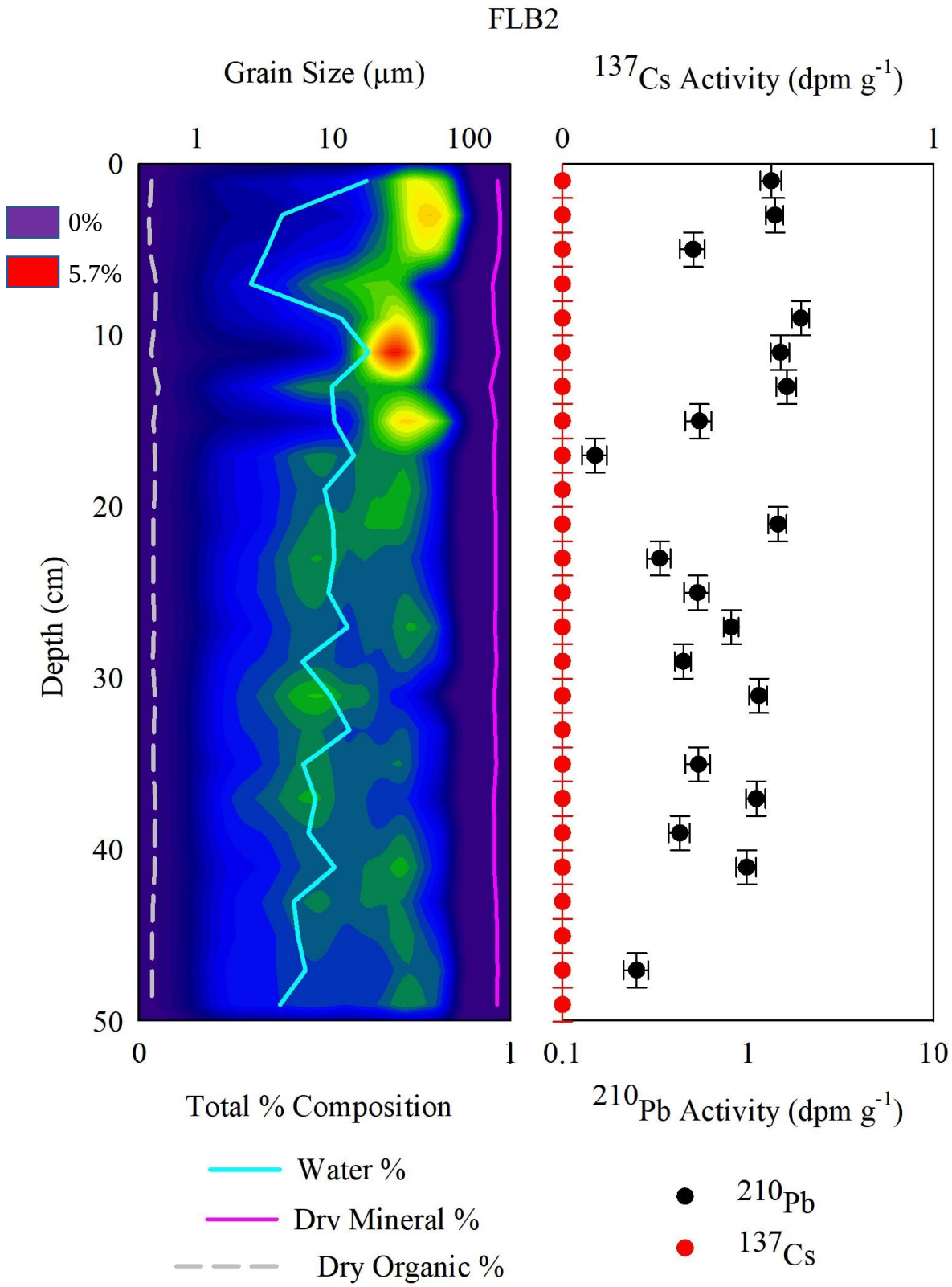
FLB2
Grain Size (µm)
1
10
100
0%
5.7%
0
10
20
30
40
50
Depth (cm)
0
1
Total % Composition
Water %
Drv Mineral %
Dry Organic %
137Cs Activity (dpm g-1)
0
1
0.1
1
10
210Pb Activity (dpm g-1)
210Pb
137Cs

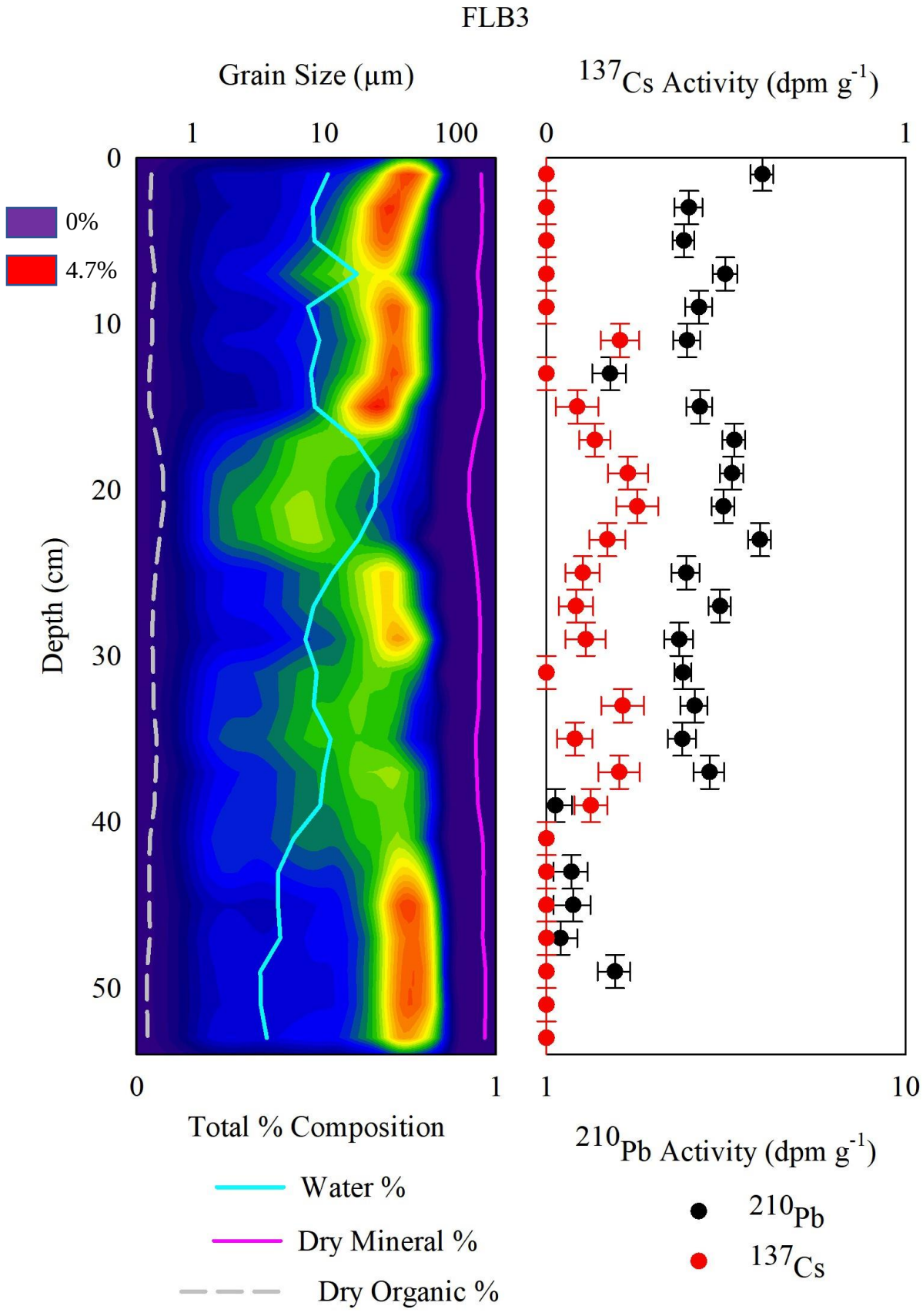
FLB3
Grain Size (µm)
1
10
100
0
0%
4.7%
10
20
30
40
50
Depth (cm)
0
1
Total % Composition
Water %
Dry Mineral %
Dry Organic %
137Cs Activity (dpm g-1)
0
1
1
10
210Pb Activity (dpm g-1)
210Pb
137Cs

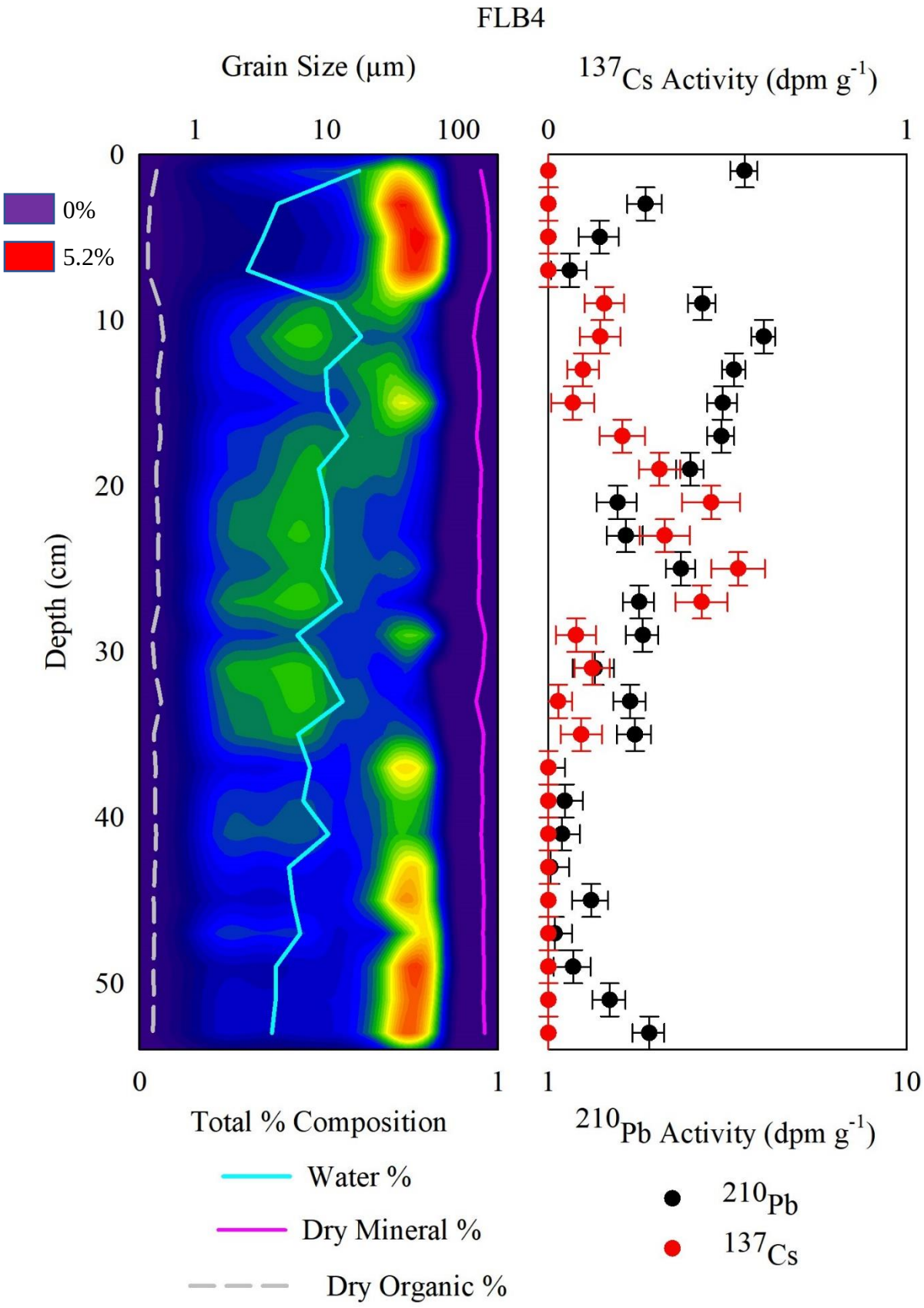
FLB4
Grain Size (µm)
1
10
100
0%
5.2%
0
10
20
30
40
50
Depth (cm)
0
1
Total % Composition
Water %
Dry Mineral %
Dry Organic %
137Cs Activity (dpm g-1)
0
1
1
10
210Pb Activity (dpm g-1)
210Pb
137Cs

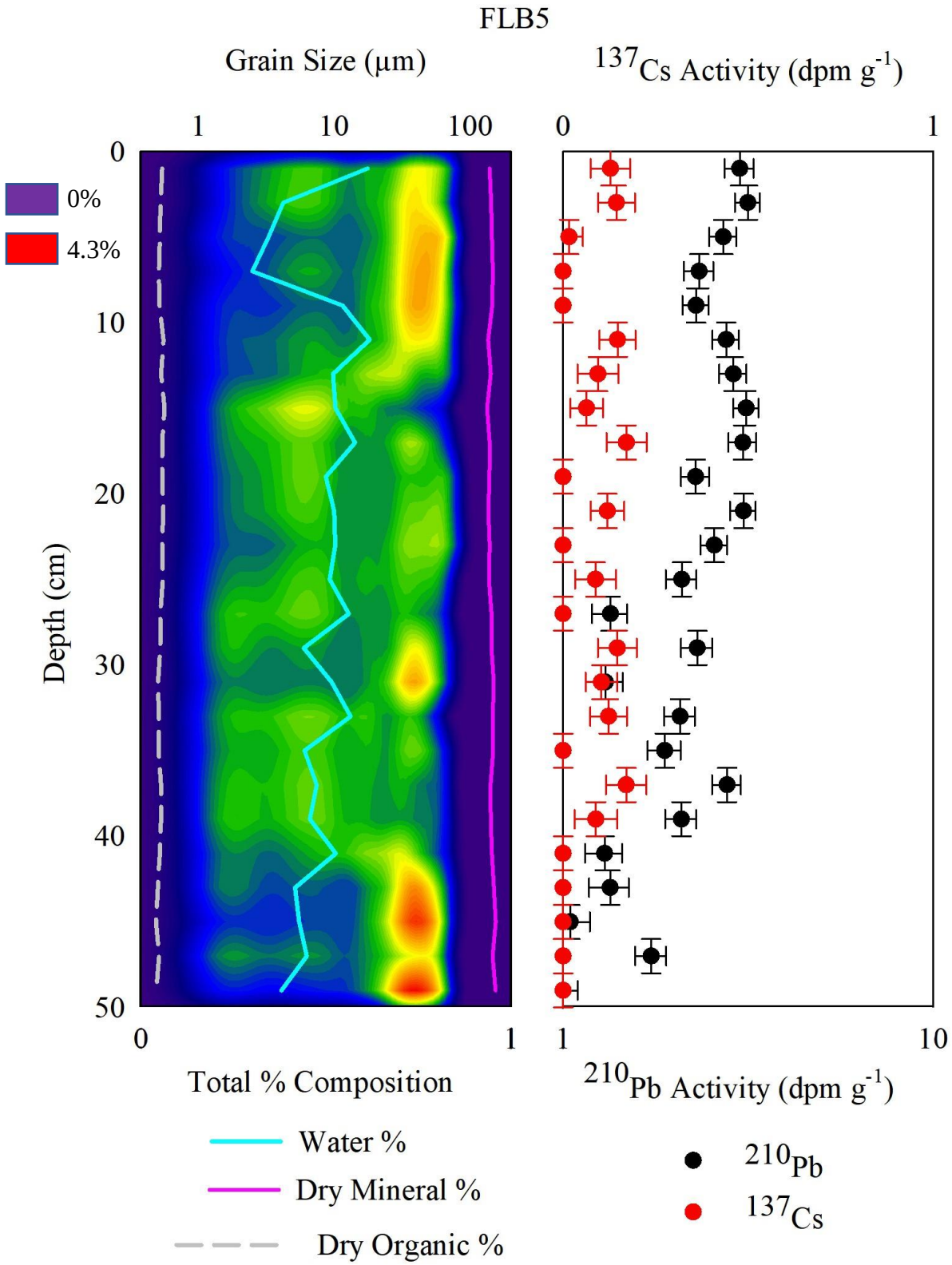
FLB5
Grain Size (µm)
1
10
100
0%
4.3%
0
10
20
30
40
50
Depth (cm)
0
1
Total % Composition
Water %
Dry Mineral %
Dry Organic %
137Cs Activity (dpm g-1)
0
1
1
10
210Pb Activity (dpm g-1)
210Pb
137Cs

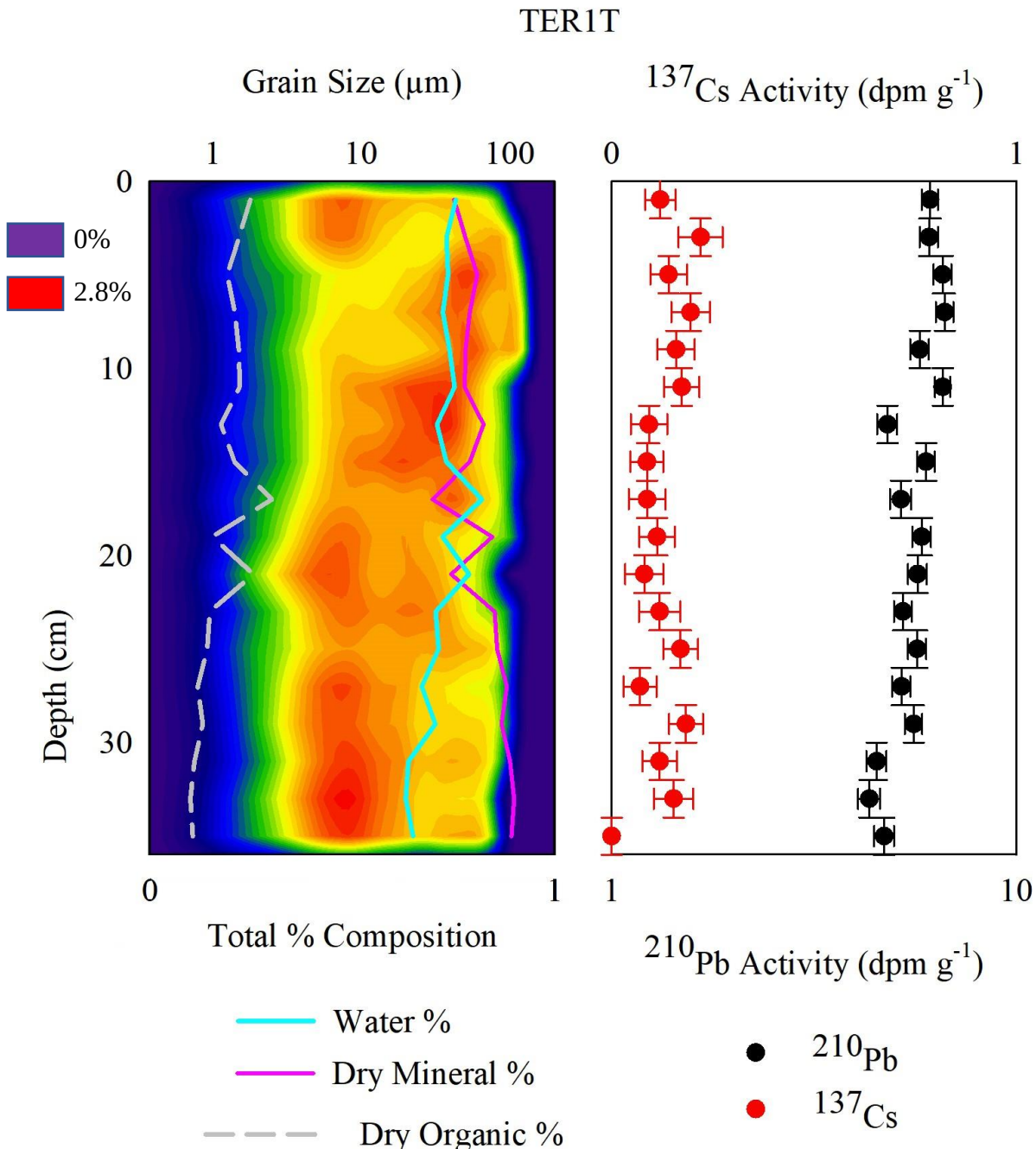
TER1T
Grain Size (µm)
1
10
100
0
0%
2.8%
10
20
30
Depth (cm)
0
1
Total % Composition
Water %
Dry Mineral %
Dry Organic %
137Cs Activity (dpm g-1)
0
1
1
10
210Pb Activity (dpm g-1)
210Pb
137Cs

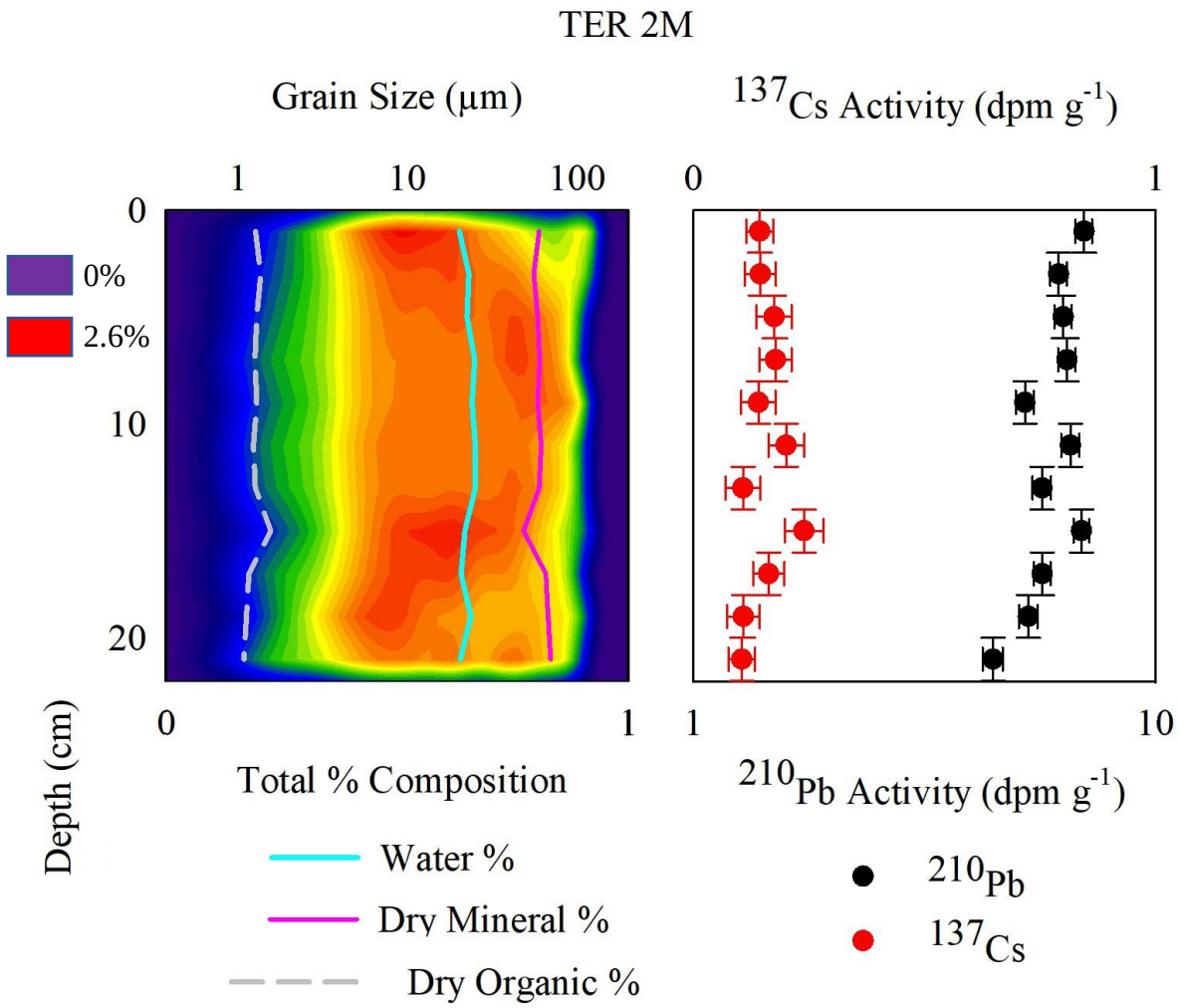
TER 2M
Grain Size (µm)
1
10
100
0
0%
2.6%
10
20
Depth (cm)
0
1
Total % Composition
Water %
Dry Mineral %
Dry Organic %
137Cs Activity (dpm g-1)
0
1
1
10
210Pb Activity (dpm g-1)
210Pb
137Cs

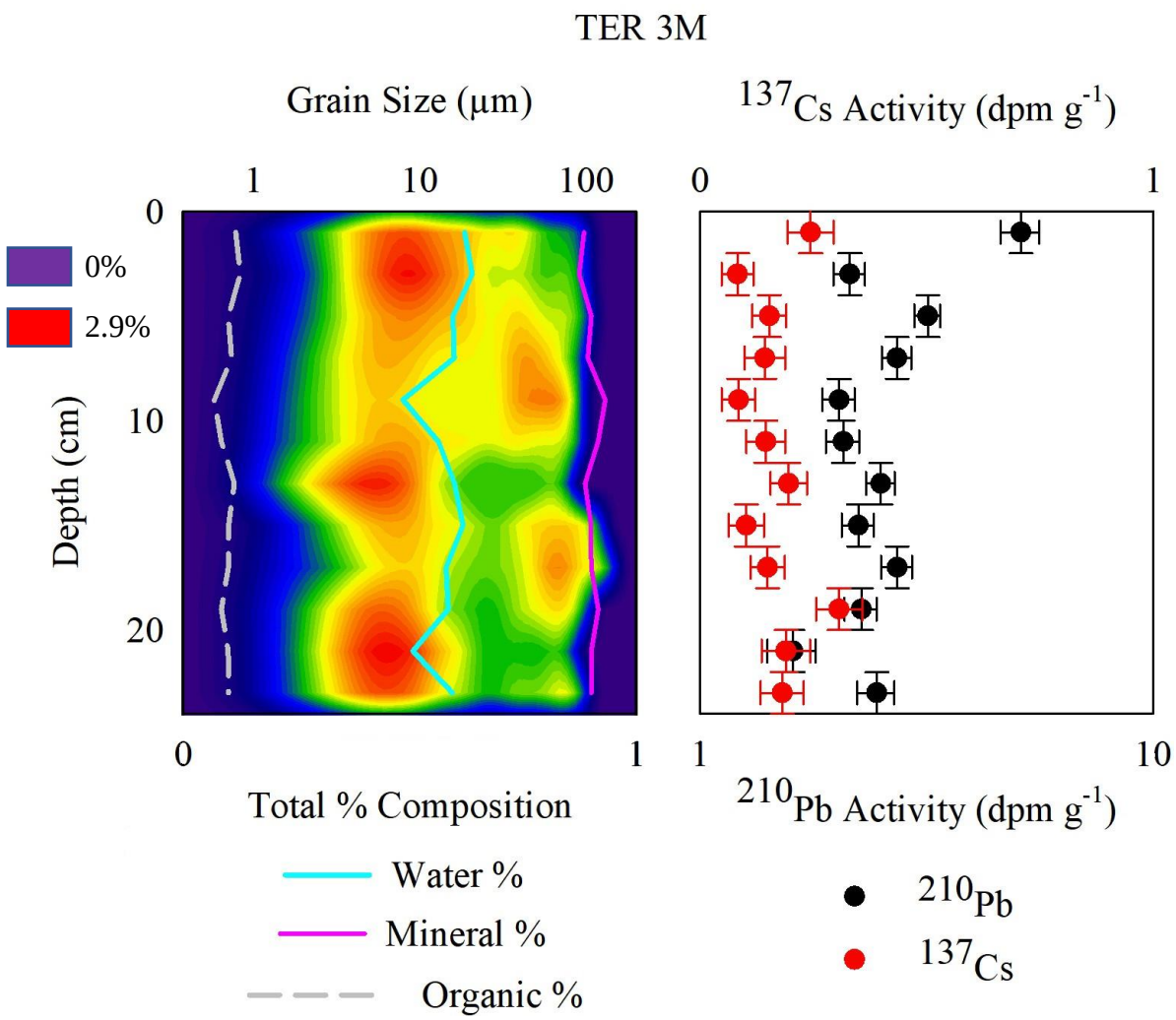
TER 3M
Grain Size (µm)
1
10
100
0
10
20
Depth (cm)
0%
2.9%
0
1
Total % Composition
Water %
Mineral %
Organic %
137Cs Activity (dpm g-1)
0
1
1
10
210Pb Activity (dpm g-1)
210Pb
137Cs

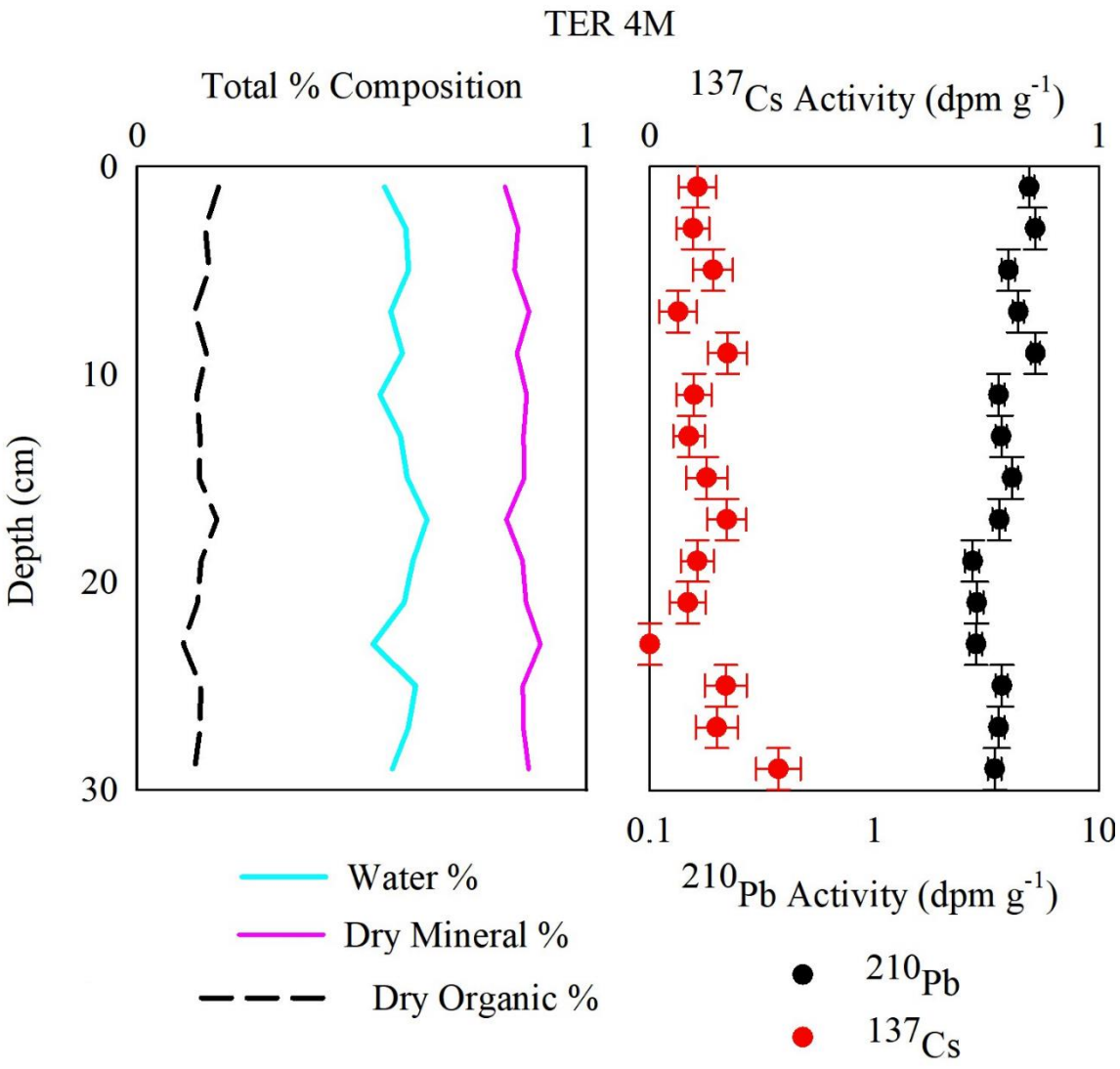
TER 4M
Total % Composition
0
1
0
10
20
30
Depth (cm)
Water %
Dry Mineral %
Dry Organic %
137Cs Activity (dpm g-1)
0
1
0.1
1
10
210Pb Activity (dpm g-1)
210Pb
137Cs

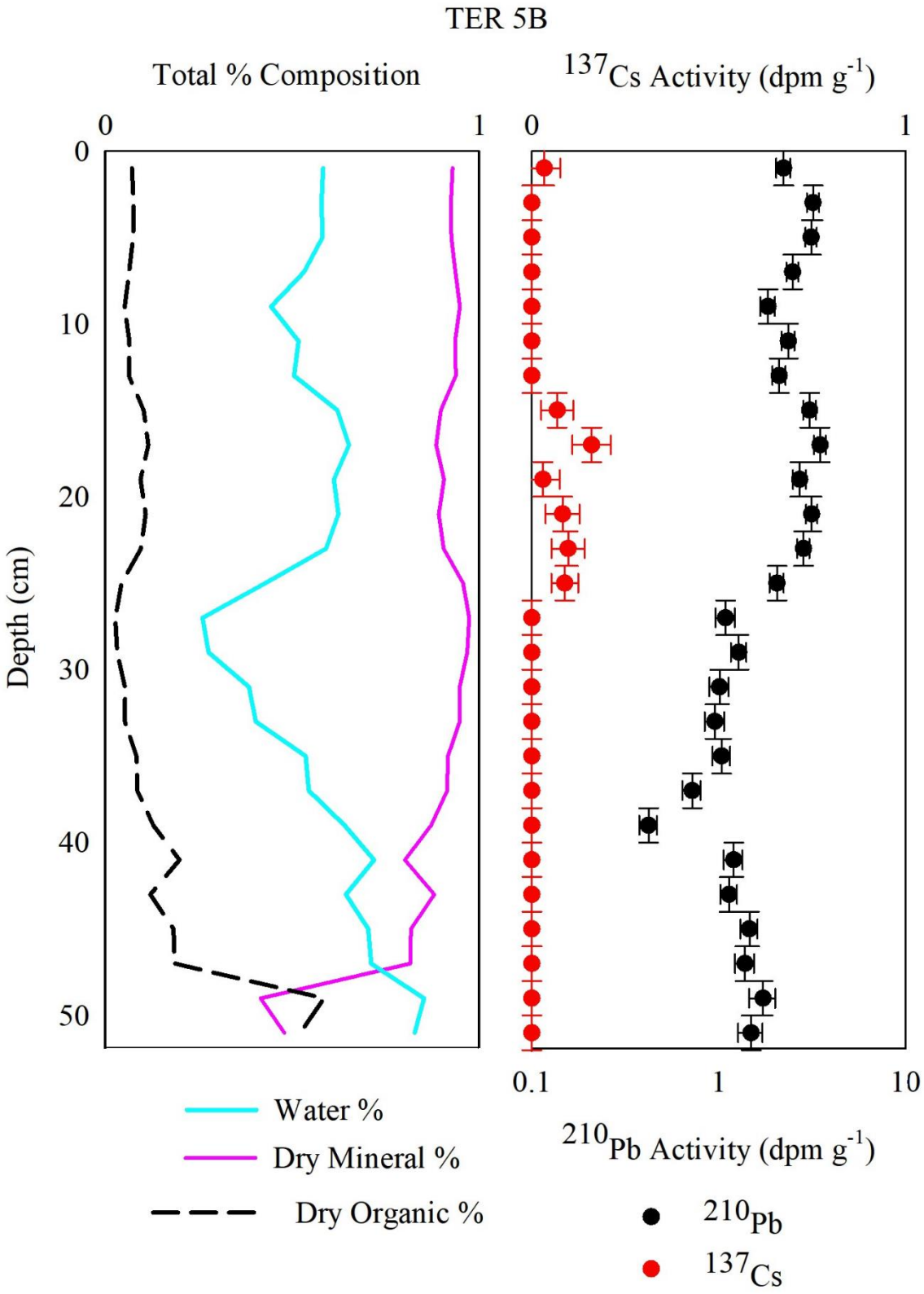
TER 5B
Total % Composition
0
1
0
10
20
30
40
50
Depth (cm)
Water %
Dry Mineral %
Dry Organic %
137Cs Activity (dpm g-1)
0
1
0.1
1
10
210Pb Activity (dpm g-1)
210Pb
137Cs

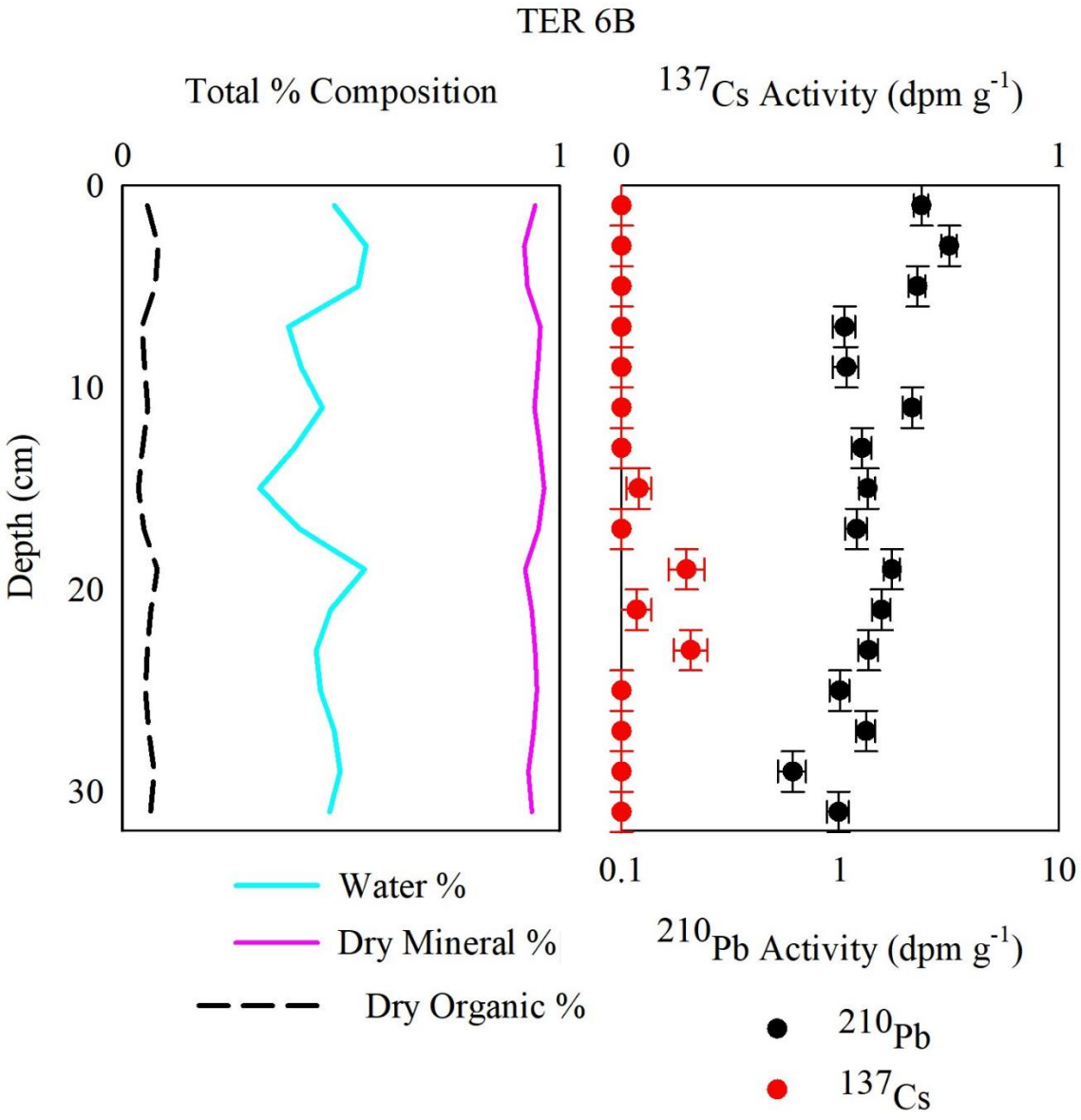
TER 6B
Total % Composition
0
1
0
10
20
30
Depth (cm)
Water %
Dry Mineral %
Dry Organic %
137Cs Activity (dpm g-1)
0
1
0.1
1
10
210Pb Activity (dpm g-1)
210Pb
137Cs

TER 7M

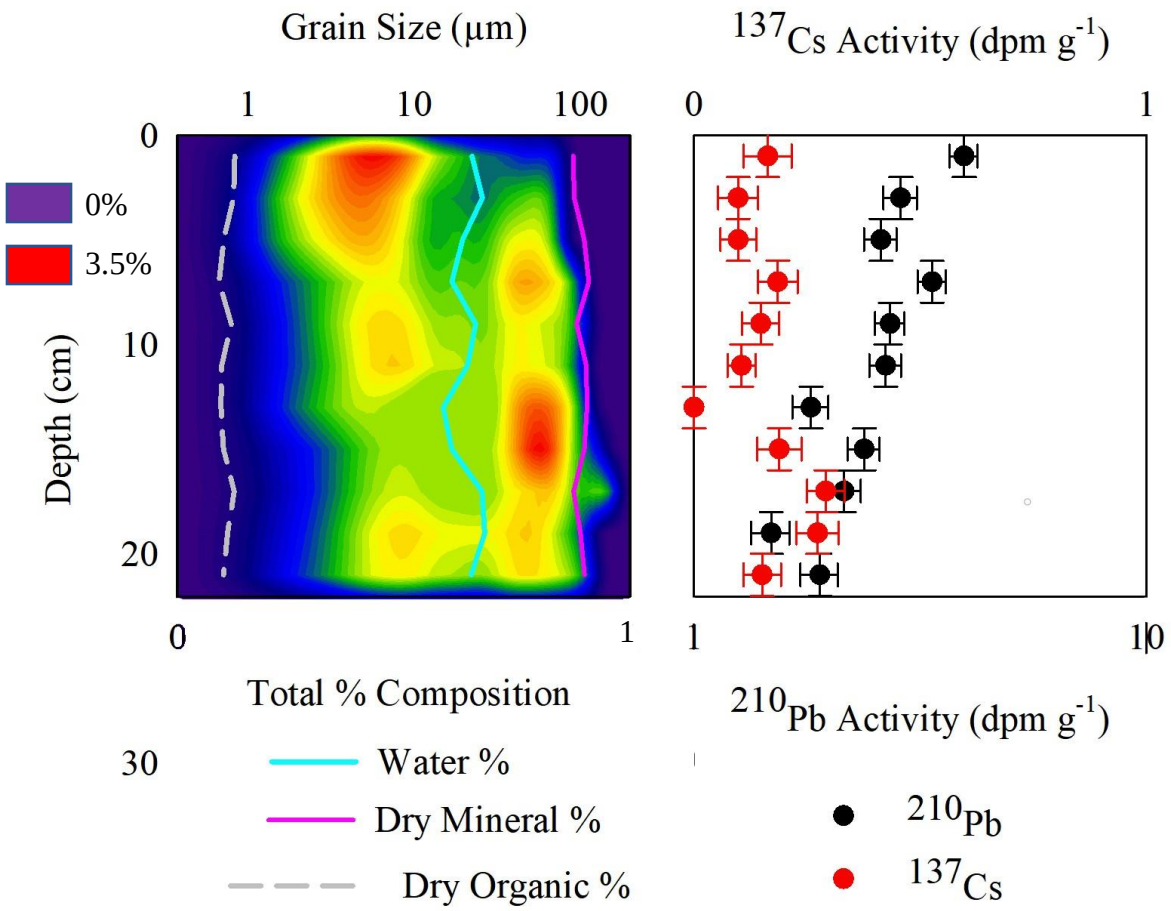
Grain Size (µm)
1
10
100
0
10
20
0%
3.5%
Depth (cm)
0
1
Total % Composition
30
Water %
Dry Mineral %
Dry Organic %
137Cs Activity (dpm g-1)
0
1
1
10
210Pb Activity (dpm g-1)
210Pb
137Cs

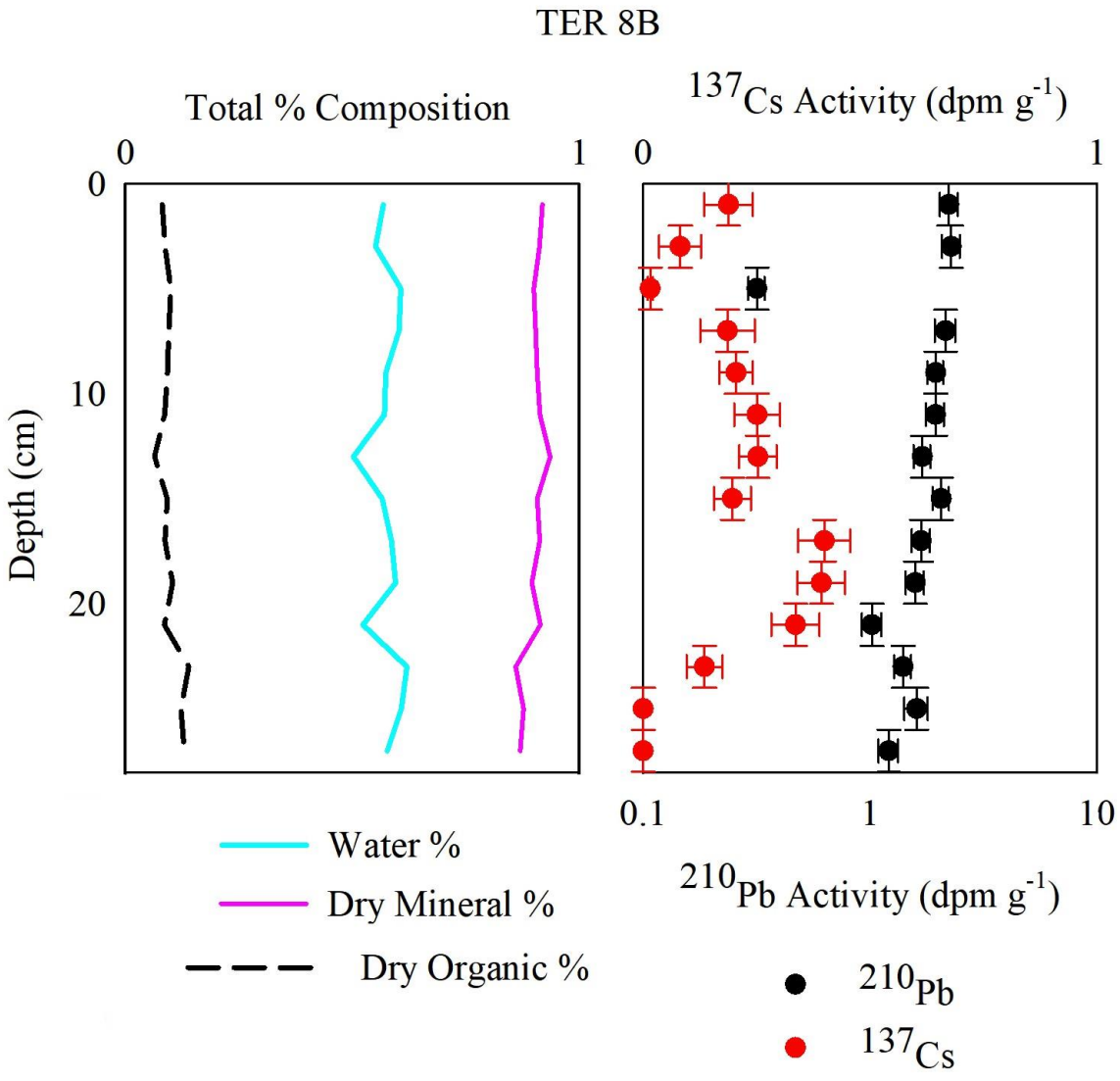
TER 8B
Total % Composition
0
1
0
10
20
Depth (cm)
Water %
Dry Mineral %
Dry Organic %
137Cs Activity (dpm g-1)
0
1
0.1
1
10
210Pb Activity (dpm g-1)
210Pb
137Cs

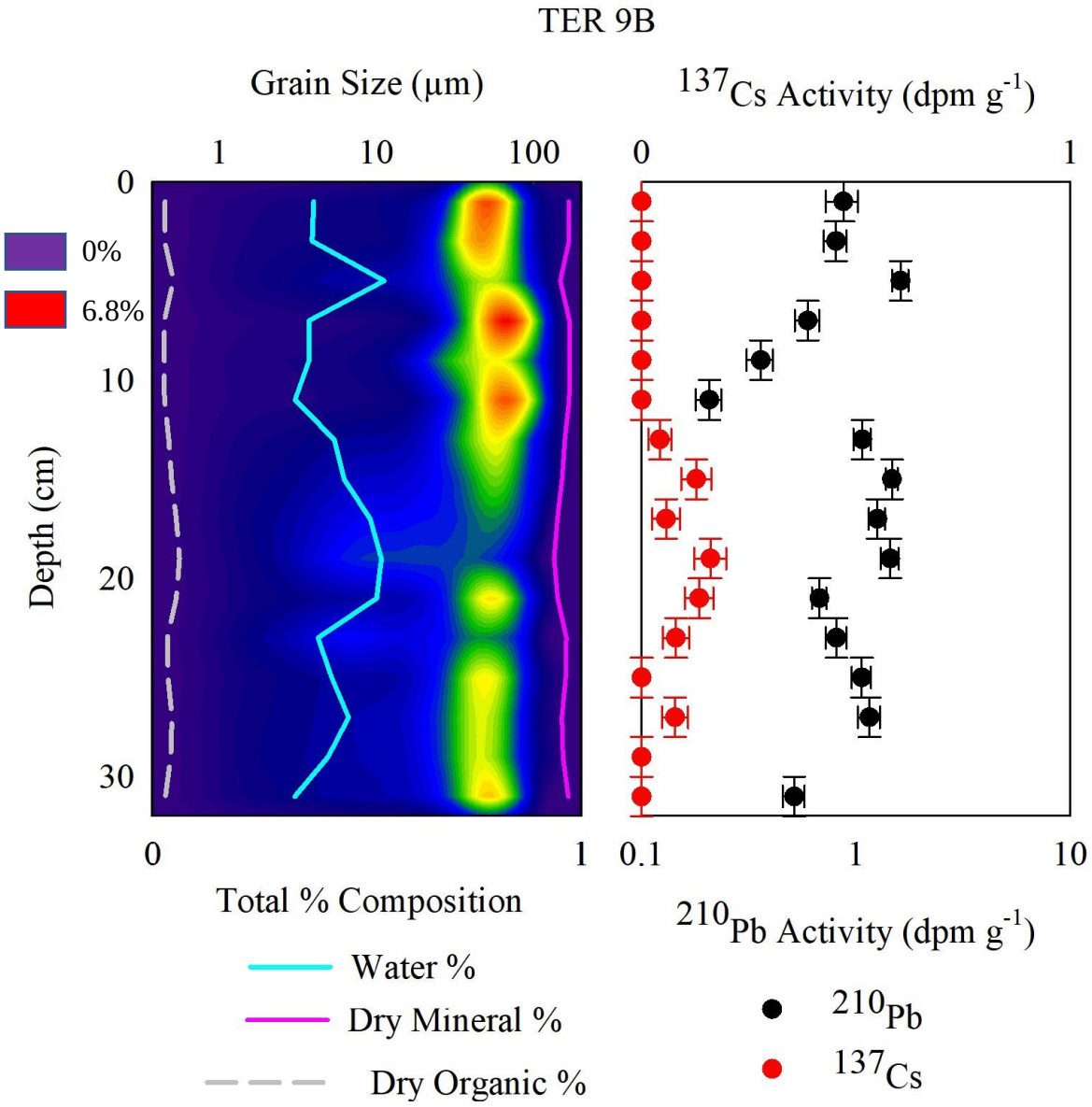
TER 9B
Grain Size (µm)
1
10
100
0
0%
6.8%
10
20
30
Depth (cm)
0
1
Total % Composition
Water %
Dry Mineral %
Dry Organic %
137Cs Activity (dpm g-1)
0
1
0.1
1
10
210Pb Activity (dpm g-1)
210Pb
137Cs

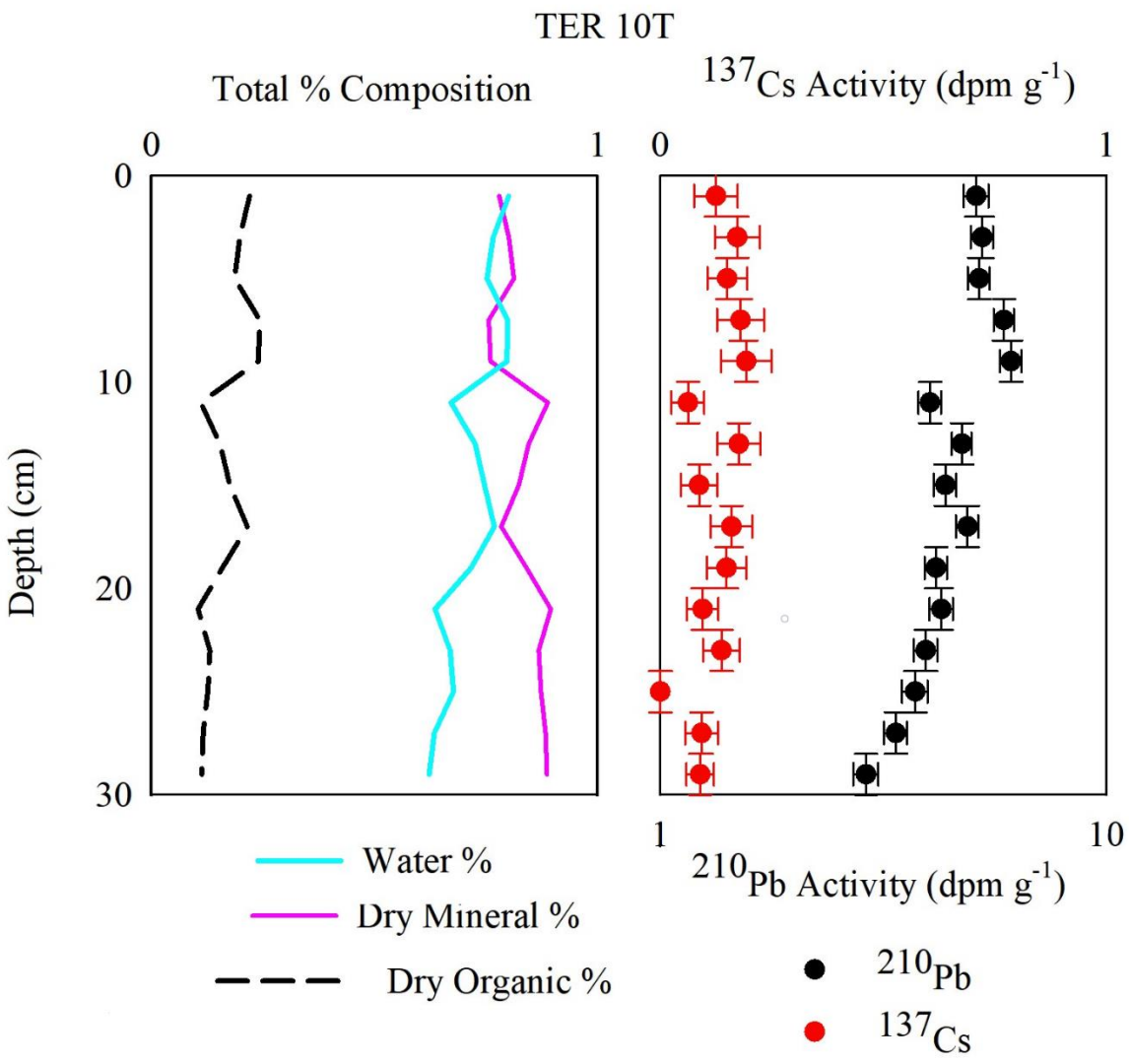
TER 10T
Total % Composition
^{137}Cs Activity (dpm g^{-1})
0
1
0
10
20
30
Depth (cm)
Water %
Dry Mineral %
Dry Organic %
1
10
^{210}Pb Activity (dpm g^{-1})
^{210}Pb
^{137}Cs

APPENDIX B. BULK DENSITY, CRITICAL EROSIONAL SHEAR STRESS, GRAIN SIZE, AND LOI DATA FOR CHAPTER 4

TER 1T

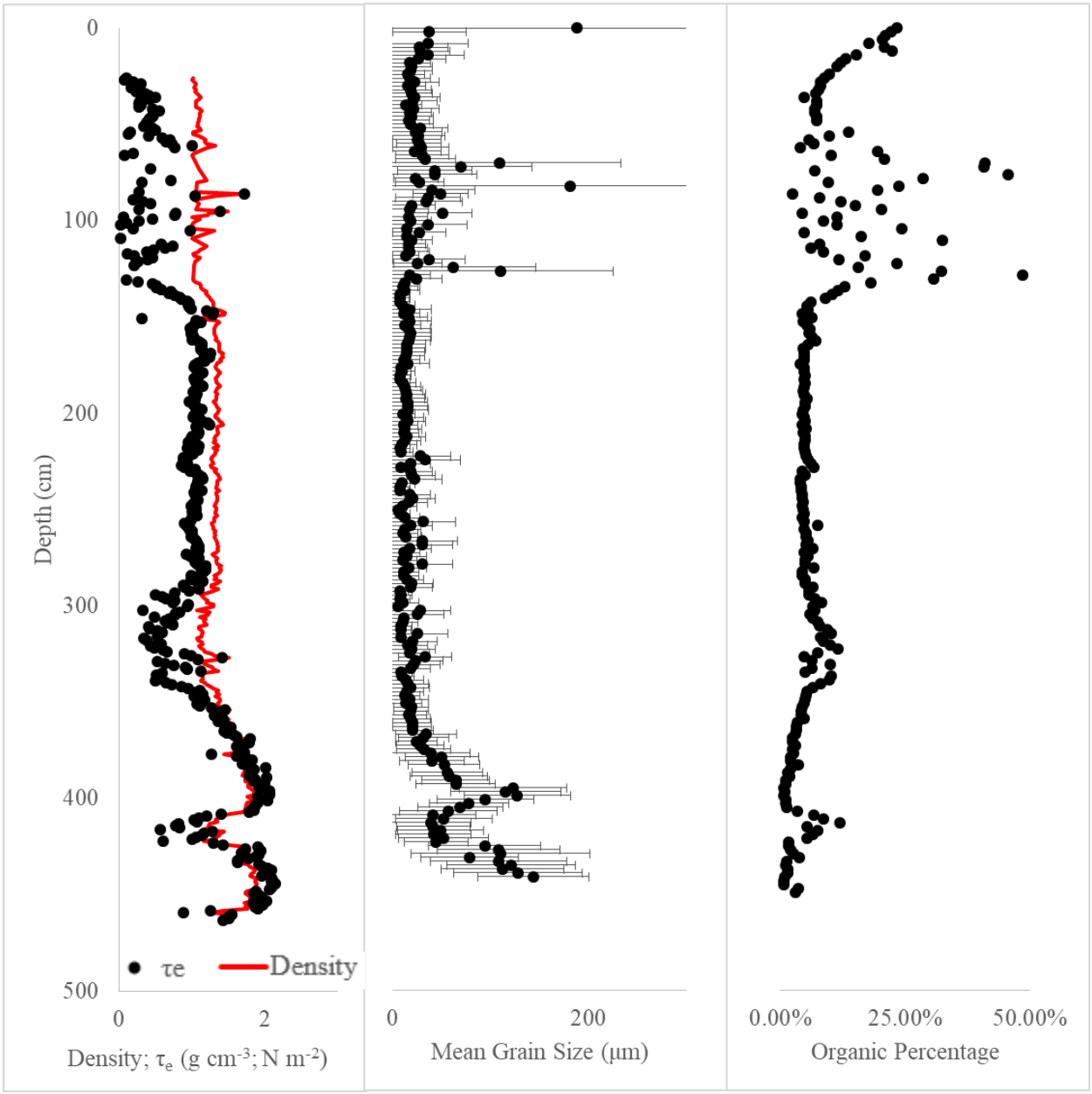

TER 2M

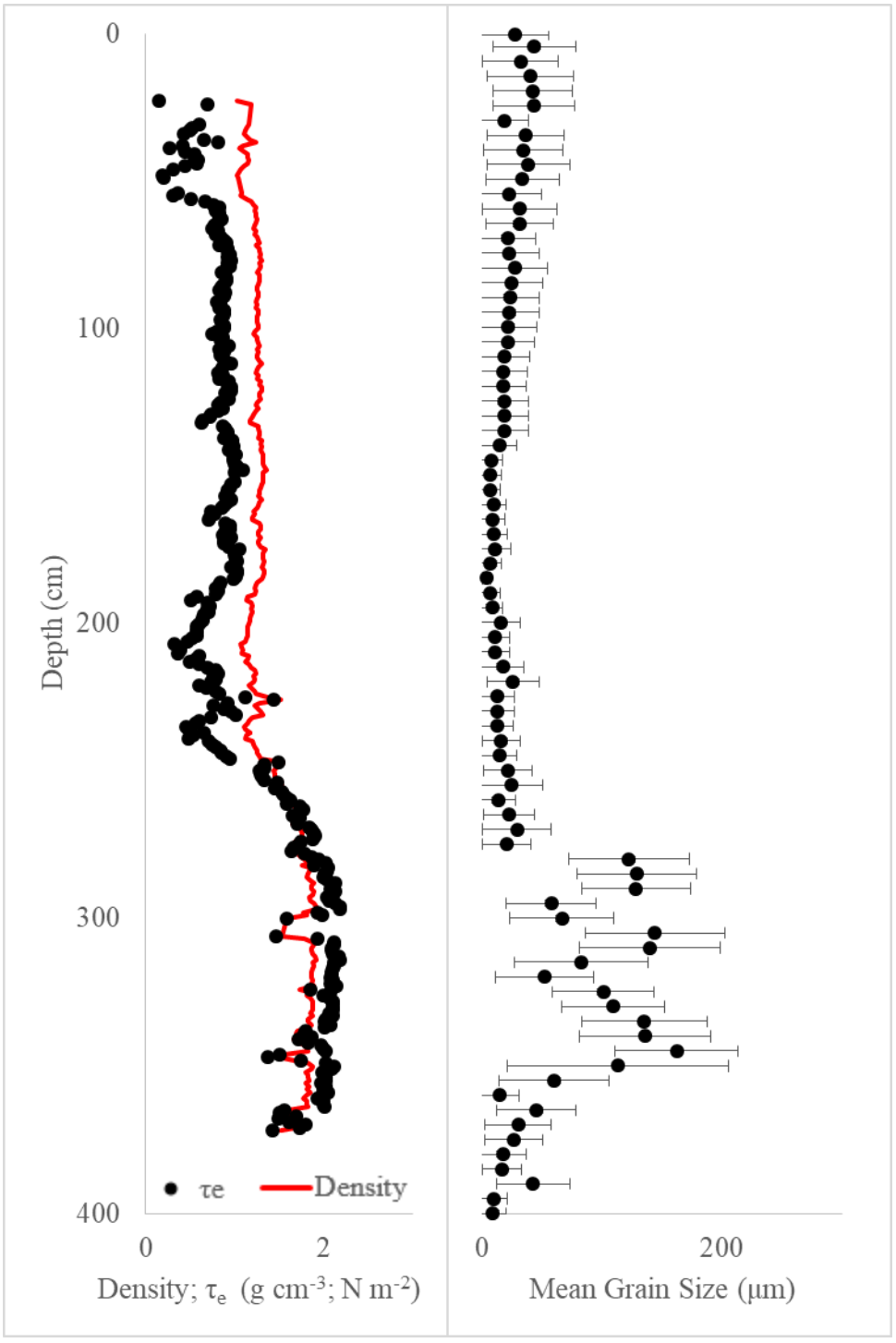
0
100
200
300
400
Depth (cm)
τe
Density
0
2
Density; τe (g cm-3; N m-2)
0
200
Mean Grain Size (µm)

TER 3M

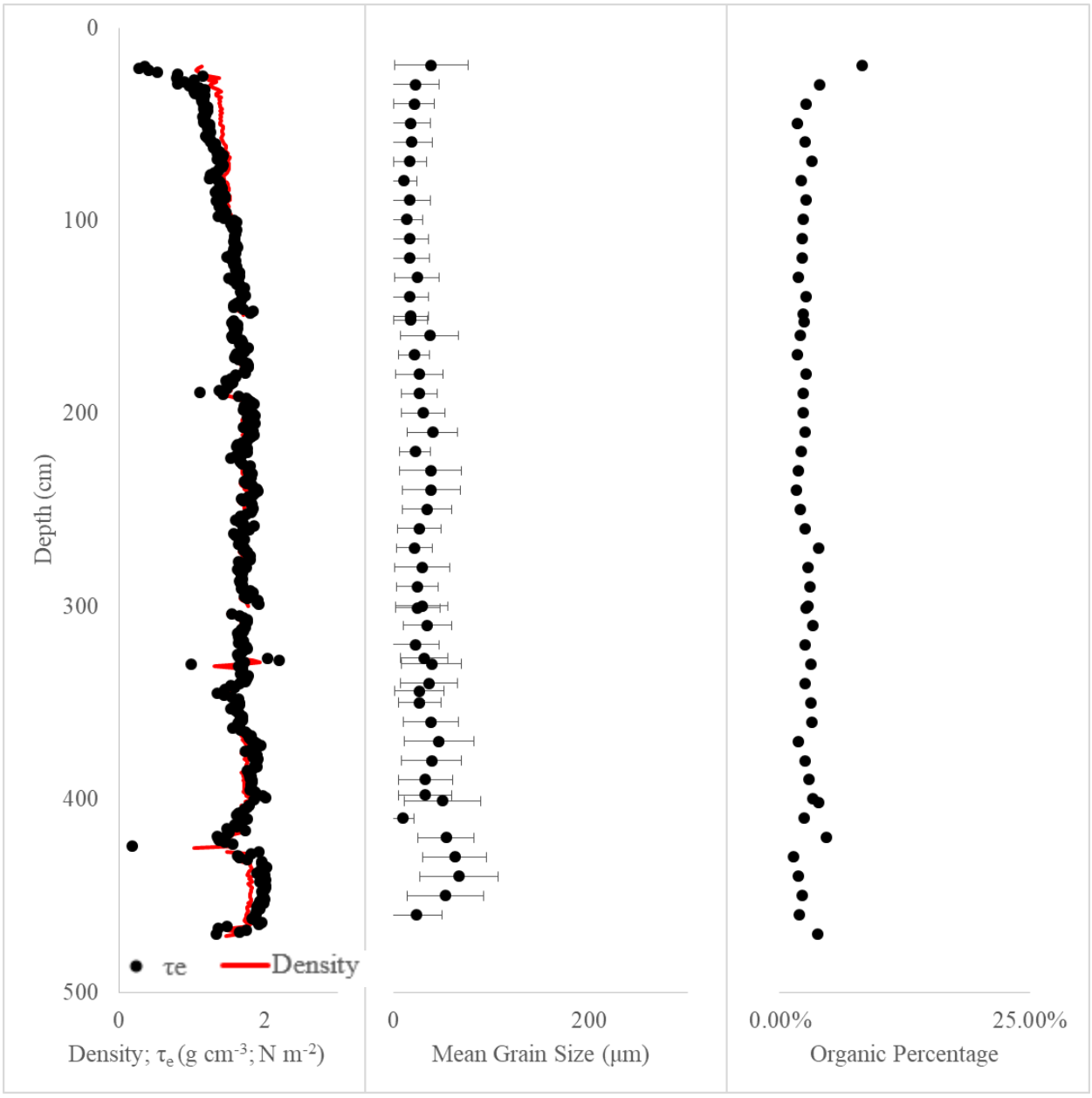
0
100
200
300
400
500
Depth (cm)
τe
Density
0
2
Density; τe (g cm-3; N m-2)
0
200
Mean Grain Size (µm)
0.00%
25.00%
Organic Percentage

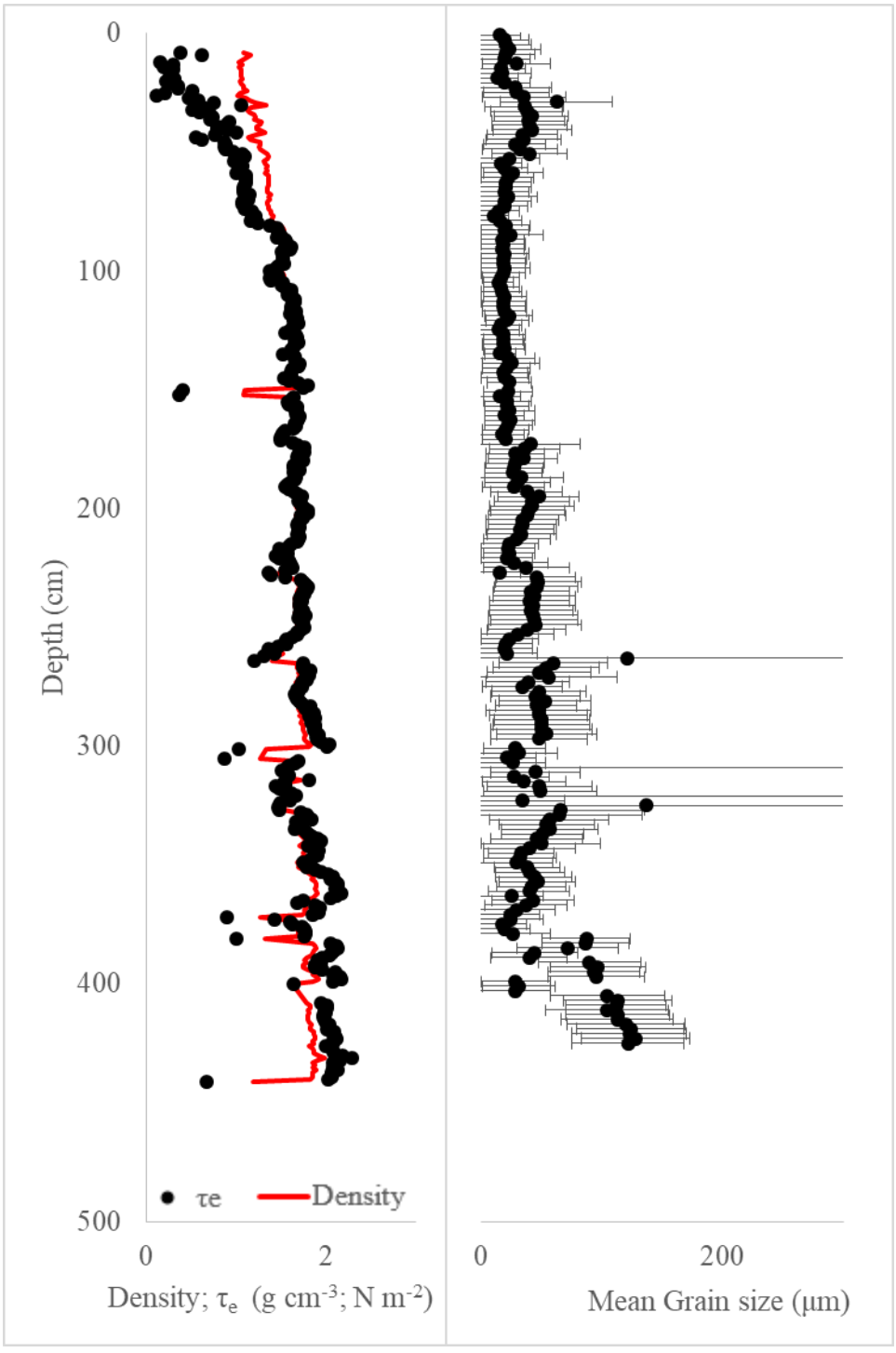
0
100
200
300
400
500
Depth (cm)
τe
Density
0
2
Density; τe (g cm-3; N m-2)
0
200
Mean Grain size (µm)

TER 5B

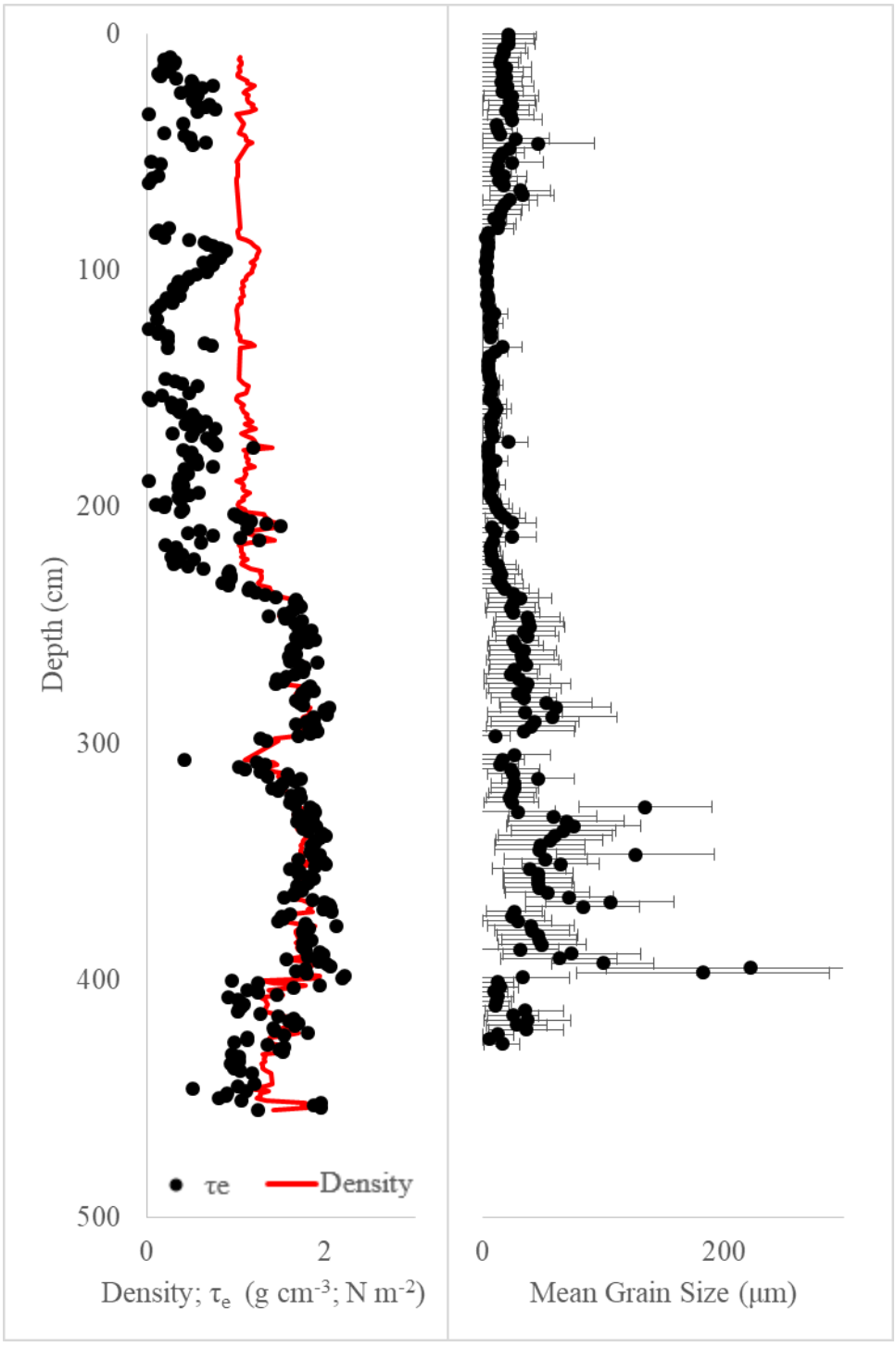
0
100
200
300
400
500
Depth (cm)
τe
Density
0
2
Density; τe (g cm-3; N m-2)
0
200
Mean Grain Size (µm)

TER 6B

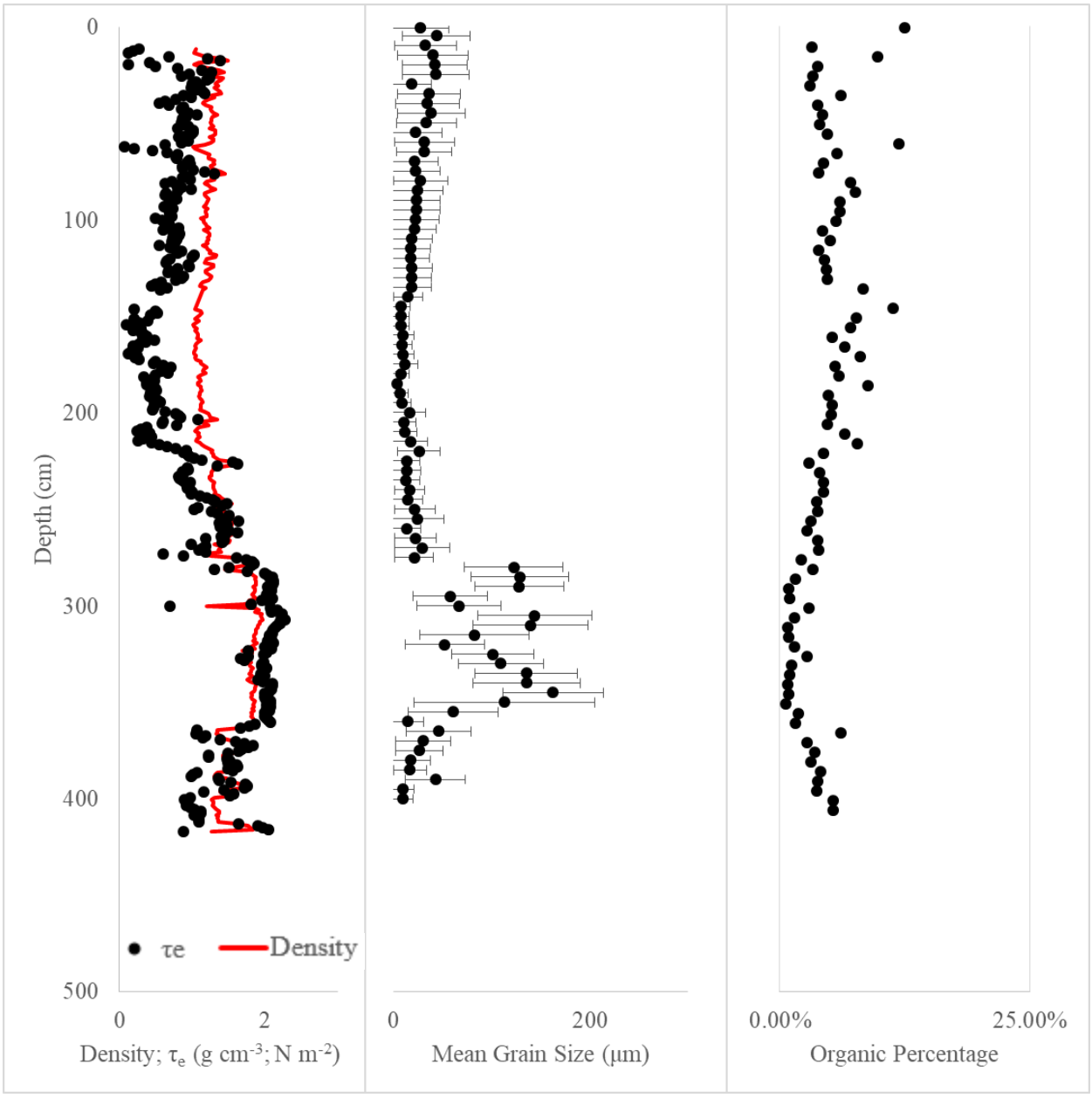
0
100
200
300
400
500
Depth (cm)
τe
Density
0
2
Density; τe (g cm-3; N m-2)
0
200
Mean Grain Size (µm)
0.00%
25.00%
Organic Percentage

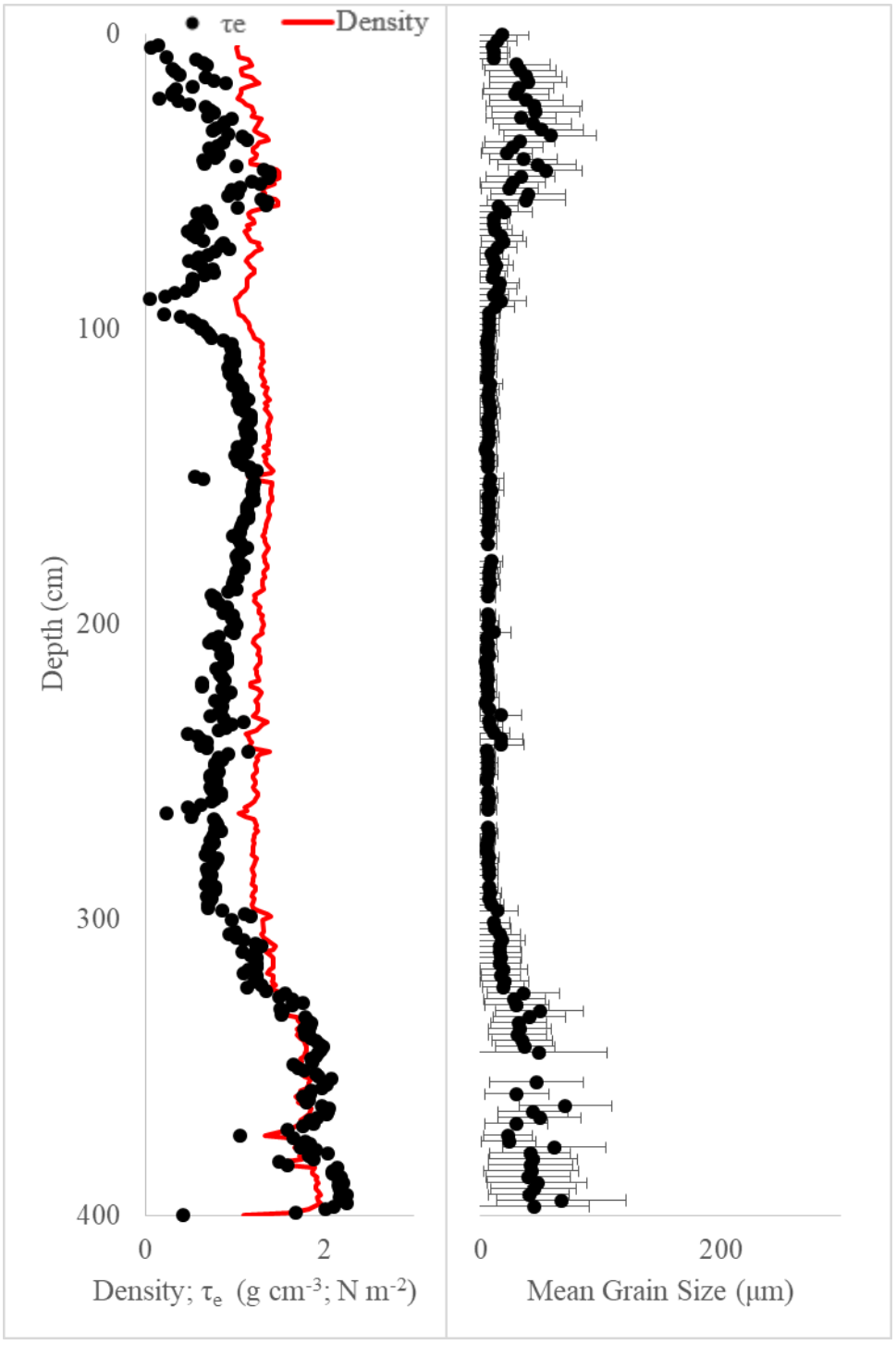
τe
Density
0
100
200
300
400
Depth (cm)
0
2
Density; τe (g cm-3; N m-2)
0
200
Mean Grain Size (µm)

TER 8B

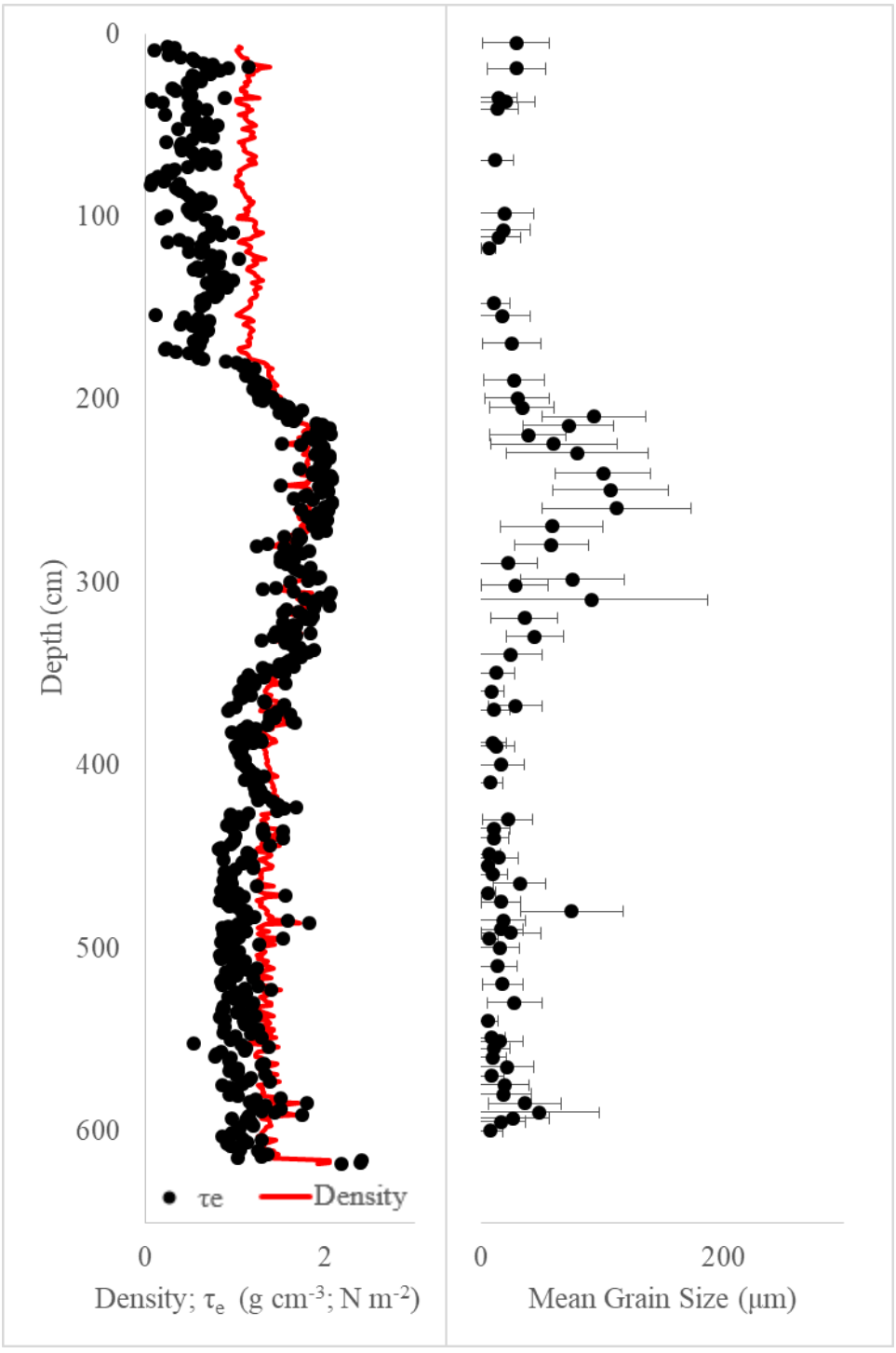
0
100
200
300
400
500
600
Depth (cm)
τe
Density
0
2
Density; τe (g cm-3; N m-2)
0
200
Mean Grain Size (µm)

TER 9B

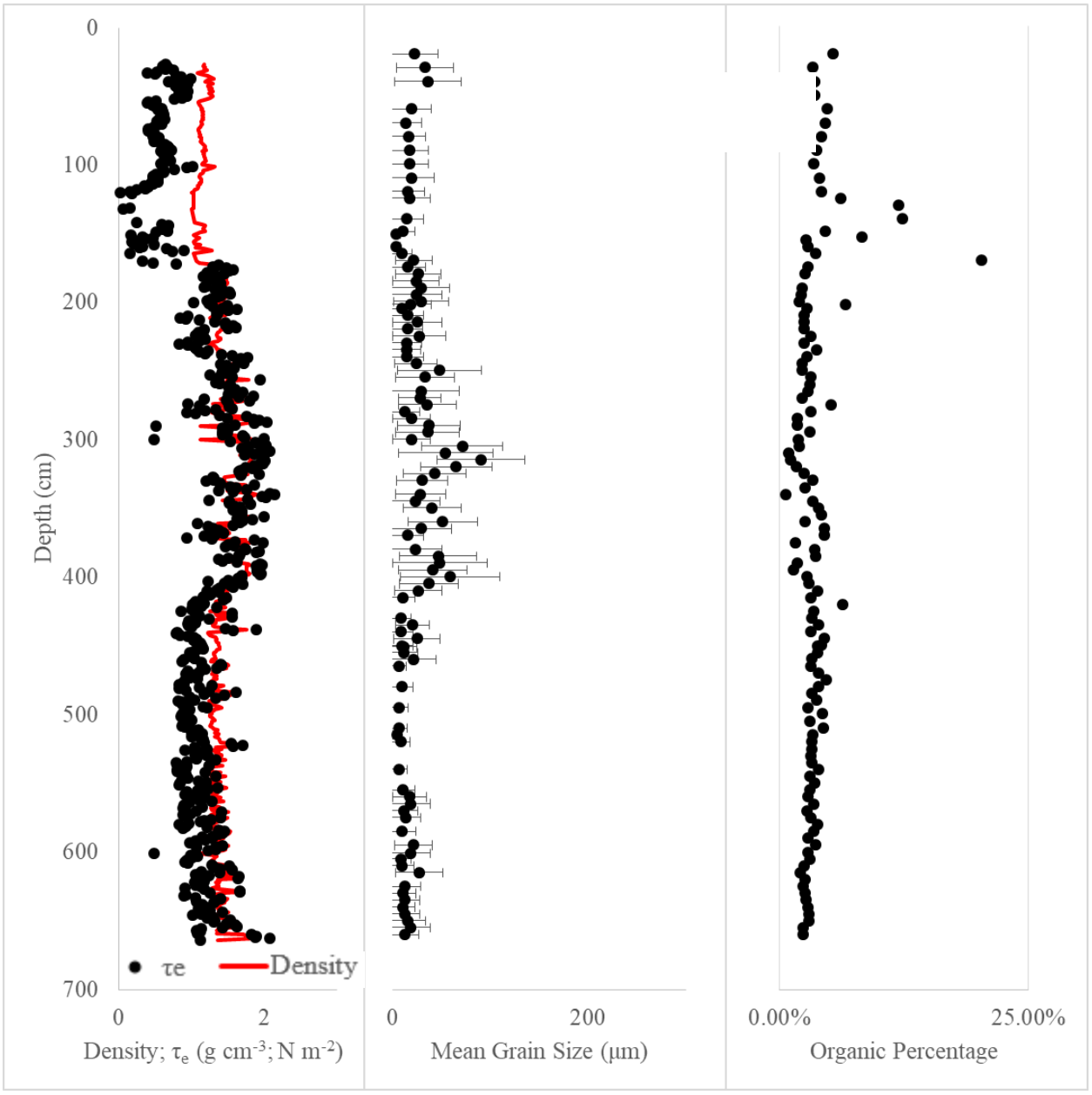
0
100
200
300
400
500
600
700
Depth (cm)
τe
Density
0
2
Density; τe (g cm-3; N m-2)
0
200
Mean Grain Size (µm)
0.00%
25.00%
Organic Percentage

TER 10T

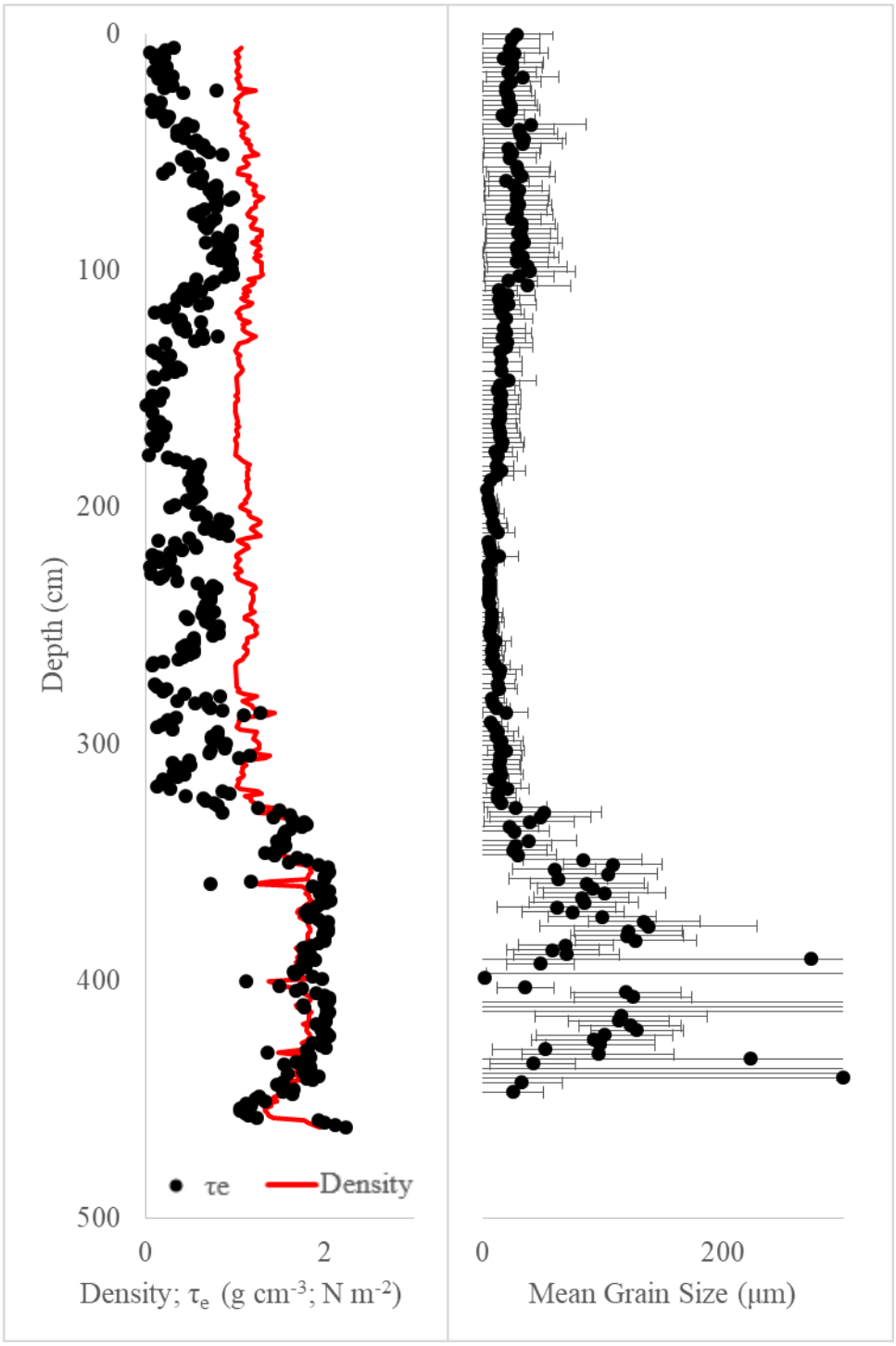
0
100
200
300
400
500
Depth (cm)
τe
Density
0
2
Density; τe (g cm-3; N m-2)
0
200
Mean Grain Size (µm)

APPENDIX C. REQUEST AND PERMISSION FOR PREVIOUSLY PUBLISHED MATERIAL

Re: Decision on your manuscript #ESCO-D-18-00044R2

Giancarlo A Restreppo
Tue 1/15/2019 4:06 PM
To: Charles Si Simenstad <simenstd@u.washington.edu>

Dr. Simenstad,

I'm about to submit my dissertation and my university requires permission from any journals before I can submit previously published work. I have my first chapter published in Estuaries and Coasts. Would you be able to tell me who I can send the request to? For reference, this is my paper: https://link.springer.com/article/10.1007/s12237-018-0453-0

Riverine Sediment Contribution to Distal Deltaic Wetlands: Fourleague Bay, LA | SpringerLink - link.springer.com

link.springer.com

The fine-sediment dispersal system of the Atchafalaya River and associated bays and wetlands provide an excellent analog for future diversions as a means to study the radius of influence that a diversion provides, in terms of fine-sediment supply.

Thank you,

Giancarlo Restreppo
PhD Candidate
Department of Geology & Geophysics
E235 Howe Russell Kniffen
Louisiana State University, Baton Rouge, LA 70803

RE: Decision on your manuscript #ESCO-D-18-00044R2

Janet Slobodien <Janet.Slobodien@springer.com>
Wed 1/16/2019 11:16 AM

To: Si Simenstad <simenstd@uw.edu>; Giancarlo A Restreppo <grestr1@lsu.edu>; Jodi Borgenicht <Jodi.Borgenicht@springer.com>

Dear Mr. Restreppo,

You can use the article in your dissertation. Per the copyright transfer agreement, "Acknowledgement needs to be given to the final publication and a link must be inserted to the published article on Springer's website, by inserting the DOI number of the article in the following sentence:

"The final publication is available at Springer via http://dx.doi.org/[insert DOI]". Author retains the right to use his/her article for his/her further scientific career by including the final published journal article in other publications such as dissertations and postdoctoral qualifications provided acknowledgement is given to the original source of publication.

Best,
Janet

Janet Slobodien
Executive Editor
Ecology and Evolutionary Biology

Springer
233 Spring Street | New York, NY 10013 | USA
T +1 (212) 460-1525
M +1 (646) 258-0091
janet.slobodien@springer.com
www.springer.com
Follow us on Twitter @SpringerEcology

VITA

Giancarlo Alessandro Restreppo is a native of Los Angeles, CA, where he earned his B.A. in anthropology from California State University, Los Angeles, in 2010. For graduate school he was drawn toward the environmental, rather than humanistic, side of science and so earned his M.S. in geology with an emphasis on hydrogeology during 2015, also from CSULA. Seeking to achieve a higher understanding of geologic and environmental interactions, he accepted an offer to obtain his PhD at Louisiana State University. Upon completion, the author will pursue a career in coastal research and restoration.